

60
7.6
B76
1981

MULTICHANNEL MAXIMUM ENTROPY METHOD OF SPECTRAL ANALYSIS
APPLIED TO OFFSHORE STRUCTURES

by

MICHAEL JEFFREY BRIGGS

B.S. University of Texas at Austin
(1970)

M.S., University of Southern California
(1974)

MARINE
BIOLOGICAL
LABORATORY
LIBRARY
WOODS HOLE, MASS.
W. H. O. I.

SUBMITTED IN PARTIAL FULFILLMENT OF THE
REQUIREMENTS FOR THE DEGREE OF
OCEAN ENGINEER

at the

MASSACHUSETTS INSTITUTE OF TECHNOLOGY

and the

WOODS HOLE OCEANOGRAPHIC INSTITUTION

June, 1981

Signature of
Author

.....
Joint Program in Ocean Engineering, Massachusetts
Institute of Technology/Woods Hole Oceanographic
Institution, and Department of Ocean Engineering,
Massachusetts Institute of Technology, June, 1981.

Certified by

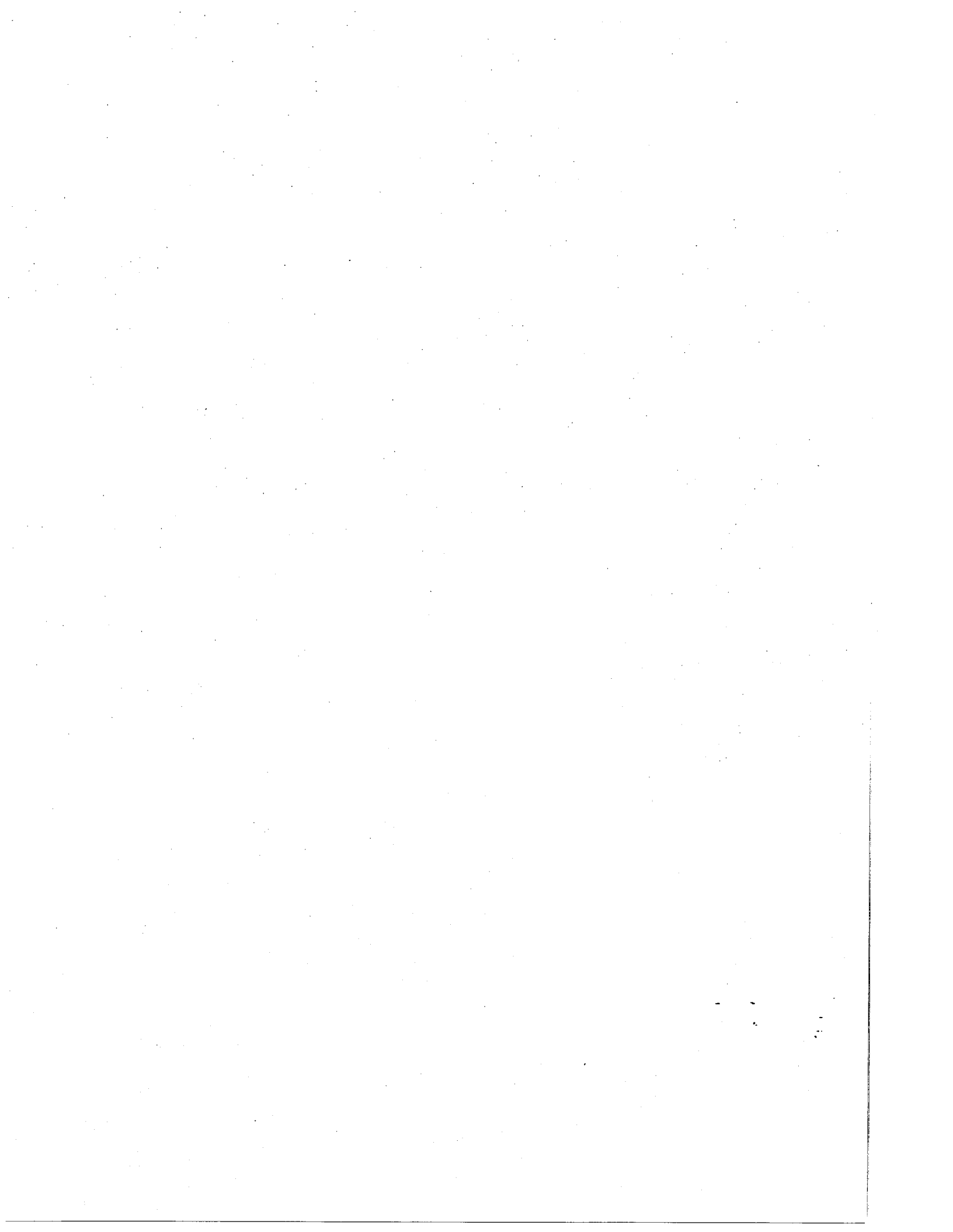
.....
J. K. Vandiver, Thesis Supervisor, MIT

Certified by

.....
W. D. Grant, Thesis Supervisor, WHOI

Accepted by

.....
Earl E. Hays, Chairman, Joint Committee on Ocean
Engineering, Massachusetts Institute of Technology/
Woods Hole Oceanographic Institution.



MULTICHANNEL MAXIMUM ENTROPY METHOD OF SPECTRAL ANALYSIS
APPLIED TO OFFSHORE STRUCTURES

by

Michael J. Briggs

Submitted to the Department of Ocean Engineering
in June, 1981 in partial fulfillment of the
requirements for the Degree of Ocean Engineer

ABSTRACT

The multichannel Maximum Entropy Method (MEM) of spectral analysis is developed and applied in the dynamic analysis of offshore structures. Two different algorithms are implemented and compared with the conventional Blackman-Tukey method. These are (1) a direct on the data or Burg method and (2) a Yule-Walker or correlation function extension method. Cross-spectral estimates of magnitude, phase, coherence squared, and transfer function are calculated. These estimates are then used in mode shape identification of a triple decked, single caisson offshore platform. The superiority of the multichannel Maximum Entropy Methods relative to conventional spectral analysis techniques in calculating these cross-spectral estimates and evaluating mode shapes is demonstrated.

Thesis Supervisor: Dr. J. Kim Vandiver
Title: Associate Professor of Ocean Engineering
Massachusetts Institute of Technology

Thesis Supervisor: Dr. William D. Grant
Title: Associate Scientist
Woods Hole Oceanographic Institution

ACKNOWLEDGEMENTS

This research was sponsored by the Branch of Marine Oil and Gas Operations of the United States Geological Survey, Department of the Interior and by the Massachusetts Institute of Technology/Woods Hole Oceanographic Institution Joint Program in Ocean Engineering. Also, Amoco permitted us to collect and process the data from one of their offshore caisson platforms located in the Gulf of Mexico.

I would like to thank my advisors in the Joint Program for their advice and encouragement and for allowing me the freedom to pursue my own research interests. Specifically they are Dr. W. D. Grant at Woods Hole and especially Dr. J. K. Vandiver of MIT.

Thanks to Mike Cook, a graduate student at MIT, for assisting Professor Vandiver in collecting the data and performing the finite element analysis of the platform.

A special thanks goes to the MIT/WHOI Joint Program for giving me the opportunity, both educationally and financially, to return to school to develop my full potential as an Ocean Engineer.

Finally, no amount of gratitude can adequately repay my wife, Mary, for her inspiration, support and sacrifice during these past three years. To her I am truly indebted.

TABLE OF CONTENTS

Title Page	1
Abstract	3
Acknowledgements	5
Table of Contents	7
List of Figures	10
List of Tables	14
List of Symbols	15
1.0 INTRODUCTION	20
2.0 CONVENTIONAL METHODS OF SPECTRAL ANALYSIS	28
2.1 Bias versus Variance Tradeoff	29
2.1.1 Windows	31
2.1.2 Data Record Segmenting	34
2.1.3 Zero Appendage	35
2.2 Spectral Estimates	36
2.3 Direct Methods of Spectral Analysis	36
2.4 Correlation Methods of Spectral Analysis	38
3.0 MAXIMUM ENTROPY METHODS OF SPECTRAL ANALYSIS	42
3.1 Autoregressive Model	42
3.2 Single Channel MEM Methods	45
3.2.1 Least Squares Filter	46
3.2.2 Levinson-Durbin Recursion	49
3.3 Multichannel MEM Methods	50
3.3.1 Direct on the Data Method	50
3.3.1.1 Derivation of Filter Coefficients Matrix	52
3.3.1.2 Spectral Matrix Estimation	54
3.3.1.3 Multichannel LWR Recursion	55
3.3.2 Correlation Method	58
3.3.2.1 Rissanen Algorithm	59
3.4 Model Order Selection Criteria	61
3.4.1 Single Channel Criteria	62
3.4.2 Multichannel Criteria	63

4.0	TRANSFER FUNCTION ESTIMATION	64
4.1	Auto and Cross-Spectral Derivation	64
4.2	Estimation Errors	68
4.2.1	Bias Errors	68
4.2.2	Random Errors	69
5.0	MULTICHANNEL SPECTRAL ANALYSIS	70
5.1	Applications to Offshore Structures	70
5.1.1	Mode Shape Identification	70
5.1.2	Dynamic Frequency Response to Wave Excitation	71
5.2	Multichannel Spectral Analysis Formulas	71
5.2.1	Time Domain Analysis	72
5.2.2	Frequency Domain Analysis	72
5.2.2.1	Autospectral Estimates	73
5.2.2.2	Cross-Spectral Estimates	73
5.2.2.3	Coherence Squared Estimates	74
5.2.2.4	Transfer Function Estimates	75
5.3	Interpretation of Cross-Spectral Estimates	76
5.3.1	Autospectral Estimates	76
5.3.2	Cross-Spectral Magnitude Estimates	76
5.3.2	Phase and Coherence Estimates	76
5.3.4	Transfer Function Estimates	77
6.0	CASE STUDY OF A SINGLE CAISSON PRODUCTION PLATFORM	78
6.1	Caisson Platform Description	78
6.2	Instrumentation	81
6.2.1	Accelerometers	81
6.2.2	Wave Staff	81
6.2.3	FM Tape Recorder	82
6.3	Summary of Load Cases	82
6.3.1	Description	82
6.3.2	Environmental Conditions	84
6.4	Test Set-up	84
6.5	Data Processing	86

7.0	COMPARISON OF MULTICHANNEL SPECTRAL ANALYSIS METHODS	90
7.1	Blackman-Tukey Method	91
	7.1.1 Effect of Window Shape	91
	7.1.2 Effect of Window Duration	91
7.2	BRGMEM Direct on the Data Method	98
7.3	Comparison of Three Multichannel Methods	108
8.0	APPLICATION OF MULTICHANNEL MEM TO CAISSON RESPONSE RECORDS	120
8.1	Dynamic Response to Wave Excitation	120
8.2	Mode Shape Identification	129
	8.2.1 Flexural Modes	129
	8.2.2 Torsional Modes	149
8.3	Spurious Noise Peaks	161
9.0	SUMMARY AND CONCLUSIONS	165
	References	169

LIST OF FIGURES

2.1	Bartlett or Triangular Lag Window	32
2.2	Periodogram Spectral Estimate	32
2.3	Blackman-Tukey Spectral Estimate	32
3.1	Linear or Shaping Filter	43
3.2	Wiener or Least Squares Filter	43
4.1	Transfer Function of a Linear, Causal System	65
4.2	Effect of Noise on Transfer Function Estimation	65
6.1	Offshore Caisson Platform	79
6.2	Schematic of Offshore Caisson Platform	80
6.3	Load Case 1 - Wave Input & Torsional Mode Shape Plan View of Wellhead Deck	83
6.4	Load Case 2 - Flexural Mode Shape Side View of Offshore Caisson Platform	83
7.1	Effect of Boxcar Window On Blackman-Tukey Method MAXLAG = 512	92
7.2	Effect of Bartlett Window on Blackman-Tukey Method MAXLAG = 512	93
7.3	Effect of Hanning Window on Blackman-Tukey Method MAXLAG = 512	94
7.4	Effect of Parzen Window on Blackman-Tukey Method MAXLAG = 512	95
7.5	Effect of Window Duration on Blackman-Tukey Method Hanning Window, NLAG = 128	96
7.6	Effect of Window Duration on Blackman-Tukey Method Hanning Window, NLAG = 128	97
7.7a	Effect of Averaging on Magnitude Cross-Spectrum BRGMEM, NSEG = 1, M = 2048, NLAG = 80	99
7.7b	Effect of Averaging on Magnitude Cross-Spectrum BRGMEM, NSEG = 9, M = 2048, NLAG = 80	100
7.7c	Effect of Averaging on Magnitude Cross-Spectrum BRGMEM, NSEG = 1, N = 18432, NLAG = 80	101

7.8a	Effect of Averaging on Phase Estimates BRGMEM, NSEG = 1, M = 2048, NLAG = 80	102
7.8b	Effect of Averaging on Phase Estimates BRGMEM, NSEG = 9, M = 2048, NLAG = 80	103
7.8c	Effect of Averaging on Phase Estimates BRGMEM, NSEG = 1, N = 18432, NLAG = 80	104
7.9a	Effect of Averaging on Coherence Estimates BRGMEM, NSEG = 1, M = 2048, NLAG = 80	105
7.9b	Effect of Averaging on Coherence Estimates BRGMEM, NSEG = 1, M = 2048, NLAG = 80	106
7.9c	Effect of Averaging on Coherence Estimates BRGMEM, NSEG = 1, N = 18432, NLAG = 80	107
7.10a	Comparison of Magnitude Cross-Spectrum BTSPEC, Hanning Window, NLAG = 80	109
7.10b	Comparison of Magnitude Cross-Spectrum BRGMEM, NSEG = 9, M = 2048, NLAG = 80	110
7.10c	Comparison of Magnitude Cross-Spectrum RYWMEM, NLAG = 80	111
7.11a	Comparison of Phase Estimates BTSPEC, Hanning Window, NLAG = 80	112
7.11b	Comparison of Phase Estimates BRGMEM, NSEG = 9, M = 2048, NLAG = 80	113
7.11c	Comparison of Phase Estimates RYWMEM, NLAG = 80	114
7.12a	Comparison of Coherence Estimates BTSPEC, Hanning Window, NLAG = 80	115
7.12b	Comparison of Coherence Estimates BRGMEM, NSEG = 9, M = 2048, NLAG = 80	116
7.12c	Comparison of Coherence Estimates RYWMEM, NLAG = 80	117
8.1	Wave Height Time History Load Case 1	121
8.2	NAW Accelerometer Time History Load Case 1	122
8.3	Wave Height Autocorrelation Load Case 1, MAXLAG = 512, N = 29696	123

8.4	NAW Accelerometer Autocorrelation Load Case 1, MAXLAG = 512, N = 29696	124
8.5	Wave and NAW Accelerometer Cross-Correlation Load Case 1, MAXLAG = 512 (pos. side), N = 29696	126
8.6	Wave Height Autospectrum Load Case 1, NLAG = 60	127
8.7	NAW Accelerometer Autospectrum Load Case 1, NLAG = 60	128
8.8	Wave Height and NAW Accelerometer Magnitude Cross-Spectrum - Load Case 1, NLAG = 60	130
8.9	Wave Height and NAW Accelerometer Coherence Estimate - Load Case 1, NLAG = 60	131
8.10	Wave Height and NAW Accelerometer Transfer Function Estimate - Load Case 1, NLAG = 60	132
8.11	NAH Accelerometer Time History Load Case 2	133
8.12	NAW Accelerometer Time History Load Case 2	134
8.13	NAH Accelerometer Autocorrelation Load Case 2, MAXLAG = 512, N = 29696	136
8.14	NAW Accelerometer Autocorrelation Load Case 2, MAXLAG = 512, N = 29696	137
8.15	NAH and NAW Accelerometer Cross-Correlation Load Case 2, MAXLAG = 512 (pos. side), N = 29696	138
8.16	NAH Accelerometer Autospectrum Load Case 2, NLAG = 80	139
8.17	NAW Accelerometer Autospectrum Load Case 2, NLAG = 80	140
8.18	NAH and NAW Accelerometer Magnitude Cross-Spectrum - Load Case 2, NLAG = 80	142
8.19	NAH and NAW Accelerometer Phase Estimates Load Case 2, NLAG = 80	143
8.20	NAH and NAW Accelerometer Coherence Estimates Load Case 2, NLAG = 80	144
8.21	NAH and NAP Accelerometer Transfer Function Estimates - Load Case 2, NLAG = 80	145

8.22	NAH and NAW Accelerometer Transfer Function Estimates - Load Case 2, NLAG = 80	146
8.23	NAH and NAB Accelerometer Transfer Function Estimates - Load Case 2, NLAG = 80	147
8.24	Finite Element Model of Offshore Caisson Platform (After Cook, 1981)	150
8.25	Comparison of Calculated Mode Shapes Using MEM Spectral Analysis and Finite Element Methods Load Case 2	151
8.26	EAW Accelerometer Time History Load Case 1	153
8.27	EAW Accelerometer Autocorrelation Load Case 1, MAXLAG = 512, N = 29696	154
8.28	EAW and EAT Accelerometer Cross-Correlation Load Case 1, MAXLAG = 512 (pos. side), N = 29696	155
8.29	EAW Accelerometer Autospectrum Load Case 1, NLAG = 60	156
8.30	EAW and EAT Accelerometer Magnitude Cross-Spectrum - Load Case 1, NLAG = 60	157
8.31	EAW and EAT Accelerometer Phase Estimates Load Case 1, NLAG = 60	158
8.32	EAW and EAT Accelerometer Coherence Estimates Load Case 1, NLAG = 60	159
8.33	EAW and EAT Accelerometer Transfer Function Estimates - Load Case 1, NLAG = 60	160
8.34	Tape Recorder Noise Autocorrelation MAXLAG = 512, N = 25600	162
8.35	Tape Recorder Noise Autospectrum NLAG = 80	164

LIST OF TABLES

6.1	Summary of Load Cases	85
6.2	Summary of Environmental Conditions	85
8.1	Summary of Cross-Spectral Estimates First Three Flexural Modes	148
8.2	Comparison of Calculated Natural Frequency Estimates	148

LIST OF SYMBOLS

A	Dummy input matrix used in solving Kronecker product sum.
A(f)	Fourier transform of AR filter coefficients, A(m). Transfer function of linear shaping filter.
A(m)	Autoregressive filter coefficients.
{A}	Column vector of prediction error filter coefficients.
AA	Intermediate pxp matrix used in Lyupanov equation recursion for forward reflection coefficients.
AB	Kronecker product sum used in solving for forward reflection coefficients.
AIC	Akaike's Theoretic Information Criteria model order criterion.
AR	Autoregressive filter.
ARMA	Autoregressive, Moving Average filter.
B	Dummy auto-power matrix used in forward and backward power recursion. Dummy input matrix used in solving Kronecker product sum.
BB	Intermediate pxp matrix used in Lyupanov equation recursion for forward reflection coefficients, CN.
Be	Resolution bandwidth, Hz.
Br	Half-power bandwidth, width between half-power points located 3 dB down on either side of spectral peak.
BRGMEM	Multichannel MEM spectral analysis computer program based on Burg (direct) method.
BT	Backward prediction error or residual.
BTM	Blackman-Tukey Method of spectral analysis.
BTSPEC	Blackman-Tukey multichannel computer program.
BZERO	Computer program to make a time series zero mean.
CB	Backward filter coefficient.
CC	Intermediate pxp matrix used in Lyupanov equation recursion for forward reflection coefficient.
CF	Forward filter coefficient.
CN	Forward reflection coefficient.
CNP	Backward reflection coefficient.
Cxy(f)	Single-Sided Coincident Spectral Density Function estimate.
D	Diagonal matrix used in computer program RYWMEM to calculate forward filter coefficient.
d(n)	Desired or true signal.
E	Dummy auto-power matrix used in forward and backward power recursion.
e(n)	Error or residual between actual and desired signal.
ET	Forward prediction error or residual.
E[]	Expectation operator for random process.

f	Cyclical frequency, Hz.
fn	Natural frequency, Hz.
fny	Nyquist or cutoff frequency, Hz.
fs	Sampling frequency, Hz.
Δf	Frequency spacing between each spectral line.
FFT	Fast Fourier Transform.
FPE	Akaike's Final Prediction Error model order criterion.
G	Dummy cross-power matrix used in forward and backward power recursion.
Gmm	Autospectral estimate of input noise, $m(t)$.
Gnn	Autospectral estimate of output noise, $n(t)$.
Guu	True input autospectrum of signal $u(t)$.
Guv	True input/output cross-spectrum of signals $u(t)$ and $v(t)$.
Gvv	True output autospectrum of $v(t)$.
Gxx(f)	Single-sided autospectral density function for channel x.
Gxy(f)	Measured input autospectral estimate. Single-sided cross-spectral density function for channels x and y.
Gxy(f)	Measured input/output cross-spectral estimate. Magnitude of cross-spectral density function, MAG.
Gyy(f)	Single-sided autospectral density function for channel y. Measured output autospectral estimate.
H(f)	Transfer or frequency response function. Fourier transform of impulse response $h(\tau)$.
H(f)	System gain factor or magnitude of $H(f)$, TRANS. True transfer function magnitude.
$h(\tau)$	Unit impulse response function.
Ha	Transfer function estimate using autospectra analysis.
Hc	Transfer function estimate using cross-spectral analysis.
Hs	Significant wave height, ft.
I	Identity matrix.
Im[]	Imaginary part of [].
j	SQRT[-1] (ie. i)
K	Number of segments, NSEG, where $K * M = N$.
k	Reflection coefficient, γ .
L	Desired number of lags of filter, filter length or model order of filter, NLAG.
LWR	Levinson-Wiener-Robinson recursion.
M	Maximum number lags or data points in a segment, MAXLAG. Dummy variable for current order of filter,

	less than or equal to filter length L.
m	Current order of filter.
m(t)	Input noise.
MA	Moving Average filter.
MEM	Maximum Entropy Method of spectral analysis.
MLM	Maximum Likelihood Method of spectral analysis.
N	Total number of data points in sample realization, DATPTS.
	Length of each segment or block, MAXLAG.
n(t)	Output noise.
NL	Number of spectral lines used to determine frequency spacing for discrete FFT, NLINES.
P	Forward power matrix.
P(L)	Error power or mean square error of order L.
p	Number of time series or components, p=2 for two channel case.
PE	Prediction error.
PP	Backward power matrix.
Qxy(f)	Single-sided Quadrature Spectral Density Function, QUAD.
R	Single channel correlation matrix.
[R]	Multichannel correlation matrix.
{r}	Column vector of autocorrelation coefficient.
RB	Backward correlation matrix, Toeplitz, square block submatrices.
RF	Forward correlation matrix, Toeplitz, square block submatrices.
Rxx(τ)	Autocorrelation function estimate for channel x, equivalent to autocovariance for zero mean random process.
Rxy(τ)	Cross-correlation function estimate for channels x and y, equivalent to cross-covariance for zero mean random process.
Ryy(τ)	Autocorrelation function estimate for channel y, equivalent to autocovariance for zero mean random process.
RYWMEM	Multichannel MEM spectral analysis computer program based on Yule Walker method of correlation extension and Rissanen algorithm.
Re[]	Real part of [].
S(M)	Prediction error matrix of order M.
SCALE	Computer program to scale a time series.
SCRIBE	Computer program to convert time history data to TSL language.
Sw(f)	White noise variance or prediction error.
Sxx	Two-sided autospectral density function for channel x.
Sxy	Two-sided cross-spectral density function for channels x and y.

S _{yy}	Two-sided autospectral density function for channel y.
T	Total length of data record, seconds, where $T=N/f_s$.
t	Dummy time variable.
TRANSL	Computer program translates TSL coded data to Fortran binary code.
U	Normalizing factor for window function, insures periodogram spectral estimate is asymptotically unbiased.
u(t)	True input signal.
V	Forward power matrix.
VP	Backward power matrix.
v(t)	True output signal.
W(f)	Fourier transform of w(n).
W(m)	Window function.
W(n)	White noise, prediction error between true and predicted value.
W _m	Weight matrix to insure positive-definiteness of forward and backward power matrices.
X(f)	Fourier transform of input signal x(t).
x(n)	Output of AR filter, true or desired value.
x(t)	Measured input signal. Channel x time history, stationary, zero mean, random process.
x _i (n)	Time series for channel i, where $i = 1, 2, \dots, p$.
x, y, z	Orthogonal set of displacement coordinates.
Y(f)	Fourier transform of response signal y(t).
y(n)	Actual or predicted signal.
y(t)	Measured output signal. Channel y time history, stationary, zero mean, random process.
z	Z to Fourier transform equivalence, $Z = \exp(-j2\pi f\Delta)$.
ZT	Z transform.
γ	Reflection coefficient, k.
γ ² _{xy} (f)	Coherence squared for channels x and y, COHSQ.
Δ	Sampling interval, seconds.
δ	Kronecker delta function, unit sample function.
ε _r	Normalized error, measure of variance of spectral estimate.
σ	Standard deviation.
σ ² (m)	Variance or Prediction error of order m.
ζ	Damping ratio.
∠x _y (f)	Absolute value of phase of G _{xy} (f), PHASE.
τ	Time delay, seconds.
∠(f)	Absolute value of phase of H _{xy} (f), PHASE.
ω	Circular frequency, rad/sec.

\otimes Kronecker (tensor) product.

$[\]^*$ Complex conjugate operator.
 $[\hat{\]}$ Estimate of $[\]$.

$[\]^T$ Matrix transpose operator

INTRODUCTION

As the petroleum industry moves into deeper and deeper waters to tap new reserves of oil and gas, the cost and size of the offshore structures increases considerably. Substantial interest has been generated in methods of detecting structural damage by measuring shifts in natural frequencies from undamaged conditions. Coppolino and Rubin [1980], Loland and Dodds [1976], Ruhl [1976, 1979] and Vandiver [1977, 1979] are but a few of the many papers that have come out in recent years on this subject. Lack of reproducibility in determination of the natural frequencies of modes higher than the fundamentals has led researchers to conclude that detection of damage by above-waterline measurement of acceleration response to environmental loads is not feasible. The fundamental problem is that non-failure related sources of change are so large as to obscure changes in natural frequency which are caused by significant levels of damage.

These problems have led researchers to consider alternate measurement techniques, including (1) below-waterline measurement of global and local modes and (2) forced excitation with shakers and impulse hammers. Rather than simple measurement of changes in natural frequencies, determination of mode shapes and transfer functions are being attempted. The success of these various

techniques will depend in part upon the development of powerful digital signal processing tools.

Design verification is another aspect of structural dynamics which can also benefit from advances in signal processing. For the design of safe fatigue-resistant structures in ever more hostile environments, it is necessary to verify by accurate measurement the adequacy of present design methods and assumptions. Predicted and measured values of natural frequencies, damping ratios, and mode shapes are but a few of the values which should be compared. Where discrepancies occur, improvements can be made in future designs.

The multichannel Maximum Entropy Method (MEM) of spectral analysis is applied in this research to the problem of mode shape and transfer function estimation. A brief review of the development of MEM follows.

In 1967, Burg introduced the concept of the Maximum Entropy Method of auto-spectral analysis. MEM is one of the family of nonlinear, data-adaptive methods of spectral analysis which is capable of generating higher resolution spectral estimates from relatively shorter data records than conventional methods [Andersen, 1974; Lacoss, 1971]. This ability to use shorter data records can be an important consideration where (1) stationarity, (2) logistics of data collection, and/or (3) computer processing time and cost are a problem. Because MEM is data-adaptive, it does not suffer

from the severe "bias versus variance" tradeoff due to finite record length requirements of conventional methods. When calculating spectral estimates at one frequency, it is able to adjust itself to be least disturbed by power at neighboring frequencies.

Entropy is a measure of the average information content contained in a signal [Burg, 1967]. Maximizing entropy therefore maximizes the information transmitted in a signal. The concept involves finding a spectral estimate corresponding to the most random or unpredictable time series whose extended correlation function satisfies the constraint that it agrees with known values.

Researchers have successfully applied the MEM method to such diverse fields as (1) econometrics [Andersen, 1974], (2) geophysics [Chave, 1980; Robinson, 1967], (3) speech communications [Markhoul, 1975], (4) neurophysics [Gersch and Sharpe, 1973; Jones, 1974], and (5) radar [Childers, 1978] among others. Campbell [1980] applied the single channel version of MEM to the dual problem of natural frequency and damping ratio estimation of offshore platforms. He was able to more accurately evaluate these two parameters as well as place 95% confidence bounds on these estimates.

Two algorithms for the multichannel MEM method of spectral analysis are implemented to demonstrate its superiority relative to conventional methods. These two algorithms are (1) a direct on the data method of Burg and (2) a correlation function extension or Yule-Walker method both originally proposed by Strand [1977]. Henceforth, these two algorithms will be referred to as the BRGMEM and RYWMEM methods respectively.

Other versions of multichannel MEM algorithms are available and have been used. Ulrych and Jensen [1974] proposed a clever extension of the single channel MEM method to derive cross-spectral estimates. Ng [1977] demonstrated the superiority of another Burg-type algorithm, as extended by Jones [1978] and Nuttall [1976], to the processing of three real sets of geological data from core samples. Morf [1978] compared the BRGMEM method with those of Jones [1978] and Morf et al. [1978] and found the BRGMEM algorithm to give as good or better resolution as these other two while generating a stable spectral estimate.

In addition to the magnitude, phase, and coherence squared estimates normally obtained using multichannel spectral analysis methods, the transfer function estimate is calculated. Auto-spectral methods give transfer function estimates with no phase information. Multichannel or cross-spectral analysis methods produce a transfer function estimate that is less biased due to noise in either the

input or output signals.

The motivation for the research contained in this thesis is to apply multichannel versions of MEM to the problems of mode shape identification and transfer function estimation in the hope that both structural monitoring and design verification technologies may benefit. Descriptions of the main sections or chapters of this thesis are given below.

In Chapter 2, a general overview of conventional methods of spectral analysis is presented. A brief history of the direct and correlation classes (Periodogram and Blackman-Tukey respectively) is given. The classical "bias versus variance" tradeoff and the methods employed to ameliorate this problem including windowing, segmenting, and zero appendage are then discussed. Finally, a discussion of the Periodogram and Blackman-Tukey methods (BTM) is presented.

Chapter 3 contains the development of the single channel and multichannel MEM methods of spectral analysis. The two different interpretations of MEM as an autoregressive (AR) and a least squares model are presented and compared. For the multichannel MEM, both the direct Burg (BRGMEM) and the correlation function extension (RYWMEM) algorithm are derived. A discussion of the model order selection criteria is then given.

In Chapter 4, a discussion of the transfer function as an unbiased estimate, when calculated from a cross-spectral analysis, is presented.

Chapter 5 presents the formulas used in cross-spectral analysis to estimate auto and cross-correlations; auto-spectra; and cross-spectral magnitude and phase, coherence squared, and transfer functions. A discussion of the interpretations of these estimates, in the context of the applications described above, is then given.

Data for an empirical analysis of the multichannel BTM and MEM algorithms was collected from an offshore, single caisson platform located in 89 ft of water in the Gulf of Mexico. Chapter 6 contains a description of this platform which telescopes from a 7 ft diameter at the mudline to 4 ft at the MLW (Mean Low Water). It is 265 ft in length overall, extending 100 ft into the mudline, and supports three decks. This platform is an ideal structure for estimating cross-spectral magnitude, phase, coherence squared, and transfer functions because of (1) the symmetry of the single, vertical caisson, (2) the lack of interference from neighboring legs, and (3) the absence of drilling activity and large unaccountable deck loads. In this chapter, a description of the instrumentation, load cases, test set-up, and data processing is given.

Chapter 7 contains a comparison of the multichannel BTM and the BRGMEM and RYWMEM algorithms. The effect of different windows (Boxcar, Bartlett, Hanning, and Parzen are available) and different window durations (ie. lengths) on the BTM are presented. Due to the large amount of computer storage and processing cost required for the BRGMEM algorithm, a segment and averaging technique similar to that used in Periodogram estimates was developed. If the individual segments are long relative to the effective correlation length, they may be assumed to be statistically independent [Baggeroer, 1979]. Each of the segments is assumed to be a realization of a stationary, Gaussian random process. The variance of the estimate is reduced by this averaging technique while the bias is only slightly increased. Thus, the method can give satisfactory results at a substantial reduction in computer costs.

As mentioned previously, the primary emphasis of this research is in the application of multichannel MEM spectral estimates, especially the transfer function, to mode shape identification. Also, the transfer function estimate is used to calculate the dynamic response of the offshore caisson platform to wave excitation. These applications of multichannel spectral analysis are presented and discussed in Chapter 8.

Finally, in Chapter 9, conclusions and recommendations for future research are presented.

CHAPTER 2
CONVENTIONAL METHODS OF SPECTRAL ANALYSIS

The first spectral estimator to be used was the periodogram. The periodogram and its variations are any of the methods which operate directly on the data by Fourier transforming to obtain the spectral estimates. Even though it is still used today, it is not a good estimator because its variance exceeds its mean value. In 1958 Blackman and Tukey introduced their autocorrelative method which involves the Fourier transform of the windowed autocorrelation function estimate. It is a moving average (MA) or all zero method which suffers from a severe "bias versus variance" tradeoff. Resolution is lost due to (1) the finite record length of the autocorrelation function estimate (assumed zero beyond known lag products) and (2) the windowing operation itself. In 1965 Cooley and Tukey sparked a revival of the Fast Fourier Transform (FFT) which had been known for many years but was not practical until the advent of the high speed digital computer. The direct method of calculating spectral estimates involving magnitude squaring of the transform of windowed data records became popular. Unfortunately, this method unreasonably assumes that the data is zero outside the selected number of lags and repeats itself periodically. Thus, the conventional methods of spectral estimation can be grouped into two broad classes: (1) those obtaining the spectral estimate by direct

manipulation of the data record and (2) those indirectly calculating the autocorrelation function estimate from the data and then Fourier transforming to the spectral estimate. Before discussing these two methods, the "bias versus variance" tradeoff with which both of these methods suffer will be discussed.

2.1 BIAS VERSUS VARIANCE TRADEOFF

First of all, some definitions are in order concerning resolution, bias, variance, and stability. Resolution means being able to discern two peaks rather than one if two closely spaced peaks are actually present. Bias is the difference between the actual (ie. true value) and the estimated value. Variance of the estimate means being able to place some confidence in the value calculated for the estimate. An estimator is said to have high stability if it has small variance. Bias, resolution, and fidelity are different ways of expressing the same concept. Likewise, so are variance and stability. We want small bias, which is the same as saying we want the resolution to be as fine as possible. Similarly, we want the variance to be as small as possible, which implies that the statistical stability of the spectral estimate is as large as possible.

According to Bendat and Piersol [1971], a measure of the resolution known as the resolution bandwidth, B_e , is given by

$$B_e = f_s / N \quad (2.1a)$$

$$B_e = SBW * f_s / L \quad (2.1b)$$

where,

- f_s : sampling frequency, Hz
- N : total number of data points in a segment, or the entire data record
- SBW : Standardized Bandwidth, function of window chosen
- L : number of lags selected

Equation 2.1a is for use with the direct on the data methods such as periodograms. Equation 2.1b is for use with the Blackman-Tukey correlation method using various windows. The resolution bandwidth is not to be confused with the frequency interval f used for calculating the spectral estimates at discrete frequencies. It is given by

$$\Delta f = f_{ny} / N_1 \quad (2.2)$$

where,

- f_{ny} = Nyquist frequency, Hz
- N_1 = number of spectral lines or frequencies

A finer Δf , although providing more points within a frequency interval, will not necessarily result in a more accurate spectral estimate. Only a decrease in the resolution bandwidth can do this.

The variance, as expressed by the normalized standard error, ϵ_r , is

$$\epsilon_r = \sqrt{L / N} \quad (2.3)$$

Thus, the "bias versus variance" requirements are conflicting: a classic tradeoff is required.

Three methods are used to alleviate this apparent contradiction. These are (1) windowing, (2) segmenting, and (3) zero appendage. Each will now be discussed.

2.1.1 Windows

Windows are necessary to reduce bias and variance and to account for the fact that a finite realization of an infinite random process is used rather than a finite time series.

Multiplication in the time domain with the lag window is equivalent to convolution in the frequency domain with the spectral window [Bloomfield, 1976; Rabiner and Gold, 1975]. Thus, the time domain lag window and the frequency domain spectral window are Fourier transform pairs. It is the particular nature of the Fourier transform that a narrow window in one domain will be wide in the other domain.

Two-sided windows, as illustrated by Figure 2.1, obey the following properties in the time domain.

$$\begin{aligned}
 w(0) &= 1 \\
 w(m) &= w(-m) & -L < m < L & \quad (2.4) \\
 w(m) &= 0 & |m| > L &
 \end{aligned}$$

The optimum window is the one which exactly reproduces the true spectrum while giving the minimum variance. In the frequency domain, convolution with a delta (Dirac or Kronecker delta) exactly reproduces a signal. However, to

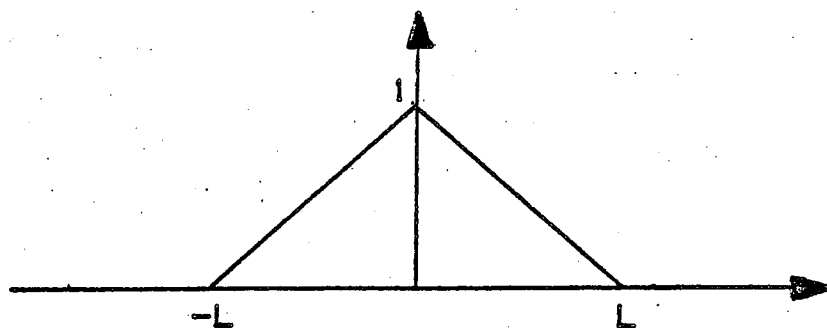


FIG. NO. 2.1: BARTLETT OR TRIANGULAR LAG WINDOW

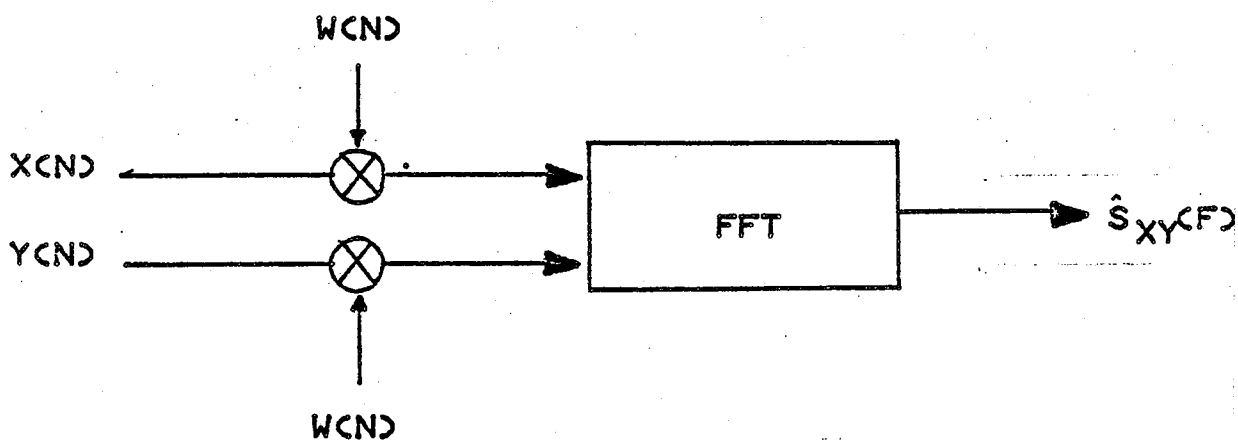


FIG. NO. 2.2: PERIODOGRAM SPECTRAL ESTIMATE

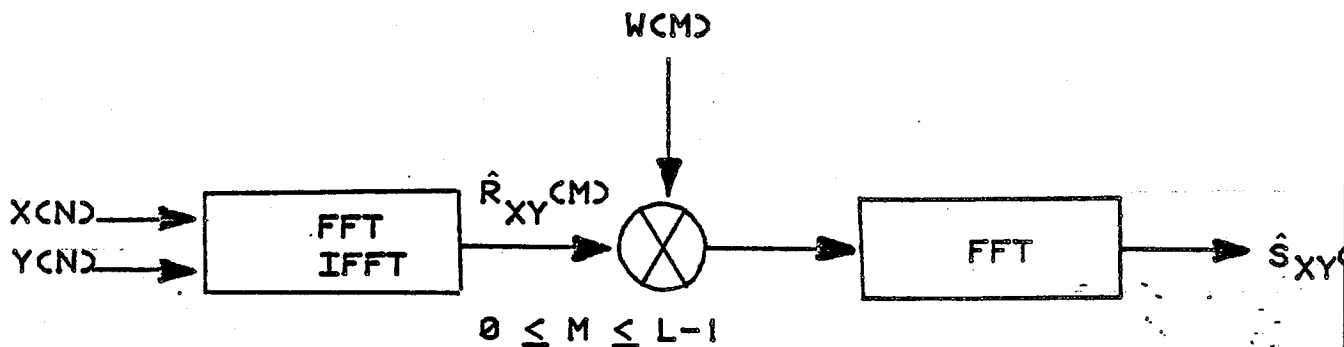


FIG. NO. 2.3: BLACKMAN-TUKEY SPECTRAL ESTIMATE

obtain minimum variance, the widest possible window is required. Thus, the classical "bias versus variance" tradeoff again. The rectangular window is the ideal window from the standpoint of minimizing the bias (ie. maximizing the resolution) as it has the narrowest main lobe. However, it also has the largest side lobes, which result in leakage of power from neighboring frequencies, thus masking the true nature of the spectrum. In addition, negative values of the spectral estimate are possible due to negative values of the spectral window resulting from the abrupt transition of the rectangular window at its bounds.

Analogous to wanting a large signal to noise ratio (SNR) to minimize the background noise effects in a signal, the sidelobes should be as small as possible relative to the main lobe. We also want the sidelobes to be positive. Smoothing the window in the time domain achieves these characteristics. The more smoothing, the better the variance and sidelobe characteristics of a window become. However, the main lobe increases correspondingly in width; thus, increasing the bias of the estimate. Finally, we want the window bandwidth to be narrower than the minimum frequency separation between the closest spaced peaks of interest in the theoretical spectrum. Otherwise, the loss of resolution could result in smearing of the power in the two adjacent peaks into only one peak.

In order to find this optimum window, many have been proposed. They include (among others) from best to worst bias:

- 1) Rectangular or Boxcar (same as no window),
- 2) Triangular or Bartlett,
- 3) Hanning, Tukey, or Raised Cosine, and
- 4) Parzen.

Each has the property that it is the convolution in the time domain with the Rectangular window and the window immediately above it in the hierarchy [Bracewell, 1978]. Of these four windows, the Hanning is ususally considered to have the best combination of properties [Jenkins and Watts; 1968; Bendat and Piersol, 1971]. The Bartlett window is often used for comparison purposes with other spectral methods. Thus, the shape as well as the duration of a window effects the outcome of a spectral estimate. More information and description of the properties of these windows and their particular shapes in the time and frequency domain can be found in references such as Bendat and Piersol [1971], Blackman and Tukey [1958], Bloomfield [1976], Jenkins and Watts [1968], Otnes and Enochson [1972], Robinson [1978], etc.

2.1.2 Data Record Segmenting

Segmental averaging involves decimating a data record of length N into K segments of length M to decrease the

variance of the spectral estimate. The assumption is made that the individual data segments are independent or uncorrelated. According to Jenkins and Watts [1968], the variance of the spectral estimate can be made as small as necessary by smoothing or averaging over shorter and shorter sub-series (ie. more segments). In the process, the bias of the estimate is increased since the data segments are shorter than the original complete data record of length N (see Eq. 2.1b). The increase in bias can be interpreted as an increase in the width of the main lobe of the segmented spectral window since the lag window is correspondingly shorter in the time domain.

2.1.3 Zero Appendage

Windowing of the correlation function estimate to make it physically realizable (ie. finite vs. infinite length), truncates it resulting in reduced resolution. By adding zeros to this windowed correlation estimate prior to Fourier transforming, the number of spectral lines or points obtained in the spectral estimate is increased. This has the effect of appearing to increase the resolution. In actuality, only the number of spectral points within a frequency band is increased with some potential for improvement in the accuracy of the estimate (see Section 2.1).

Filling of the data record with additional zeros (for spectral estimation applications) in order to inhibit the

effects of circular convolution when performing FFT's is usually not warranted in terms of the added computational costs (especially when using stochastic data).

2.2 SPECTRAL ESTIMATES

The theoretical definition of the power spectrum, $S(f)$, given by Crandall [1973] is the Fourier transform of the correlation function, $R(\tau)$,

$$S(f) = \int_{-\infty}^{\infty} R(\tau) \exp[-j2\pi f\tau] d\tau \quad (2.5)$$

If the correlation function is obtained from a sample function of an ergodic random process $x(t)$

$$R(\tau) = \lim_{T \rightarrow \infty} (1/T) \int_{-T/2}^{T/2} x(t) x(t + \tau) d\tau \quad (2.6)$$

In reality, however, we are not given an infinite time series nor are we allowed to sum the autocorrelation over infinite positive and negative lags. Instead, the spectral estimate is obtained by the discrete Fourier transform [Oppenheim and Schaffer, 1975] given by

$$S(m) = \Delta \sum_{n=0}^{L-1} R(n) w(n) \exp[-j2\pi fm\Delta] \quad (2.7)$$

Thus, both the time series and the correlation function estimate are finite and assumed to be zero beyond a certain limit.

2.3 DIRECT METHODS OF SPECTRAL ANALYSIS

Four different direct methods are used. All are

variations of the periodogram [Childers, 1978; Jones, 1965; Rabiner and Gold, 1975]. They are:

- (1) Periodogram,
- (2) Smooth the periodogram,
- (3) Segment and average the periodogram, and
- (4) Segment, window, and average the periodogram.

The periodogram spectral estimate, $S(f)$, involves a magnitude squaring of the Fourier transform of the data record. The data may or may not be windowed (see Figure 2.2). It is given by

$$S(2\pi f) = (1/NU) \left| \sum_{n=0}^{N-1} x(n) w(n) \exp[-j2\pi fn] \right|^2 \quad (2.8)$$

where U is a normalizing factor for the window function to assure that the spectral estimate is asymptotically unbiased. It is often assumed to be unity and is defined as

$$U = (1/N) \sum_{n=0}^{N-1} w^2(n) \quad (2.9)$$

Smoothing the periodogram consists of averaging adjacent periodogram spectral estimates with even or uneven weighting (ie. a form of windowing).

The third variation on the periodogram is due to Bartlett and involves segmenting the data into overlapping or non-overlapping (juxtaposed) segments to reduce the variance of the estimate. Overlapping results in reduced variance and less wastage of the available data. Instead of

using the original total record length, N , the shorter segmented record length of M is used and the estimates are averaged over the K segments to obtain the final spectral estimates.

The final method is identical to the Bartlett method except that the windowing of each of the segments is performed prior to calculating the periodogram. This method is attributable to Welch and is often called the "modified periodogram." Again, the segments may be overlapped or non-overlapped with the corresponding reduction in variance.

2.4 CORRELATION METHODS OF SPECTRAL ANALYSIS

Again, four variations of the basic Blackman-Tukey correlation method of spectral analysis are available [Childers, 1978]. They are:

- (1) No window on correlation function estimates obtained using entire record length,
- (2) Window correlation function estimates obtained using entire record length,
- (3) No window on correlation function estimates obtained by segmenting the data record, and
- (4) Window correlation function estimates obtained by segmenting the data record.

The differences among these four variations of the correlation methods are (1) whether the correlation function estimates are calculated using the entire data record of length N or a segmented version of K segments of length M (see Section 2.1.2); and (2) whether a window is used on

these correlation function estimates prior to Fourier transforming to the spectral estimates. Figure 2.3 illustrates the basic operations involved. The correlation function estimates are calculated from the data (entire record or segments) by Fourier transforming and then inverse Fourier transforming. Next, a window can be applied to these estimates as desired to obtain the spectral estimates. Figure 2.3 is sufficiently general to represent all four versions as a Boxcar window, which is equivalent to no window, could be used.

A biased cross-correlation function estimate at discrete lags, $R(m)$, is given by

$$R_{xy}(m) = (1/N) \sum_{n=0}^{N-m-1} x(n) y(n+m) \quad 0 \leq m \leq L-1 \quad (2.10a)$$

$$R_{yx}(m) = (1/N) \sum_{n=0}^{N-m-1} y(n) x(n+m) \quad 0 \leq m \leq L-1 \quad (2.10b)$$

where m is the current number of lags. Strictly speaking, a covariance function estimate, rather than a correlation function estimate, is obtained if a zero mean process is used in Eq. 2.10. However, for simplicity, we will continue to call $R(m)$ the correlation function estimate. The maximum lag value L of the correlation function is usually chosen to be of the order of 10% or less of the total number of data points N in the record. This is done to avoid aliasing effects of the circular convolution when the FFT is used to compute Eq. 2.10 [Oppenheim and Schaffer, 1975]. It also reduces the bias somewhat.

A biased correlation function estimate is calculated to insure positive definiteness of the spectral estimate (ie. no negative values). An unbiased estimate could be obtained by replacing the division by N with division by $(N - m)$ in Eq. 2.10. An unbiased estimate has smaller mean square error but will not necessarily guarantee a positive-definite spectral estimate.

The corresponding power spectral estimate, $S(f)$, is calculated by performing a Fourier transform of the windowed or unwindowed correlation function estimate (see Figure 2.3)

$$S_{xy}(n) = \Delta \sum_{m=0}^{L-1} R_{xy}(m) w(m) \exp[-j\pi mn/NL]$$

$$0 \leq n \leq NL-1 \quad (2.11)$$

Windowing is applied prior to Fourier transforming to reduce the undesirable effects of using a finite length correlation function instead of the theoretical infinite sequence [Rabiner and Gold, 1975]. The first variation (listed at the beginning of this section) is equivalent to using a Boxcar window or no window. The second variation would require the use of one of the windows described in Section 2.1.1.

The third and fourth variations involve segmenting of the original data record. The correlation function estimate is calculated for each segment, averaged, and then transformed. The fourth variation, involving windowing of the correlation function estimates from each segment prior

to transforming, is the particular Blackman-Tukey procedure used in this research as a comparison with the multichannel MEM algorithms. Note that whether the segments are averaged and transformed or transformed and averaged makes no difference in the spectral estimates obtained.

CHAPTER 3
MAXIMUM ENTROPY METHODS OF SPECTRAL ANALYSIS

In this chapter, the single and multichannel MEM methods of spectral analysis are developed. Both the direct on the data approach (BRGMEM) and the correlation extension method (RYWMEM) are explained. A discussion of the importance of the model order selection is then presented. In order to facilitate understanding of the Maximum Entropy concept, a discussion of MEM as a Autoregressive (AR) model is given.

3.1 AUTOREGRESSIVE MODEL

Perhaps the simplest model which can be used to understand the MEM method is the autoregressive or AR model proposed by Van den Bos [1971]. Figure 3.1 depicts a white noise with unit variance discrete signal $w(n)$ which is input into a linear or shaping filter $H(f)$. The corresponding output $x(n)$ (true or desired value) is given in the time domain by

$$x(n) = \sum_{m=1}^L A(m) x(n - m) + w(n) \quad n=1, L \quad (3.1)$$

where,

- $x(n)$: output of AR filter, true or desired value
- $A(m)$: AR filter coefficients of model order m
- L : desired AR filter order



FIG. NO. 3.1: LINEAR OR SHAPING FILTER

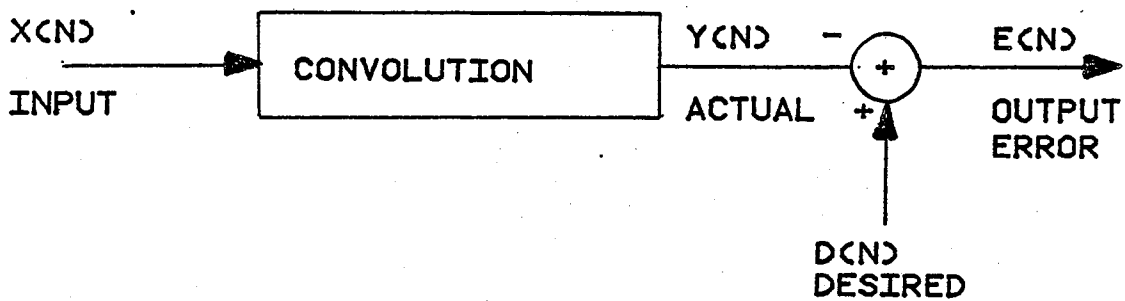


FIG. NO. 3.2: WIENER OR LEAST SQUARES FILTER

$w(n)$: white noise, innovation, or prediction error between true and predicted (actual) value

Note that the notation " $n=1, L$ " will be used to denote the operation $n = 1, 2, 3, \dots, L$ in the remainder of this thesis. The summation operation of the AR coefficients with the L past values of the output x represents a convolution operation which gives the predicted value.

Multiplying both sides of Eq. 3.1 by the z operator (ie. $z = \exp[-j2\pi f\Delta]$) and taking the corresponding z or Fourier transform, the frequency domain equivalent is

$$X(f) = \sum_{m=1}^L A(m) \exp[-j2\pi fm\Delta] X(f) + W(f) \quad (3.2)$$

Noting that the exponential term is the result of the delay property of Fourier transforms, we can rearrange Eq. 3.2 into the following standard frequency domain form:

$$X(f) = A(f) W(f) \quad (3.3)$$

where the transfer function of the shaping filter, $A(f)$, is given by

$$A(f) = \left\{ 1 - \sum_{m=1}^L A(m) \exp[-j2\pi fm\Delta] \right\}^{-1} \quad (3.4)$$

Finally, multiplying Eq. 3.3 by its complex conjugate and taking expectations, the two-sided spectral estimate for the autoregressive process between the Nyquist frequency, f_{ny} , is given by

$$S_x(f) = |A(f)|^2 S_w(f) \quad -f_{ny} < f < f_{ny} \quad (3.5)$$

$$= \frac{2 \sigma^2(L) \Delta}{\left| \left\{ 1 - \sum_{m=1}^L A(m) \exp[-j2\pi f m \Delta] \right\} \right|^2}$$

where $\sigma^2(L)$ or $S_w(f)/2\Delta$ is the white noise variance or prediction error and the denominator is the magnitude squared of the Fourier transform of the AR filter coefficients. The Δ is the time increment in seconds between sampled data points. Note that the one in the denominator of Eq. 3.5 is actually the $A(0)$ AR filter coefficient term.

Thus, the MEM filter can be cast into a form which most structural dynamicists are familiar with. The MEM spectral estimate is obtained by (1) calculating the AR filter coefficients out to the desired filter order L , (2) calculating the prediction error due to a white noise signal at filter order L , (3) taking the magnitude squared of the Fourier transform of the AR coefficients, and (4) performing the operations indicated in Eq. 3.5.

3.2 SINGLE CHANNEL MEM METHODS

With this understanding of the MEM as an AR model, the development of the single channel MEM method is presented. It is developed in terms of a least squares filter. The Levinson-Durbin recursive scheme which utilizes the special Toeplitz symmetry of the correlation matrix is also

discussed.

3.2.1 Least Squares Filter

The Wiener, prediction error, and whitening filter are all variations on the least squares filter. The main difference among them is the interpretation given to the error series between the desired and actual signals. Many authors including Baggeroer [1979], Haykin [1979], Kanasewich [1976], Robinson [1967], and Wiener [1977] have expounded on their characteristics. Basically, a mean square error term is minimized in such a way that the input signal is whitened (or the output becomes uncorrelated) as the filter order is increased.

In the time domain, the error series $e(n)$ is defined as the difference between the desired (or true) signal $d(n)$ and the actual (or predicted) signal $y(n)$ where

$$e(n) = d(n) - y(n) \quad n=1, L \quad (3.6)$$

In the classical Wiener filter, the actual output $y(n)$ is given by the convolution sum of L past values of input $x(n)$

$$y(n) = \sum_{m=1}^L A(m) x(n - m) \quad n=1, L \quad (3.7)$$

where L is the order or number of lags selected for the filter. Figure 3.2 illustrates how a given input signal $x(n)$ is converted into the desired output signal $e(n)$ such that $y(n)$ is the best approximation to the desired signal $d(n)$ in a mean square sense. The desired signal $d(n)$ is

chosen to be a unit sample function.

In a whitening filter, the desired signal $d(n)$ is chosen to be white noise and zero mean with unit variance such that the input is progressively "whitened" as the filter order is increased.

Finally, for the prediction error filter, the desired signal is chosen as the input signal $x(n)$ advanced one time unit ahead (hence, the prediction error terminology). The error series of Eq. 3.6 can equivalently be written as

$$\begin{aligned} e(n) &= d(n) - y(n) && n=1, L && (3.8) \\ &= x(n) - \sum_{m=1}^L A(m) x(n - m) \end{aligned}$$

Thus, $x(n)$ represents the desired or current value of the output and the convolution sum represents the actual or past values. The prediction error filter coefficients are given by the $A(m)$'s. Thus, the output $e(n)$ is made as completely random or unpredictable as possible (ie. made white or uncorrelated).

According to least squares theory, a mean square error or error power, $P(L)$, is defined as the expected value ($E[]$) of the square of the error signal $e(n)$

$$\begin{aligned} P(L) &= E[e^2(n)] && (3.9) \\ &= E[(x(n) - \sum_{m=1}^L A(m) x(n - m))^2] \end{aligned}$$

The energy contained in this error power is minimized by

requiring that the derivative with respect to each filter coefficient $A(n)$ satisfy

$$\partial P(L) / \partial A(n) = 0 \quad n=1, L \quad (3.10)$$

Expanding and solving Eq. 3.10 for the filter coefficients, $A(n)$, a set of L simultaneous equations known as the Yule-Walker equations are obtained

$$[R] \{A\} = \{r\} \quad (3.11)$$

or in matrix form:

$$\begin{bmatrix} R(0) & R(1) & R(2) \dots R(L-1) \\ R(1) & R(0) & R(1) \dots R(L-2) \\ R(2) & R(1) & R(0) \dots R(L-3) \\ \vdots & \vdots & \vdots & \vdots \\ R(L-1) & R(L-2) & R(L-3) \dots R(0) \end{bmatrix} \begin{Bmatrix} A(1) \\ A(2) \\ A(3) \\ \vdots \\ A(L) \end{Bmatrix} = \begin{Bmatrix} R(1) \\ R(2) \\ R(3) \\ \vdots \\ R(L) \end{Bmatrix}$$

where,

- $[R]$: $L \times L$ matrix of autocorrelation coefficients, 0 to $L-1$ lags
- $\{A\}$: $L \times 1$ column vector of prediction error filter coefficients
- $\{r\}$: $L \times 1$ column vector of autocorrelation coefficients, 0 to $L-1$ lags

A special Toeplitz symmetry of the correlation matrix can be exploited if a final equation known as the error or prediction error power equation is added to the Yule-Walker equations (Eq. 3.11). This error equation is

$$\begin{aligned} P(L) &= E[e^2(n)] & (3.12) \\ &= R(0) - \sum_{m=1}^L A(m) R(m) \end{aligned}$$

By rearranging the Yule-Walker equation and adding the error equation as the first row, the Normal or Wiener-Levinson equations are obtained. They are given by

$$\sum_{m=0}^L A(m) R(n - m) = P(L) \quad \begin{matrix} n=0 \\ n=1, L \end{matrix} \quad (3.13)$$

or in matrix form:

$$\begin{bmatrix} R(0) & R(1) & R(2) & \dots & R(L) \\ R(1) & R(0) & R(1) & \dots & R(L-1) \\ R(2) & R(1) & R(0) & \dots & R(L-2) \\ \vdots & \vdots & \vdots & \ddots & \vdots \\ R(L) & R(L-1) & R(L-2) & \dots & R(0) \end{bmatrix} \begin{pmatrix} 1 \\ -A(1) \\ -A(2) \\ \vdots \\ -A(L) \end{pmatrix} = \begin{pmatrix} P(L) \\ 0 \\ 0 \\ \vdots \\ 0 \end{pmatrix}$$

where the prediction error term $P(L)$ is equal to the variance $\sigma^2(L)$ and we now have $L+1$ simultaneous equations to solve. The Levinson-Durbin recursive algorithm is then used to solve for the prediction error filter coefficients $A(m)$. Note that these filter coefficients are the same as the autoregressive (AR) filter coefficients of Eq. 3.4 except for sign. The spectral estimate can then be calculated by Eq. 3.5.

3.2.2 Levinson-Durbin Recursion

The Levinson-Durbin recursion is an algorithm that takes advantage of the special Toeplitz symmetry of the Normal equations whereby all diagonals in the correlation matrix of Eq. 3.14 are the same. Therefore, a reduction of the order of L^2 multiplies and L storage locations are required as compared to L^3 multiplies and L^2 storage locations. The recursion algorithm utilizes linear superposition to update the filter coefficients to the next higher model order using an intermediate variable known as the reflection coefficients. The algorithm consists of the

following steps:

- (1) Determine updated filter coefficients from
 - (a) correlation matrix,
 - (b) past values of the filter coefficients, and
 - (c) past values of the prediction error;
- (2) Update prediction error for next filter order using
 - (a) past prediction error and
 - (b) past reflection coefficient; and
- (3) Return to step 1 to update filter coefficients until desired filter order is achieved.

These recursion equations have been presented in numerous publications including Campbell [1980], Claerbout [1976], and Haykins [1979] to name just a few.

3.3 MULTICHANNEL MEM METHODS

There are two basic methods of multichannel MEM which are developed in this thesis. They are (1) the direct on the data method of Burg (BRGMEM) and (2) the Yule-Walker or correlation extension method (RYWMEN).

3.3.1 Direct on the Data Method

There are three different algorithms which have been developed for the direct on the data or Burg method. They are:

- (1) Whittle, Jones, Nuttall Algorithm
[Jones, 1978; Nuttall, 1978],
- (2) Square Root Normalized Levinson-Wiener-Robinson
[Morf, 1978], and
- (3) Levinson-Wiener-Robinson (LWR) Algorithm
[Strand, 1977].

The Jones procedure was developed simultaneously and independently as that of Nuttall. It is based on the forward filter coefficients and does not necessarily give positive definite or stable spectral estimates. The analytical procedure used is to minimize the trace of the sum of weighted forward and backward error matrices by suitable choice of correlation coefficients.

The Morf algorithm utilizes square root normalized (averaging) of the forward and backward filter coefficients prior to calculating the spectral estimate matrix. According to Morf [1978], it gives about the same resolution as the Strand algorithm.

The Strand algorithm employs a least squares estimate of the reflection coefficients with inverse power weighting to guarantee a positive-definite covariance matrix and a resulting stable spectral estimate. Strand [1977] has demonstrated superior spectral resolution using this method while avoiding the problems inherent in the correlation extension method.

It consists of the following steps:

- (1) Input channel x and channel y time series and other input parameters;
- (2) Initialize the LWR recursion parameters: forward and backward errors and forward and backward powers;
- (3) Perform LWR Recursion for forward filter coefficients and prediction error by solving bilinear or Lyapunov equation;

- (4) Calculate optimum model order according to Akaike's FPE Model Order Criterion (see Section 3.4 for references); and
- (5) Calculate spectral matrix estimates using forward filter coefficients and prediction error.

A discussion of the Strand derivation of the filter coefficients, the spectral matrix, and the LWR recursion will now be presented.

3.3.1.1 Derivation of Filter Coefficients Matrix. Let $x(n)$ be a wide sense stationary, zero mean time series of p -channels (in our case, $p=2$).

$$\{x(n)\}^T = \{x_1(n) \ x_2(n) \ x_3(n) \dots x_p(n)\} \quad n=1, N \quad (3.14)$$

where $x_1(n)$ represents the N total data points in time series or channel 1, $x_2(n)$ the same for channel 2, etc. The T stands for the matrix transpose of a real matrix.

Analogous to the prediction error filter model for single channel time series, the forward and backward filter errors of length M (M less than or equal to L), E_T and B_T respectively, are

$$E_T(M, n) = x(n) + \sum_{m=1}^M CF(M, m)^T x(n - m) \quad n=1, M \quad (3.15a)$$

$$B_T(M, n) = x(n) + \sum_{m=1}^M CB(M, m)^T x(n + m) \quad n=1, M \quad (3.15b)$$

where the real forward and backward filter coefficient. $p \times p$ matrices, CF and CB , respectively are defined by

$$CF(M, m)^T = [I \ CF(M, 1)^T \ CF(M, 2)^T \dots CF(M, M)^T] \quad (3.16a)$$

$$CB(M,m)^T = [I \quad CB(M1)^T \quad CB(M2)^T \dots CB(MM)^T] \quad (3.16b)$$

where I is a $p \times p$ identity matrix, M is the current model order, and m is the coefficient number.

The expected mean-square values of ET and BT should be minimized in order to have the optimum filter. Therefore, applying this least squares criterion

$$E\{[ET(M,n)]^T [ET(M,n)]\} = \text{minimum} \quad (3.17a)$$

$$E\{[BT(M,n)]^T [BT(M,n)]\} = \text{minimum} \quad (3.17b)$$

As discussed in the single channel models, the result of carrying out Eq. 3.17 are the Normal equations for the forward and backward filter coefficients [Wiggins and Robinson, 1965]. They are defined by

$$[RF] \{CF(M,m)\} = \{V\} \quad (3.18a)$$

$$[RB] \{CB(M,m)\} = \{VP\} \quad (3.18b)$$

where,

[RF] : forward R-matrix, Toeplitz, square block submatrices

[RB] : backward R-matrix, Toeplitz, square block submatrices

$\{V\}^T$: forward power matrix, $[P(M) \ 0 \ 0 \ \dots \ 0]$

$\{VP\}^T$: backward power matrix, $[PP(M) \ 0 \ 0 \ \dots \ 0]$

The R_4 element or $p \times p$ submatrix for a lag of 4 for the two channel case ($p=2$) is

$$\{R_4\} = \begin{bmatrix} R_{11}(4) & R_{12}(4) \\ R_{21}(4) & R_{22}(4) \end{bmatrix} \quad (3.19)$$

where the diagonals are the autocorrelations and the

off-diagonals are the cross-correlations between channels 1 and 2.

The forward and backward prediction errors, $P(M)$ and $PP(M)$, respectively satisfy

$$\begin{aligned} P(M) &= E[ET(M,n) ET(M,n)^T] & (3.20a) \\ &= \{CF(M,m)\}^T [RF] \{CF(M,m)\} \end{aligned}$$

$$\begin{aligned} PP(M) &= E[BT(M,n) BT(M,n)^T] & (3.20b) \\ &= \{CB(M,m)\}^T [RB] \{CB(M,m)\} \end{aligned}$$

and are positive-definite if the R-matrices are.

3.3.1.2 Spectral Matrix Estimation. The single-sided, multichannel MEM spectral matrix for a positive-definite set of forward power (prediction error) matrices is a function of the Fourier transform of the forward filter coefficient matrix [Burg, 1975; Ioannidis, 1975; Jones, 1974].

$$G(f) = 2\Delta [CF^{-1}(1/z)]^* P(M) [CF^{-1}(1/z)] \quad (3.21)$$

where the forward filter coefficient matrix CF is defined as

$$CF(z) = I + CF(M1)z + CF(M2)z^2 + \dots + CF(MM)z^M \quad (3.22)$$

where $z = \exp[-j2\pi f\Delta]$. Since the forward power, P satisfies the condition that it is greater than zero, the filter coefficient matrices are nonsingular and invertible. Equation 3.21 reduces to Eq 3.5 for the single channel case if matrices are replaced by vectors and vectors by scalars.

The inverse matrix operations become divisions and the product of the filter coefficients with their complex conjugates gives the magnitude squared as before.

The backward filter coefficient matrix could equivalently be used to calculate the spectral matrix of Eq. 3.21. It would be given by

$$G(f) = 2\Delta [CB^{-1}(z)]^* PP(M) [CB^{-1}(z)] \quad (3.23)$$

where the backward filter coefficient matrix is defined by

$$CB(z) = I + CB(M1)z + CB(M2)z^2 + \dots + CB(MM)z^M \quad (3.24)$$

3.3.1.3 Multichannel LWR Recursion. The multichannel MEM algorithm presented here is known as the Levinson-Wiener-Robinson (LWR) recursion. Additional details on this procedure may be found in Strand [1977] and Ioannidis [1975].

Prior to the LWR recursive algorithm, the forward and backward filter coefficients, CF and CB are zeroed and initialized. The forward and backward powers, P and PP, are also initialized to the zero lag correlation product and equivalenced to each other.

$$P(0) = 1/N \sum_{m=1}^N x(m) x(m)^T \quad (3.25)$$

$$= PP(0)$$

where N is the total number of data points in the time series. Finally, the Akaike Final Prediction Error (FPE, see Section 3.4) value for order zero is calculated.

The master loop of the recursion consists of steps which can be broken down and summarized as follows:

(1) Forward Error ET. The forward error or residual ET is initialized.

$$ET(0,n) = x(n) \quad n=1, N-1 \quad (3.26)$$

(2) E, B, and G Matrices. The E, B, and G p x p matrices used in the recursion for the forward and backward powers are defined as

$$E = 1/W_m * \sum_{n=1}^{N-M} ET(M,n) ET(M,n)^T \quad (3.27a)$$

$$B = 1/W_m * \sum_{n=1}^{N-M} BT(M,n) BT(M,n)^T \quad (3.27b)$$

$$G = 1/W_m * \sum_{n=1}^{N-M} BT(M,n) ET(M,n)^T \quad (3.27c)$$

where W_m is a weight to insure positive-definiteness of the forward and backward power matrices, P and PP.

(3) Forward Reflection Coefficient CN. The forward reflection coefficient CN is calculated by solving a bilinear or Lyapunov equation given by

$$AA (CN) + CN (BB) = CC \quad (3.28)$$

where the p x p matrices AA, BB, and CC are defined as

$$AA = (PP(M))^{-1} * B \quad (3.29A)$$

$$BB = (P(M))^{-1} * E \quad (3.29B)$$

$$CC = -2 * (PP(M))^{-1} * G \quad (3.29C)$$

The method involves the calculation of the Kronecker Product sum AB [Bellman, 1960] given by

$$AB = A \otimes I + I \otimes B^T \quad (3.30)$$

where,

- I : Identity p x p matrix
- A : input p x p matrix
- B : input p x p matrix
- \otimes : Kronecker (tensor) product

(4) Backward Reflection Coefficient CNP. The backward reflection coefficient CNP is calculated based on the forward reflection coefficient CN as

$$CNP(M) = P(M-1)^{-1} (CN(M))^T PP(M-1) \quad (3.31)$$

(5) Forward and Backward Filter Coefficient CF and CB. The forward and backward filter coefficients, CF and CB, are updated by the recursive relationships using the forward and backward reflection coefficients CN and CNP.

$$CF(M,m) = CF(M-1,m) + CB(M-1,M-m) CN(M) \quad m=1, M-1 \quad (3.32a)$$

$$CB(M,m) = CB(M-1,m) + CF(M-1,M-m) CNP(M) \quad m=1, M-1 \quad (3.32b)$$

(6) Forward and Backward Errors ET and BT. The forward and backward errors (residuals) are updated using the forward and backward reflection coefficients CN and CNP.

$$ET(M+1,m) = ET(M,m+1) + (CN(M))^T BT(M,m+1) \quad m=1, Wm-1 \quad (3.33a)$$

$$BT(M+1,m) = BT(M,m) + (CNP(M))^T ET(M,m) \quad m=1, Wm-1 \quad (3.33b)$$

(7) Forward and Backward Powers P and PP. The "modern Levinson recursion" is then used to update the forward and backward powers, P and PP with the forward and backward reflection coefficients, CN and CNP.

$$P(M) = P(M-1) - (CN(M))^T PP(M-1) CN(M) \quad (3.34a)$$

$$PP(M) = PP(M-1) - (CNP(M))^T P(M-1) CNP(M) \quad (3.34b)$$

(8) Akaikes Final Prediction Error Criterion. Finally, the next value of the Akaike's FPE model order selection criterion is calculated. One loop of the recursion is now complete.

(9) Return. The model order is updated, if it is less than the model order L selected, and the recursion is repeated.

3.3.2 Correlation Method

The correlation, Yule-Walker, or R-method is a correlation extension method based on the Rissanen [1973] recursion. It involves the triangular decomposition of the R-matrix into a diagonal form from which psuedo-forward filter coefficients are calculated [Strand, 1977; Ulrych and Bishop, 1975]. Strand has noted superior resolution with the direct on the data approach relative to this

method. However, he notes that it has not been severely tested using a large number of lags. Ioannidis [1975] has used the method with much success however.

The basic procedure consists of:

- (1) Input correlation matrix and other input parameters,
- (2) Initialize Rissanen algorithm,
- (3) Perform Rissanen recursion,
- (4) Calculate FPE optimum model order, and
- (5) Calculate estimate of spectral matrix.

3.3.2.1 Rissanen Algorithm. The Rissanen algorithm is a recursive procedure for the simultaneous decomposition of the forward and backward correlation matrices, RF and RB , into the block diagonal forms

$$[B] \quad [RF] \quad [B]^* = \{D\} \quad (3.35a)$$

$$[BS] \quad [RB] \quad [BS]^* = \{DS\} \quad (3.35b)$$

where,

$$[B] = \begin{bmatrix} I & & & & \\ B(21) & I & & & \\ B(31) & B(32) & I & & \\ \vdots & \vdots & \vdots & \ddots & \\ \vdots & \vdots & \vdots & \vdots & \\ B(M+1,1) & B(M+1,2) & \dots & B(M+1,M) & I \end{bmatrix} \quad (3.36a)$$

$$[BS] = \begin{bmatrix} I & & & & \\ BS(21) & I & & & \\ BS(31) & BS(32) & I & & \\ \vdots & \vdots & \vdots & \ddots & \\ \vdots & \vdots & \vdots & \vdots & \\ BS(M+1,1) & BS(M+1,2) & \dots & BS(M+1,M) & I \end{bmatrix} \quad (3.36b)$$

$$\{D\} = [D(1) \quad D(2) \quad D(3) \quad \dots \quad D(M+1)] \quad (3.37a)$$

$$\{DS\} = [DS(1) DS(2) DS(3) \dots DS(M+1)] \quad (3.37b)$$

where the * denotes Hermetian conjugation and the D and DS matrices are block diagonal. Substituting Eqs. 3.36 and 3.37 into Eq. 3.35 and performing the Rissanen recursion gives

$$\sum_{m=0}^M B(M+1, m+1) RF(M-m) = D(M+1) \quad (3.38a)$$

$$\sum_{m=0}^M BS(M+1, m+1) RB(M-m) = DS(M+1) \quad (3.38b)$$

Taking the Hermetian conjugate of Eq. 3.38 and comparing with Eq. 3.18, the equivalence of BS and B to the forward and backward filter coefficients, CF and CB, is given by

$$CF(Mj) = [BS^*(M+1, M-j+1)] \quad j=1, M \quad (3.39a)$$

$$CB(Mj) = [B^*(M+1, M-j+1)] \quad j=1, M \quad (3.39b)$$

The corresponding forward and backward powers, P and PP, are given by

$$P(M) = DS(M+1) \quad M=0, \dots \quad (3.40A)$$

$$PP(M) = D(M+1) \quad M=0, \dots \quad (3.40B)$$

Only two rows of the B and BS matrices are required in storage at any one time. These correspond to the current row denoted by B and BS, and a previous or past row denoted by B1 and BS1. Therefore, the amount of computer storage required is minimized.

Thus, the forward filter coefficients are obtained by a triangular decomposition of the forward and backward correlation matrices into a form equivalent to the direct on the data method of Burg. The interested reader is referred to the papers by Strand [1977] and Rissanen [1973] for more details on this method.

3.4 MODEL ORDER SELECTION CRITERIA

The nonlinear methods of spectral analysis such as MEM are only as good as the number of lags selected for model order or filter length. As the filter length is increased beyond the optimum, the variance of the spectral estimate increases resulting in spurious detail. The model order selection criteria attempt to prevent this from happening by calculating the optimum number of lags or model order for the filter. These criteria are nothing more than "cost functions" [Campbell, 1980] which are evaluated up to the number of lags designated; then the optimum is selected as the value corresponding to the minimum. Thus, these criteria give the best mean square model order estimate which effects a compromise between high resolution and high variance. Several different model order selection criteria have been proposed.

It is generally felt that these criteria should only be used as guidelines. A bracketing technique, similar to the window closing technique of Jenkins and Watts [1968] for

conventional spectral analysis, should be used to determine real convergence. The problems inherent in these criteria are discussed by Akaike [1969], Gersch and Sharpe [1973], and Ulrych and Bishop [1975] among others.

The two most popular criteria are (1) Akaike's Final Prediction Error (FPE) mean square prediction error scheme and (2) Akaike's Information Theoretic Criterion (AIC). The formulas for these two criteria will be presented for both the single channel and multichannel MEM methods of spectral analysis.

3.4.1 Single Channel Criteria

The formulas for Akaike's FPE and AIC criteria for a zero mean process are

$$\text{FPE}(M) = \{ [N + (M+1)] / [N - (M+1)] \} * \sigma^2(M) \quad (3.41)$$

$$\text{AIC}(M) = N * \sigma^2(M) + 2M / N \quad (3.42)$$

where,

- M : particular order of the MEM filter,
- N : total number of data points in time series,
- $\sigma^2(m)$: prediction error for MEM filter of order M.

The log of the FPE model order asymptotically approaches the value calculated by the AIC formula. The maximum value chosen for the number of lags for the optimum filter is usually of the order of 3 times the square root of the total number of data points, N [Campbell,1980].

3.4.2 Multichannel Criteria

The basic difference between the single channel and multichannel versions of Akaike's FPE and AIC model order criteria is that the multichannel formulas deal with matrices rather than vectors. As the equations below illustrate, the determinant of the prediction error matrix is required. Also, note that the total number of channels or time series is used in the formulas.

$$\text{FPE}(M) = \frac{[N + (M_p + 1)]}{\det |S(M)|} \cdot [N - (M_p + 1)]^p \quad (3.43)$$

$$\text{AIC}(M) = N * \ln [S(M)] + 2p/(pM + 1) \quad (3.44)$$

where,

p : total number of time series or channels

$S(M)$: prediction error matrix of order M .

Additional description of these model order criteria can be found in Haykin [1978], Ioannidis [1975], Jones [1974], and Kanasewich [1976].

CHAPTER 4
TRANSFER FUNCTION ESTIMATION

In this chapter, a derivation and comparison of the transfer function (frequency response function) using auto and cross-spectral methods is presented. A discussion of the two types of estimation errors, bias and random errors, follows this.

4.1 AUTO AND CROSS-SPECTRAL DERIVATION

For an ideal, causal, stable, linear physical system as shown in by Figure 4.1; the system output, $y(t)$, is related to the input, $x(t)$, by the convolution or superposition integral

$$y(t) = \int_0^{\infty} h(\tau) x(t - \tau) d\tau \quad (4.1)$$

where $h(\tau)$ is the unit impulse response. The transfer function or frequency response function is related to the impulse response function by the Fourier transform

$$H(f) = \int_0^{\infty} h(\tau) \exp[-j2\pi f\tau] d\tau \quad (4.2)$$

The Fourier transform of the output is

$$Y(f) = \int_0^{\infty} y(t) \exp[-j2\pi ft] dt \quad (4.3)$$

Substituting Eq. 4.1 into Eq. 4.3 yields the following expression

$$Y(f) = H(f) X(f) \quad (4.4)$$

Two equations are obtained if we multiply Eq. 4.4 once with its complex conjugate and once with the complex conjugate of the input signal $x(t)$. They are

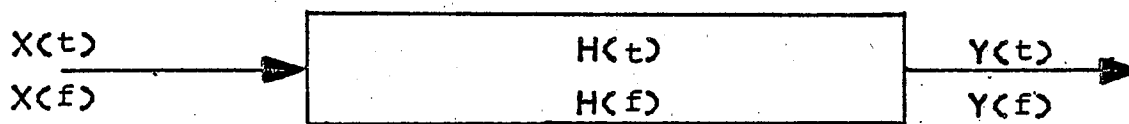


FIGURE NO. 4.1
TRANSFER FUNCTION OF A LINEAR, CAUSAL SYSTEM

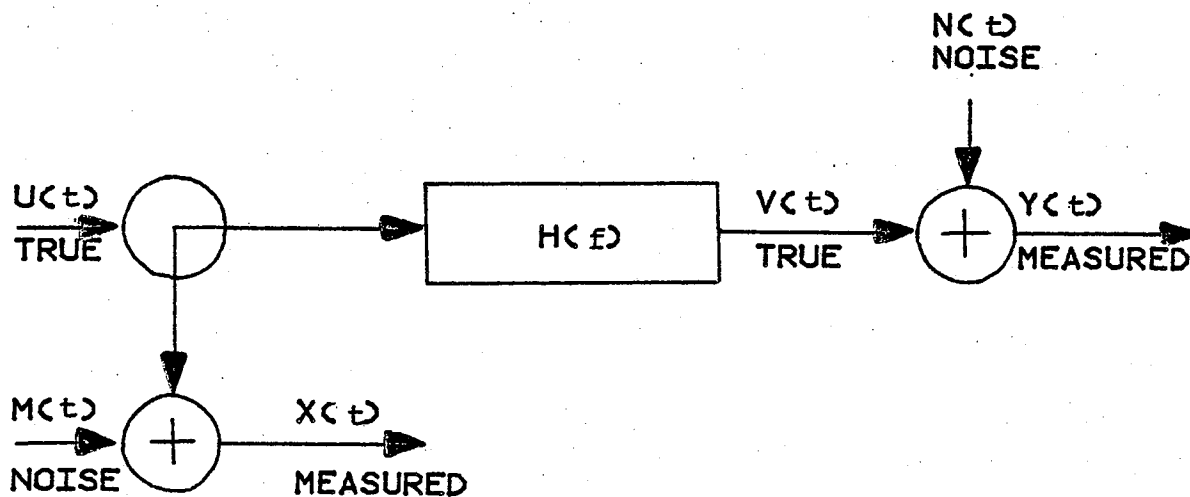


FIGURE NO. 4.2
EFFECT OF NOISE ON TRANSFER FUNCTION ESTIMATION

$$|Y(f)|^2 = |H(f)|^2 |X(f)|^2 \quad (4.5a)$$

$$X^*(f)Y(f) = H(f) |X(f)|^2 \quad (4.5b)$$

which when we take expectations and multiply by $2/T$ becomes the single-sided auto and cross-spectra in terms of the transfer function $H(f)$.

$$G_{yy}(f) = |H(f)|^2 G_{xx}(f) \quad (4.6a)$$

$$G_{xy}(f) = H(f) G_{xx}(f) \quad (4.6b)$$

Note that we have taken a simplistic and direct approach to derive these results. They could equally well have been computed by taking the Fourier transforms of the auto and cross-correlations, $R_{xx}(t)$ and $R_{xy}(t)$ respectively.

Equation 4.6a is the autospectral result; whereas, Eq. 4.6b is based on cross-spectral analysis. The advantages of cross-spectral analysis versus autospectral analysis for the transfer function estimate are (1) phase information can be obtained, and (2) the estimate is not as easily biased by noise in the input or output signal.

Consider a system [Bendat and Piersol, 1971] such as illustrated in Figure 4.2 where the input $x(t)$ and the output $y(t)$ measurements are related to the actual input $u(t)$ and output $v(t)$ signals through the noise terms $m(t)$ and $n(t)$ by

$$x(t) = u(t) + m(t) \quad (4.7a)$$

$$y(t) = v(t) + n(t) \quad (4.7b)$$

The noise terms are assumed to be uncorrelated with the

signals and with each other. Performing the manipulations as described in this section, true and measured single-sided auto and cross-spectral estimates are given by

$$G_{vv} = |H|^2 G_{uu} \quad (4.8a)$$

$$G_{uv} = H G_{uu} \quad (4.8b)$$

$$G_{xx} = G_{uu} + G_{mm} \geq G_{uu} \quad (4.9a)$$

$$G_{yy} = G_{vv} + G_{nn} \geq G_{vv} \quad (4.9b)$$

$$G_{xy} = G_{uv} \quad (4.9c)$$

where frequency dependence f has been omitted to simplify the notation. Substituting Eqs. 4.8 and 4.9 into Eq. 4.6 and rearranging, the following relationships for the transfer function estimates are obtained for the autospectral ($H_a(f)$) and cross-spectral ($H_c(f)$) derivations.

$$|H_a|^2 = \frac{G_{vv} + G_{nn}}{G_{uu} + G_{mm}} = |H|^2 \left[\frac{1 + G_{nn}/G_{vv}}{1 + G_{mm}/G_{uu}} \right] \quad (4.10a)$$

$$|H_c| = \frac{G_{uv}}{G_{uu} + G_{mm}} = |H| \left[\frac{1}{1 + G_{mm}/G_{uu}} \right] \quad (4.10b)$$

where,

$|H|$: true transfer function

$|H_a|$: autospectral derived transfer function

$|H_c|$: cross-spectral derived transfer function

Thus, regardless of the amount of input noise; if output noise is present, the autospectral derivation for the transfer function estimate will always give a biased estimate of the true transfer function. The cross-spectral derivation, however, will give an unbiased estimate of the true value when the input noise satisfies the inequality

$$G_{mm} \ll G_{uu} \quad (4.11)$$

regardless of the amount of output noise, G_{nn} . Therefore, the cross-spectral method of calculating the transfer function estimate is always superior to the estimate calculated using only autospectra whenever independent noise is present.

4.2 ESTIMATION ERRORS

Estimation errors are (1) bias errors due to resolution deficiencies and (2) random errors due to variance extremes.

4.2.1 Bias Errors

The bias errors are attributable to:

- (1) extraneous input noise,
- (2) resolution bias errors,
- (3) nonlinear system effects, and
- (4) correlation of unmeasured inputs with measured inputs.

Extraneous input noise will always cause the transfer function estimate to be underestimated unless the noise is (1) part of the excitation, (2) uncorrelated with the input of interest, and/or (3) actually passes through the system.

Resolution bias errors may be resolved by obtaining a narrow enough resolution bandwidth, B_e , to resolve closely spaced peaks and troughs.

If the system is nonlinear, then only a linear approximation of the transfer function can be obtained. The transfer function estimate is the best linear approximation in a least squares sense to the true value however.

4.2.2 Random Errors

Random errors are due to:

- (1) measurement or computational noise,
- (2) uncorrelated, unmeasured inputs that contribute to the output, and
- (3) system nonlinearities.

The same explanations as presented above for the bias errors apply here also. The interested reader can find additional information on transfer function estimation and error evaluation in Bendat and Piersol [1971, 1980].

CHAPTER 5 MULTICHANNEL SPECTRAL ANALYSIS

In this chapter, applications of multichannel spectral analysis are presented. The multichannel formulas and some discussion on their interpretation is then given.

5.1 APPLICATIONS TO OFFSHORE STRUCTURES

The primary emphasis of this research and thesis is in the application of multichannel spectral estimates, especially the transfer function, to mode shape identification. In addition, the transfer function estimate can be used where actual input data, such as wave heights, are measured. In this case, a transfer function estimate of the dynamic platform response to ocean wave excitation is available.

5.1.1 Mode Shape Identification

In mode shape analysis, the resonant frequencies of the structure are first identified and then the order and shape of the normal modes can be determined. The more transducers (accelerometers) used, the easier the task of identifying the modes, especially the higher modes. Usually, the number of accelerometers used determines the highest order mode which can be determined.

Normally, multichannel spectral analysis estimates include only autospectra and cross-spectral magnitude, phase, and coherence estimates. As discussed in Chapter 4, the cross-spectral transfer function estimate tends to be an unbiased estimate in comparison with autospectral derivations. Thus, the transfer function estimates obtained from multichannel spectral analysis are particularly useful in mode shape identification. They can be used to give relative displacements between accelerometer locations.

5.1.2 Dynamic Response to Wave Excitation

If a wave staff is used to collect input wave excitation, then a dynamic response (transfer function) can be calculated for the response of different accelerometers on the structure. This information is particularly useful in the verification of theoretical (ie. computer models) models for future design purposes.

5.2 MULTICHANNEL SPECTRAL ANALYSIS FORMULAS

The equations used in multichannel spectral analysis are presented from the time domain and the frequency domain standpoint. Both the $x(t)$ and $y(t)$ time series are assumed to be zero mean, real random processes. A number of excellent references are available and include Bendat and Piersol [1971, 1980], Crandall [1973], and Jenkins and Watts [1968].

5.2.1 Time Domain Analysis

Correlations tell how well future values can be predicted based on past values. The autocorrelation function estimate (actually covariance for a zero mean random process) is defined as

$$R_{xx}(\tau) = R_{xx}(-\tau) = E[x(t) x(t + \tau)] \quad (5.1)$$

and is a real, even function of lag τ . The cross-correlation function estimate (again, cross-covariance) satisfies

$$\begin{aligned} R_{xy}(\tau) &= R_{yx}(-\tau) = E[x(t)y(t+\tau)] \\ &= E[y(t)x(t-\tau)] \end{aligned} \quad (5.2)$$

and is a real function of lag τ .

5.2.2 Frequency Domain Analysis

The frequency domain equivalent of the correlation functions are the spectral density function estimates. The spectra and the correlations are Fourier transform pairs and satisfy the Wiener-Khintchine relations:

$$S(f) = \int_{-\infty}^{\infty} R(\tau) \exp(-j2\pi f \tau) d\tau \quad (5.3a)$$

$$R(\tau) = 1/2\pi \int_{-\infty}^{\infty} S(f) \exp(j2\pi f \tau) df \quad (5.3b)$$

All spectra defined in this thesis are one-sided as opposed to two-sided (f varies over 0 to ∞ rather than $-\infty$ to ∞) and satisfy

$$G(f) = 2 S(f) \quad 0 < f < \infty \quad (5.4)$$

The total area under the curves are equivalent. Single-sided correlations and spectra are also Fourier

transform pairs of one another.

The autospectral and cross-spectral estimates of magnitude, phase, and coherence are now discussed.

5.2.2.1 Autospectral Estimates. The two-sided autospectral estimates satisfy

$$S_{xx}(f) = S_{xx}(-f) \quad (5.5)$$

and are real, non-negative, and even functions of frequency f .

5.2.2.2 Cross-Spectral Estimates. The two-sided cross-spectral estimate is defined as

$$\begin{aligned} S_{xy}(f) &= S_{yx}(-f) = S_{xy}^*(-f) & -\infty < f < \infty & (5.6) \\ &= C_{xy}(f) - jQ_{xy}(f) \end{aligned}$$

It is a complex-valued function of frequency f . It consists of (1) the coincident or co-spectra density function, $C_{xy}(f)$, which is real-valued even function of frequency f ; and the quadrature spectral density function, $Q_{xy}(f)$, which is a real-valued, odd function of frequency f . These satisfy

$$\begin{aligned} C_{xy}(f) &= C_{xy}(-f) & -\infty < f < \infty & (5.7) \\ &= 0.5 * [G_{xy}(f) + G_{yx}(f)] \end{aligned}$$

The quadrature component satisfies

$$\begin{aligned} Q_{xy}(f) &= -Q_{xy}(-f) & -\infty < f < \infty & (5.8) \\ &= j/2 * [G_{xy}(f) - G_{yx}(f)] \end{aligned}$$

It is shifted in time 90 degrees from the co-spectra density function estimate. The corresponding values for the

single-sided cross-spectrum are defined for frequency over the interval $[0, \infty]$ only.

The cross-spectra given by Eq. 5.6 for the two-sided cross-spectrum can be alternately defined in terms of a magnitude and phase for the single-sided cross-spectrum as

$$G_{xy}(f) = |G_{xy}(f)| \exp[-j\theta_{xy}(f)] \quad 0 < f < \infty \quad (5.9)$$

where the magnitude, $|G_{xy}(f)|$, and the phase, $\theta_{xy}(f)$, are defined as

$$|G_{xy}(f)| = \text{SQRT} [C_{xy}^2(f) + Q_{xy}^2(f)] \quad 0 < f < \infty \quad (5.10a)$$

$$\theta_{xy}(f) = \text{ARCTAN} [Q_{xy}(f) / C_{xy}(f)] \quad 0 < f < \infty \quad (5.10b)$$

The magnitude is real-valued and even and the phase is real-valued and odd function of frequency f .

5.2.2.3 Coherence Squared Estimates. Another way to display the cross-spectra is the coherence squared (or coherence, if square root is taken) which is a form of normalizing the cross-spectra. It is defined as

$$\gamma^2_{xy}(f) = G_{xy}^2(f) / \{G_{xx}(f) * G_{yy}(f)\} \quad (5.11)$$

And is a measure of the fraction or portion of one signal which is due to the other. It satisfies the inequality

$$0 \leq \gamma^2_{xy}(f) \leq 1 \quad (5.12)$$

When it has a value of zero, $x(t)$ and $y(t)$ are said to be incoherent or uncorrelated (independent if normal) at the particular frequency [Bendat and Piersol, 1971, 1980; Enochson, 1976]. When the coherence is zero for all frequencies, then $x(t)$ and $y(t)$ are statistically

independent. When the coherence equals unity at a particular frequency, $x(t)$ and $y(t)$ are said to be fully coherent, correlated, or dependent.

5.2.2.4 Transfer Function Estimates. The transfer function estimate, can be obtained by either an auto or cross-spectral estimate. However, as discussed in Chapter 4, the cross-spectral estimate is better since output noise is rejected. It is defined as

$$\begin{aligned} H_{xy}(f) &= G_{xy}(f) / G_{xx}(f) & 0 < f < \infty & \quad (5.13) \\ &= H_r(f) - jH_i(f) \end{aligned}$$

where $G_{xx}(f)$ is considered to be the input signal whether or not it actually is an excitation. Analogous to the cross-spectral estimate, the transfer function is composed of (1) a component, $H_r(f)$, which is a real-valued, even function of frequency f ; and (2) a component, $H_i(f)$, which is a real-valued, odd function of frequency f . It can be defined in terms of a magnitude (ie. gain), $|H_{xy}(f)|$, and phase, $\phi_{xy}(f)$. These must satisfy

$$H_{xy}(f) = |H_{xy}(f)| \exp[-j\phi_{xy}(f)] \quad 0 < f < \infty \quad (5.14)$$

where,

$$|H_{xy}(f)| = |G_{xy}(f)| / G_{xx}(f) \quad 0 \leq f < \infty \quad (5.15)$$

$$\begin{aligned} \phi_{xy}(f) &= \arctan [H_i(f) / H_r(f)] \\ &= \theta_{xy}(f) \end{aligned}$$

Thus, the phase, $\phi_{xy}(f)$, of the transfer function estimate is identical to the phase of the cross-spectral estimate $\theta_{xy}(f)$.

5.3 INTERPRETATION OF CROSS-SPECTRAL ESTIMATES

The primary use of the cross-spectral estimates will be in mode shape identification. A brief discussion of the possible interpretations of each of the autospectra and cross-spectral magnitude, phase, coherence, and transfer function estimates will be presented.

5.3.1 Autospectral Estimates

the autospectral density estimates reveal peaks which may be due to either normal modes of the structure, machine noise, or excitation peaks.

5.3.2 Cross-spectral Magnitude Estimates

The cross-spectral magnitude estimates should be used in conjunction with the autospectra estimate to locate natural frequencies and half-power damping estimates.

5.3.3 Phase and Coherence Estimates

The phase and coherence (or coherence squared) estimates should be used in conjunction with the auto and cross-spectral magnitude estimates to determine modal characteristics. Coupling between modes can cause the phase values to be other than zero or 180 degrees. Extraneous noise in the measurement at a particular location will cause the coherence value between that accelerometer and all

others to be less than unity. Other possible explanations for low coherence values could be (1) a nonlinear relationship between the output signals, (2) different contributions from uncorrelated sources, and (3) wave excitation at an angle to the structure causing no response from one of the accelerometers. The predicted modal deflections will be underpredicted if the coherence is much less than unity.

Generally, mode shape identification should not be made unless a coherence of near unity and a phase of near zero or 180 degrees is obtained with all other outputs.

5.3.4 Transfer Function Estimates

The transfer function estimates should be used in conjunction with the other cross-spectral estimates. For mode shape identification, relative acceleration amplitudes between two accelerometers can be used in place of relative displacements to determine mode shapes. Resolution bias errors or system nonlinearities will cause the coherence and the transfer function estimate not to peak at the same frequencies of system normal modes.

CHAPTER 6 CASE STUDY OF A SINGLE CAISSON PRODUCTION PLATFORM

In order to compare the multichannel MEM algorithms with the conventional Blackman-Tukey approach, data was collected and analyzed for an offshore caisson platform located in the Gulf of Mexico and operated by Amoco. The data was collected in March, 1981 by Prof. J. K. Vandiver, Mike Cook, a Graduate Research Assistant, and Don Green, an Amoco engineer. In this Chapter, a description of the platform, instrumentation, load cases, test set-up, and data processing is presented.

6.1 CAISSON PLATFORM DESCRIPTION

The offshore caisson platform is located in 89 ft of water in the Gulf of Mexico. It consists of a single, vertical cylindrical caisson which telescopes from a 7 ft diameter at the mudline to 4 ft at the MLW. Figure 6.1 is a three-dimensional view of the structure. It supports three decks: a helicopter, production, and wellhead deck. Figure 6.2 shows that it is 265 ft overall; extending 100 ft below the mudline, 89 ft through the water column, and 76 ft above the surface. Due to the symmetry of the single caisson and the resultant lack of interference from adjacent legs, it makes an ideal structure for an empirical study.

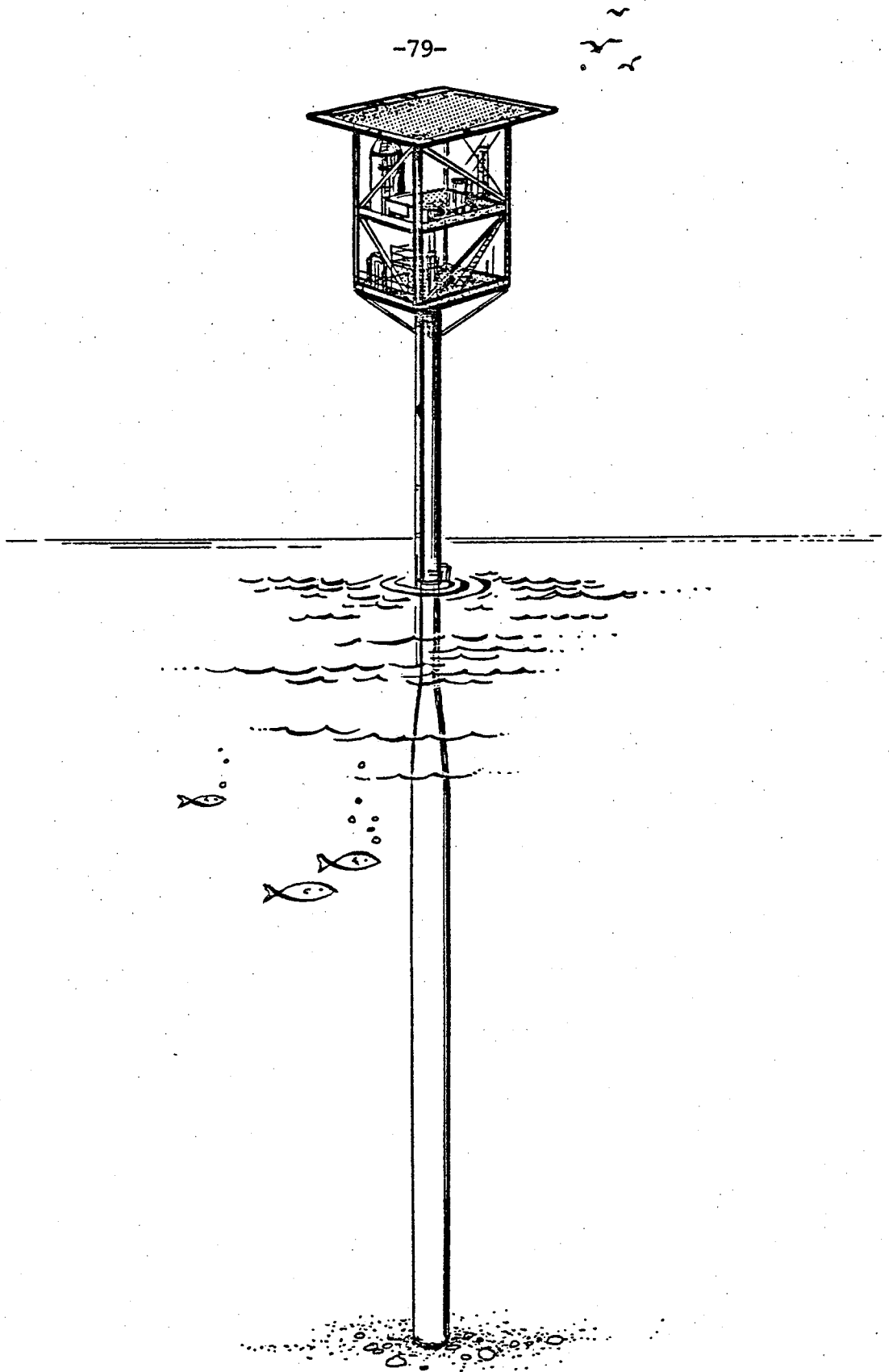


FIGURE NO. 6.1
OFFSHORE CAISSON PLATFORM

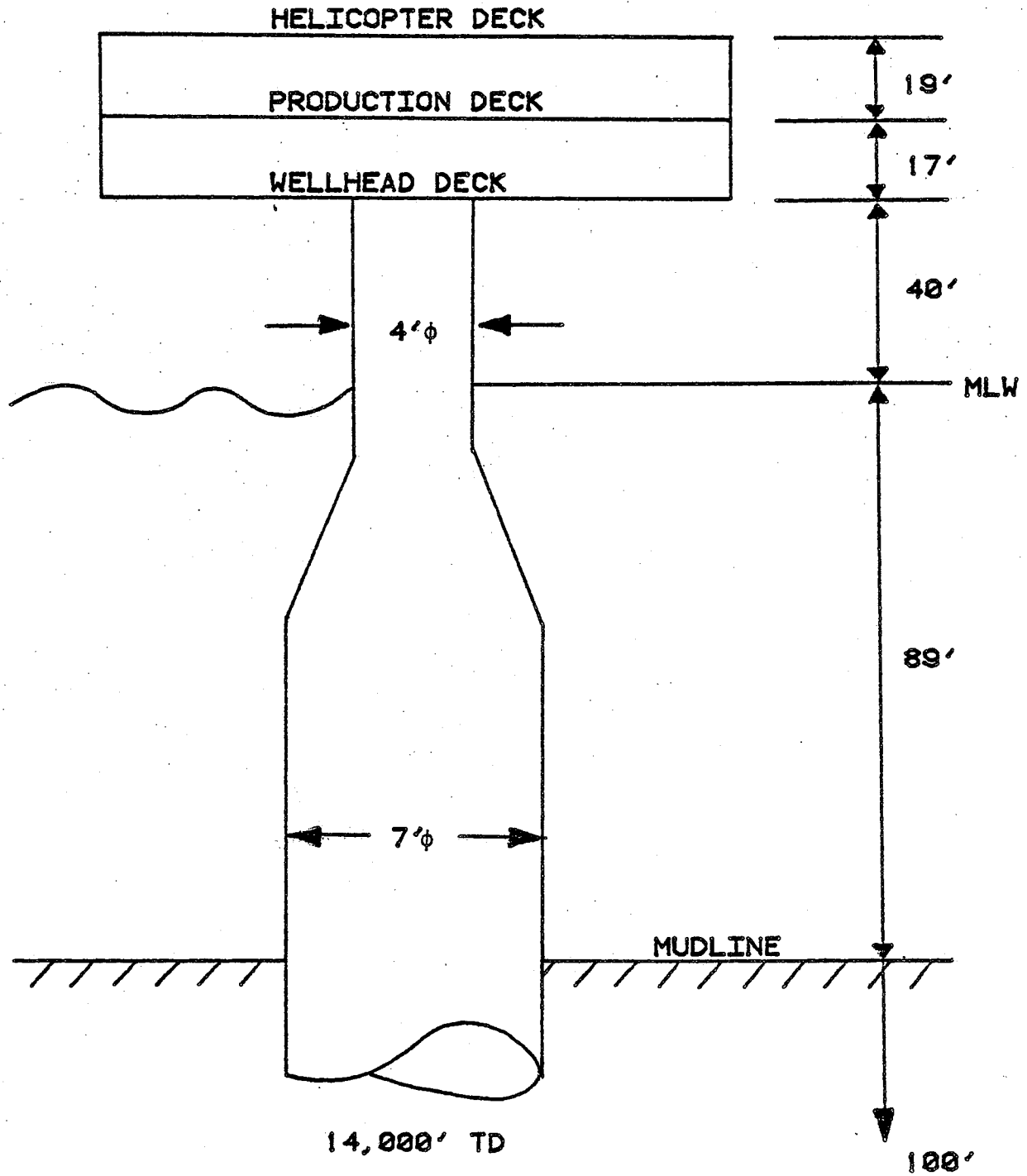


FIGURE NO. 6.2
SCHEMATIC OF OFFSHORE CAISSON PLATFORM

6.2 INSTRUMENTATION

The instrumentation for this series of tests consisted of as many as four accelerometers, a wave staff, and a Tandberg 4 channel FM tape recorder.

6.2.1 Accelerometers

The accelerometers used were Endevco QA 116-16 force balance type. They can measure up to ± 1 g, resolve down to 10^{-6} g's, and have a sensitivity of 1 volt per g.

6.2.2 Wave Staff

The wave staff is a capacitance type which converts changes in surface elevation to variations in voltage output. A variable capacitor is formed using an insulated wire. The wire and water act as the two plates of the capacitor while the wire insulation provides the dielectric. Two Colpitts oscillators form the detection circuitry. One oscillator acts as a reference signal while the second oscillator frequency is governed by the capacitance of the sensor.

The wave staff was suspended from one side of the wellhead deck. The lower end was heavily weighted to prevent it from being deflected from the vertical due to wave or current action.

6.2.3 FM Tape Recorder

A Tandberg 4 channel FM tape recorder, Model 100, was used to record the data. It uses standard 1/4 in. tape and records simultaneously on four channels with the option to override channel four with voice commentary.

6.3 SUMMARY OF LOAD CASES

The results from two of the five load cases conducted on the caisson platform are presented in this thesis. They are described below.

6.3.1 Description

Load Case No. 1 was designed to measure input wave excitation and platform flexure and torsional modes. The wave staff and three accelerometers, all placed in the same horizontal plane on the wellhead deck, were used. A biaxial pair was placed in the center of the deck oriented north and east. A third accelerometer was placed in the middle of the north side of the deck and was also oriented in an easterly direction to facilitate torsional mode identification (see Figure 6.3).

Load Case No. 2 was designed to measure the flexural mode shapes of the platform. Four accelerometers were placed in the same vertical plane running through the centerline of the platform with accelerometers oriented in a

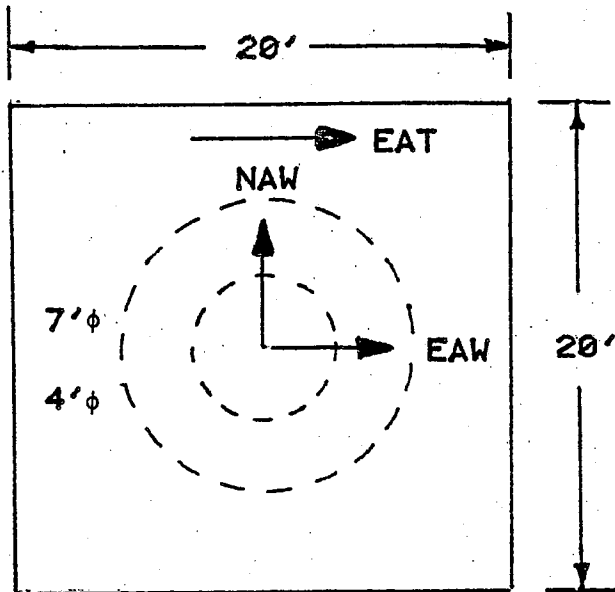


FIGURE NO. 6.3
LOAD CASE 1: WAVE INPUT & TORSIONAL MODE SHAPE
PLAN VIEW OF WELLHEAD DECK

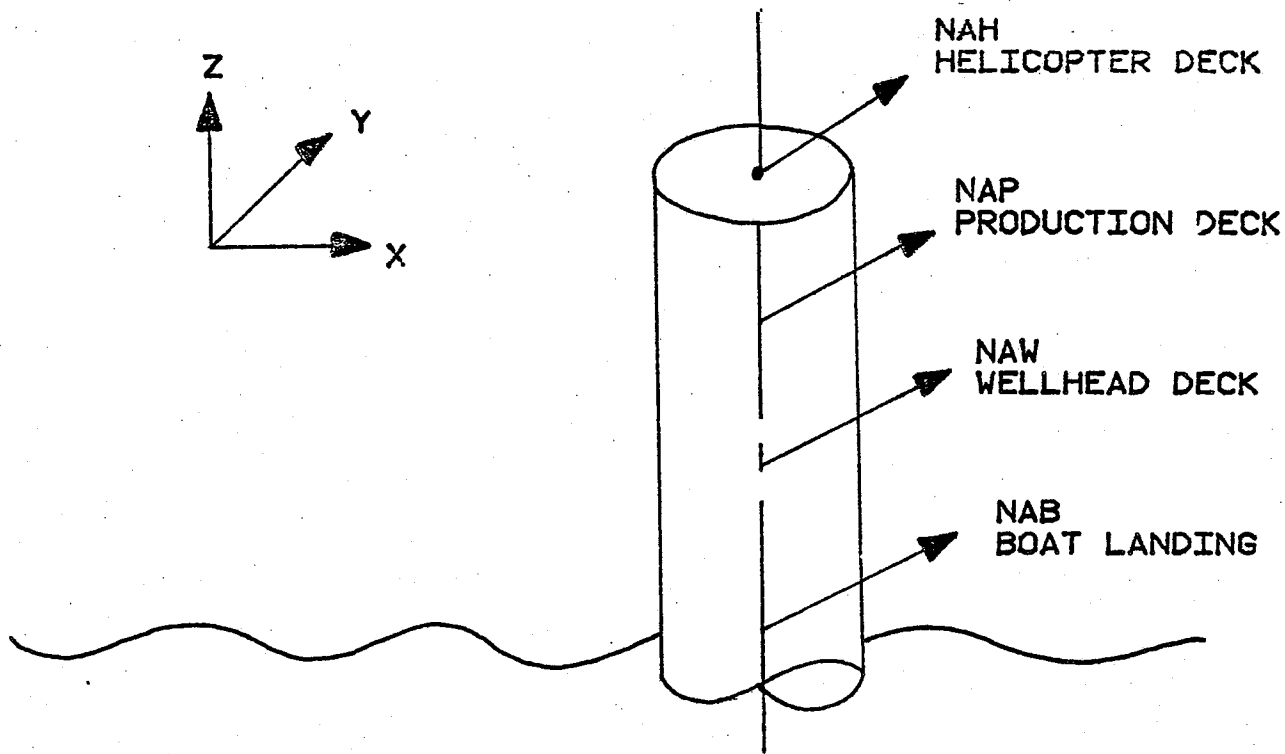


FIGURE NO. 6.4
LOAD CASE 2: FLEXURAL MODE SHAPE
SIDE VIEW OF OFFSHORE CAISSON PLATFORM

northerly direction (see Figure 6.4). A summary of this data for the two load cases is presented in Table 6.1.

6.3.2 Environmental Conditions

An anemometer was used to measure wind speeds. Visual observation was used to determine sea state conditions in all load cases where the wave staff was not used. In Load Case 1, the RMS wave amplitude was calculated from the power density spectrum calculated from the measured wave staff data. The significant wave height was then calculated from this data. Table 6.2 summarizes these environmental conditions.

6.4 TEST SET-UP

The wave staff was fixed to the platform. The two possible mounting locations were from the boat landing and from the center of the north side of the wellhead deck. Mounting the staff off of the boat landing would have insured less motion of the sensor element, but would have resulted in interference from the caisson. Therefore, the wave staff was mounted from the wellhead deck, some 40 ft above the MLW. The suspended 30 lb weight helped to stabilize the gage.

TABLE 6.1
SUMMARY OF LOAD CASES

<u>Load Case</u>	<u>Description</u>	<u>Date</u>	<u>Input</u>	<u>Output</u>
1	Wave Input Torsion Mode Shape Load Case	3/28/81	Wave Staff	Lateral plane, Biaxial & single Accelerometers
2	Flexural Mode shape Load Case	3/25/81	None	Vertical plane, 4 colinear Accelerometers

TABLE 6.2
SUMMARY OF ENVIRONMENTAL CONDITIONS

<u>Load Case</u>	<u>Description</u>	<u>Wind, knots</u>	<u>Sea State, ft</u>
1	Wave Input and Torsion Mode Shape Load Case	10-12	Seas Hs = 3.32'
2	Flexural Mode shape Load Case	ENE @ 20	Seas 5-8'

Note:
Significant wave height calculated from RMS wave
amplitude of wave PSD

The FM tape recorder was located in a centralized place on the production deck and all cables were connected as required. The amplifier gain was selected to give an accelerometer output of 100 volts per g. Data was recorded on the four channels at 1-7/8 ips.

The only machinery operating on the platform was a diesel generator on the production deck.

6.5 DATA PROCESSING

Prior to calculating the spectral estimates, using either conventional or MEM methods, the data was processed using the following programs:

- (1) SCRIBE - converts FM tape source for each channel into digital TSL form,
- (2) TRANSL - translates TSL code into Fortran code,
- (3) BZERO - makes a time series zero mean, and
- (4) SCALE - scales a time series for proper voltage conversion factor.

A sampling rate, f_s , of 6.4 Hz (0.16 second interval) was used in the data reduction. A total of 80 minutes (4800 sec, 30720 data points) of data was collected.

The multichannel Burg direct on the data method is implemented in the program BRGMEM. Data is accepted directly as input. The correlation based programs, the Blackman-Tukey program BTSPEC and the Yule-Walker MEM program RYWMEM, require auto and cross-correlations as

input. These are calculated using the programs ACORPM and XCOR for the auto and cross-correlations respectively. These correlations were calculated to lag lengths of 512 points or 80 seconds. This value was chosen as an appropriate tradeoff between resolution and variance. A total of 29696 points were used (58 segments of 512 points each).

CHAPTER 7 COMPARISON OF MULTICHANNEL SPECTRAL ANALYSIS METHODS

In this chapter, a comparison of the different multichannel methods of spectral analysis is made. These include the Blackman-Tukey (BTSPEC), and MEM direct on the data (BRGMEM) and correlation extension methods (RYWMEM). First, a discussion of the effect of the four different windows and the window duration on the Blackman-Tukey method is presented. Then, the effect of the segmenting and averaging procedure on the MEM direct on the data (BRGMEM) method is discussed. Finally, a comparison of all three methods is made.

For all comparisons, the Load Case 2 Helicopter and Wellhead deck accelerometers are used. As discussed previously in Section 6.5, the BTSPEC and RYWMEM programs require correlations as input. The BRGMEM program calculates the cross-spectral estimates directly from the data. A sampling frequency of 6.4 Hz was used to digitize a total of 80 minutes (4800 seconds, 30,720 data points). An "overlap and save" technique was used to calculate the correlation function estimates from 58 segments of 512 points each (29,696 points).

7.1 BLACKMAN-TUKEY METHOD

In this section the effect of different window shapes and durations on the multichannel Blackman-Tukey method is discussed.

7.1.1 Effect of Window Shape

The effect of different windows, as discussed in Chapter 2.0, on the multichannel Blackman-Tukey method will be presented. The windowing is performed on the correlation function estimates prior to Fourier transforming for the spectral estimates. Figures 7.1 - 7.4 illustrate the effect of the Boxcar, Bartlett, Hanning, and Parzen windows respectively on the magnitude cross-spectral estimate for a window duration or length of 512 lags (ie. the entire correlation lag length). The corresponding resolution bandwidths, B_e , are 0.00625, 0.01875, 0.01667, and 0.00057 Hz respectively. Obviously, as discussed in Section 2.1.1, only the Hanning window is capable of giving a satisfactory "bias versus variance" tradeoff without severe sidelobe leakage. This leakage is very evident in Figures 7.1 and 7.4.

7.1.2 Effect of Window Duration

Figures 7.5 and 7.6 show the magnitude cross-spectral

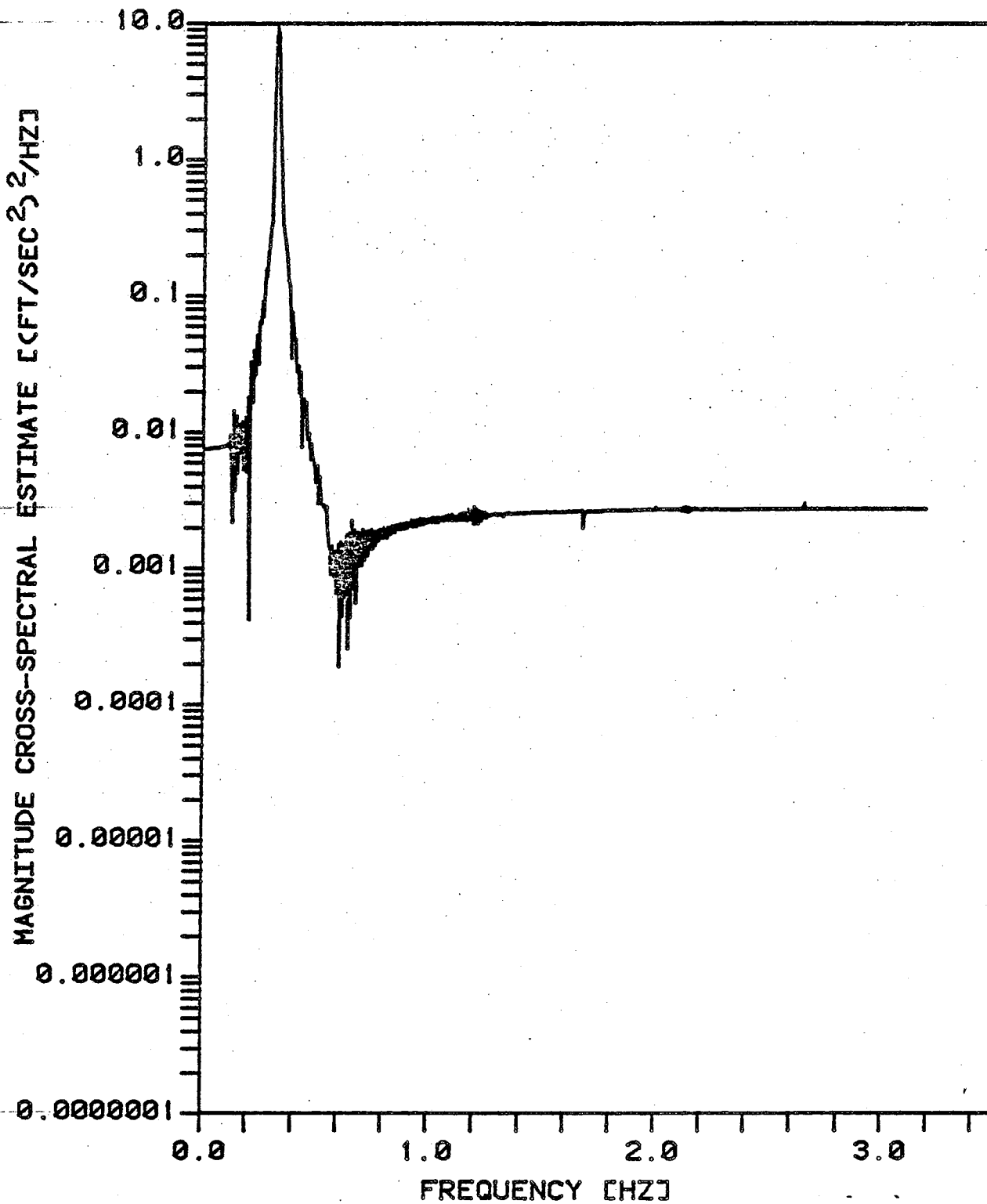


FIGURE NO. 7.1
EFFECT OF BOXCAR WINDOW ON BLACKMAN-TUKEY METHOD
MAXLAG = 512

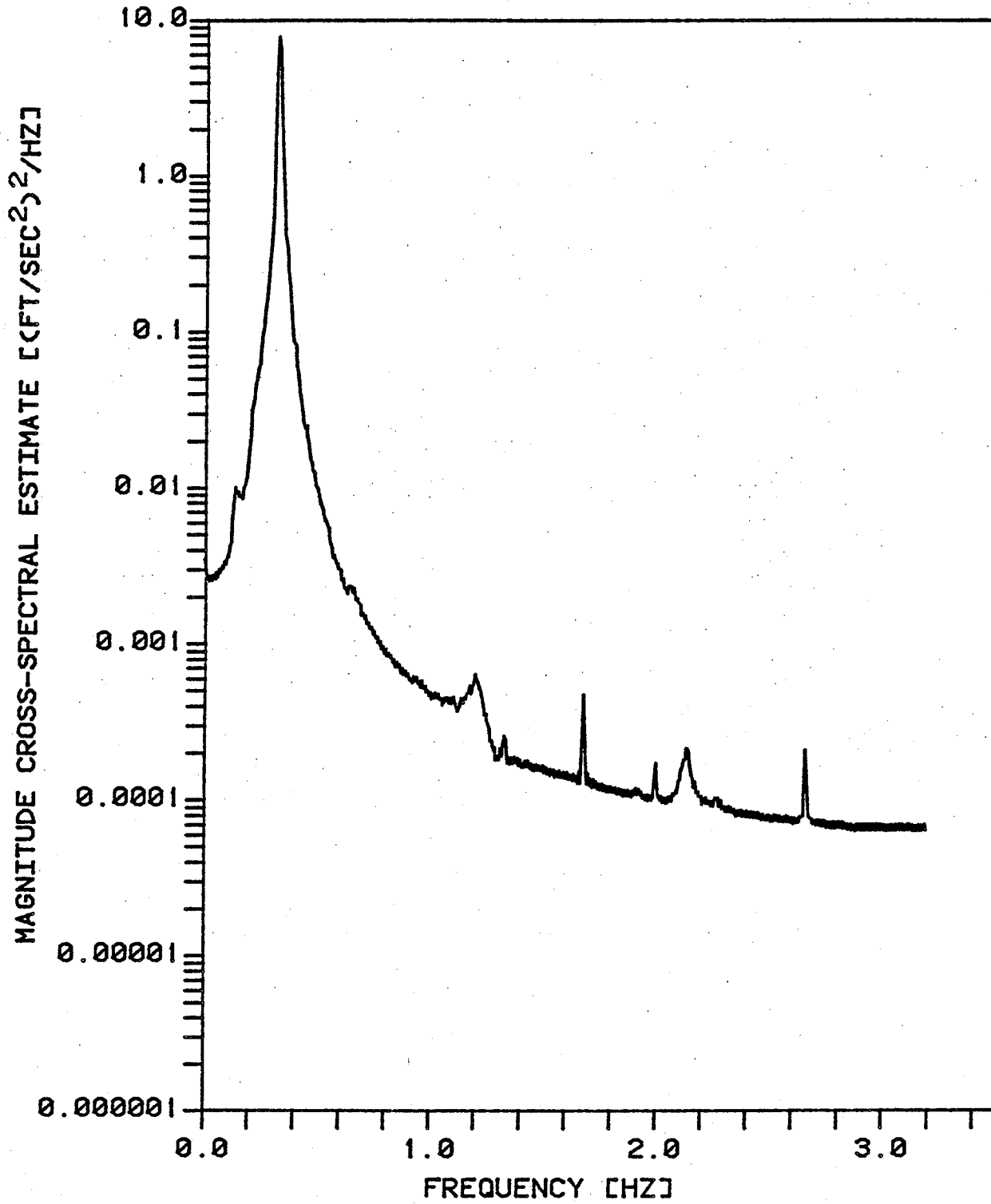


FIGURE NO. 7.2
EFFECT OF BARTLETT WINDOW ON BLACKMAN-TUKEY METHOD
MAXLAG = 512

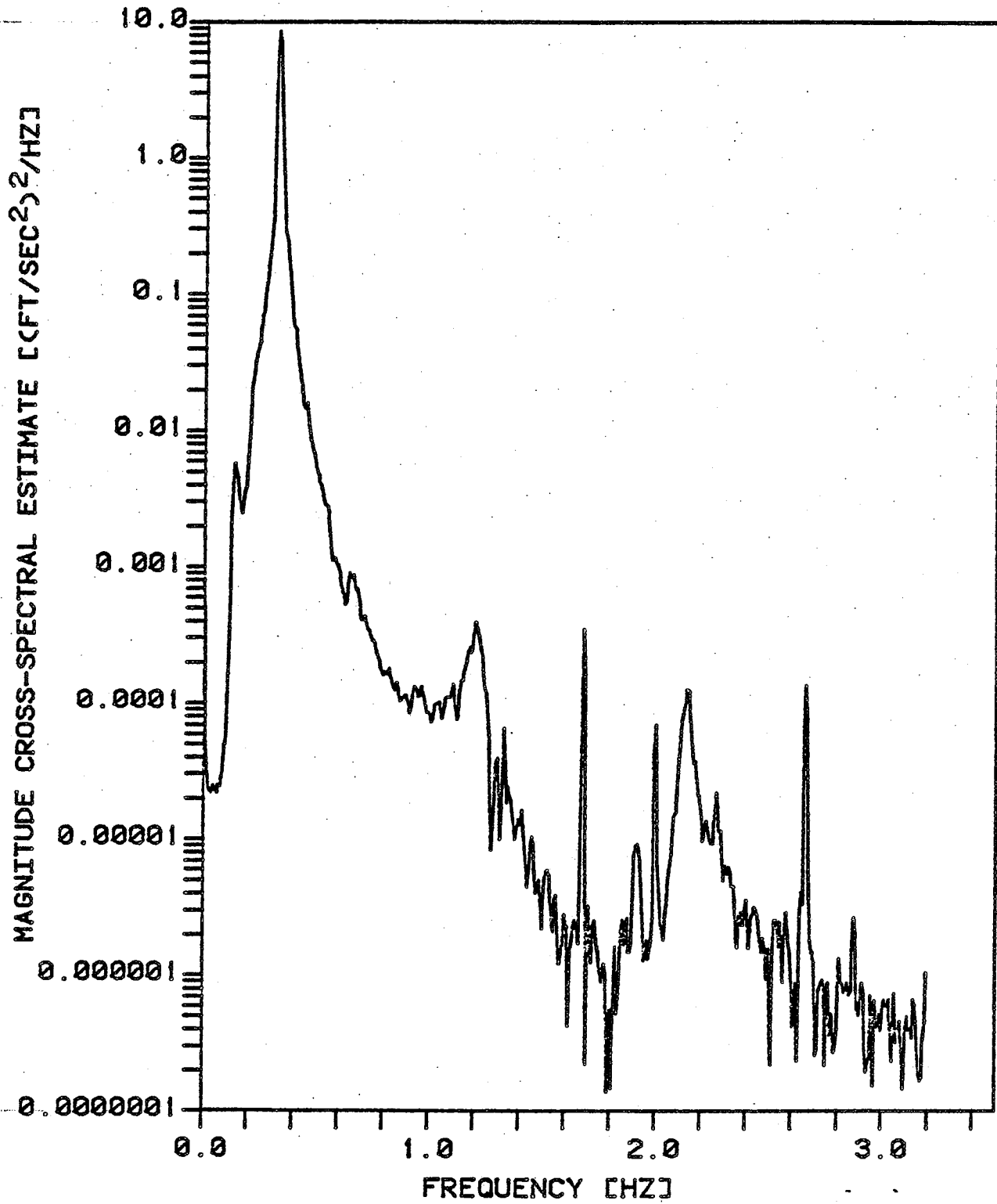


FIGURE NO. 7.3
EFFECT OF HANNING WINDOW ON BLACKMAN-TUKEY METHOD
MAXLAG = 512

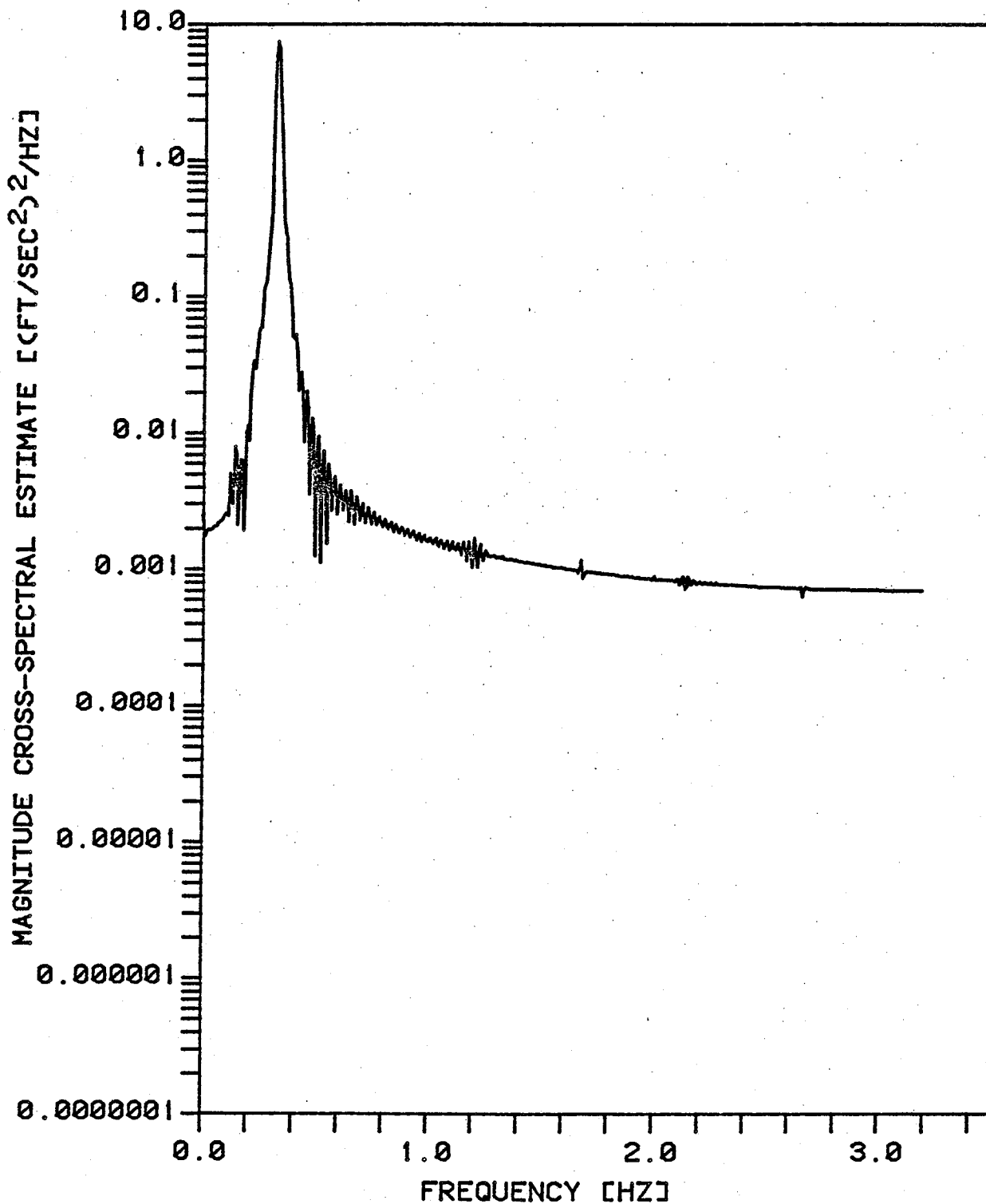


FIGURE NO. 7.4
EFFECT OF PARZEN WINDOW ON BLACKMAN-TUKEY METHOD
MAXLAG = 512

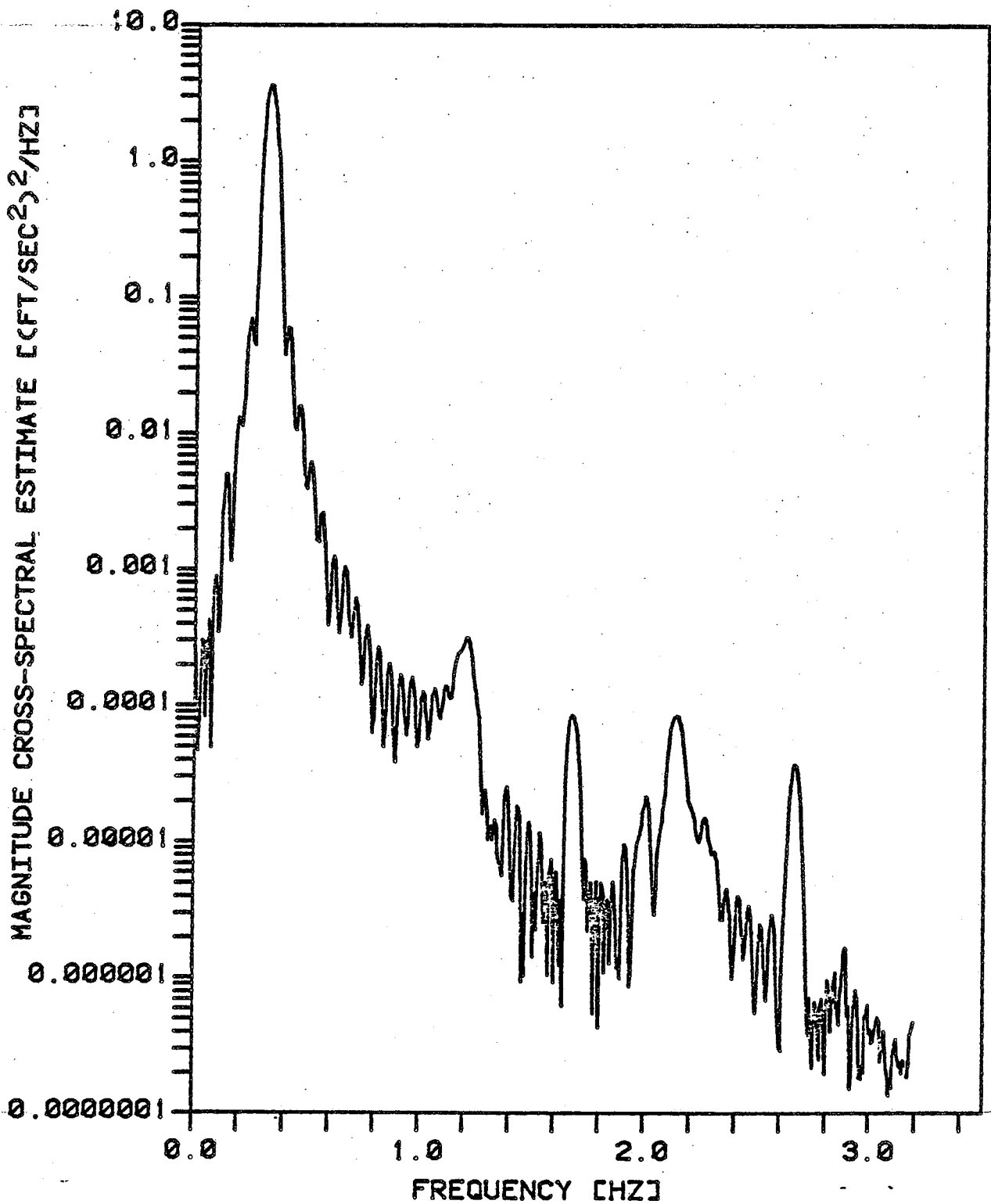


FIGURE NO. 7.5
EFFECT OF WINDOW DURATION ON BLACKMAN-TUKEY METHOD
HANNING WINDOW, NLAG = 128

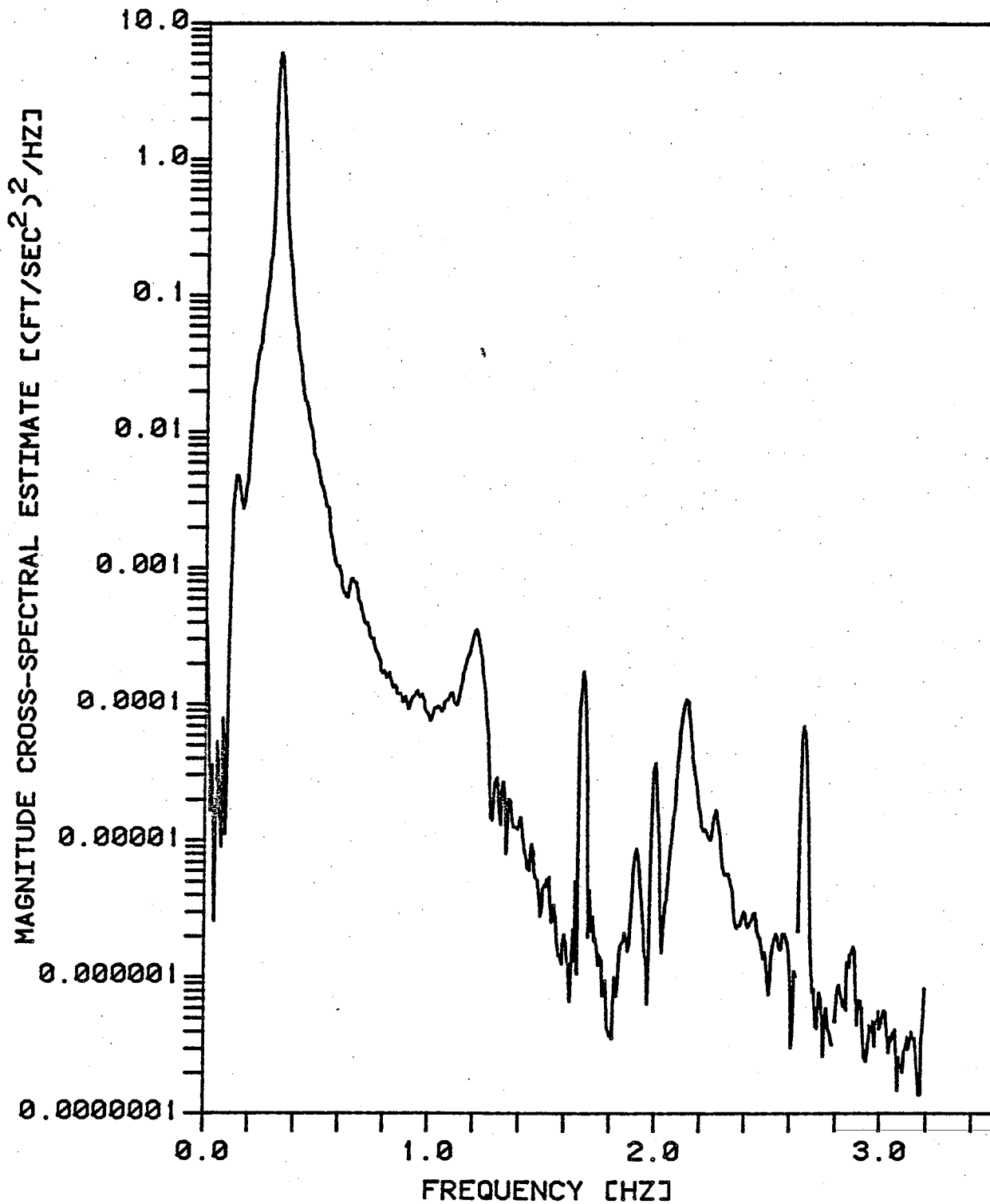


FIGURE NO. 7.6
EFFECT OF WINDOW DURATION ON BLACKMAN-TUKEY METHOD
HANNING WINDOW, NLAG = 256

estimate calculated using the Hanning window for window durations of 128 and 256 lags respectively. The corresponding resolution bandwidths, B_e , are 0.06667 and 0.03333 Hz respectively. Comparing these two figures with Figure 7.3 for 512 lags, a window duration of at least 256 lags is required to give satisfactory results. The effect of sidelobe leakage on the cross-spectral magnitude estimate in Figure 7.5 can be clearly seen.

7.2 BRGMEM DIRECT ON THE DATA METHOD

The effect of segmenting and averaging, analogous to that used for periodograms to decrease the variance at a small loss of resolution, is shown in this section. Figures 7.7 - 7.9 represent the multichannel spectral estimates for the magnitude cross-spectrum, phase, and coherence squared respectively. Note that the phase estimates are the absolute value of the phase estimate to eliminate rapid crossovers between ± 180 degrees. A series of three graphs for each estimate, numbered a, b, and c, are shown for the different segment and averaging combinations listed below.

- (1) Graph a:
1 segment of 2048 points (320 sec),
- (2) Graph b:
9 segments of 2048 points (2880 sec total), and
- (3) Graph c:
1 segment of 18432 points (2880 sec).

A lag of 80 was selected as the optimum model order (filter

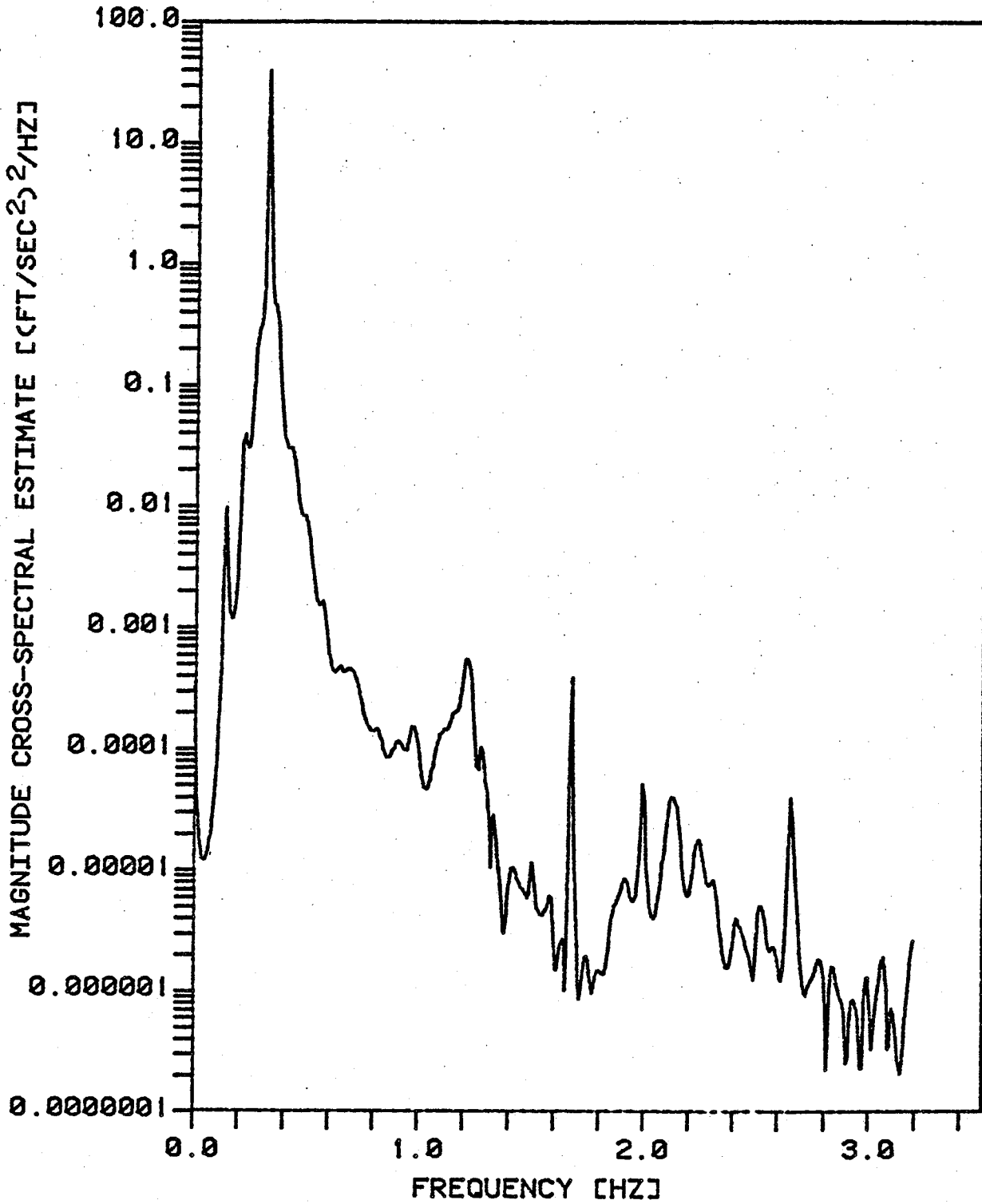


FIGURE NO. 7.7A
EFFECT OF AVERAGING ON MAGNITUDE CROSS-SPECTRUM
BRGMEM, NSEG = 1, M = 2048, NLAG = 80

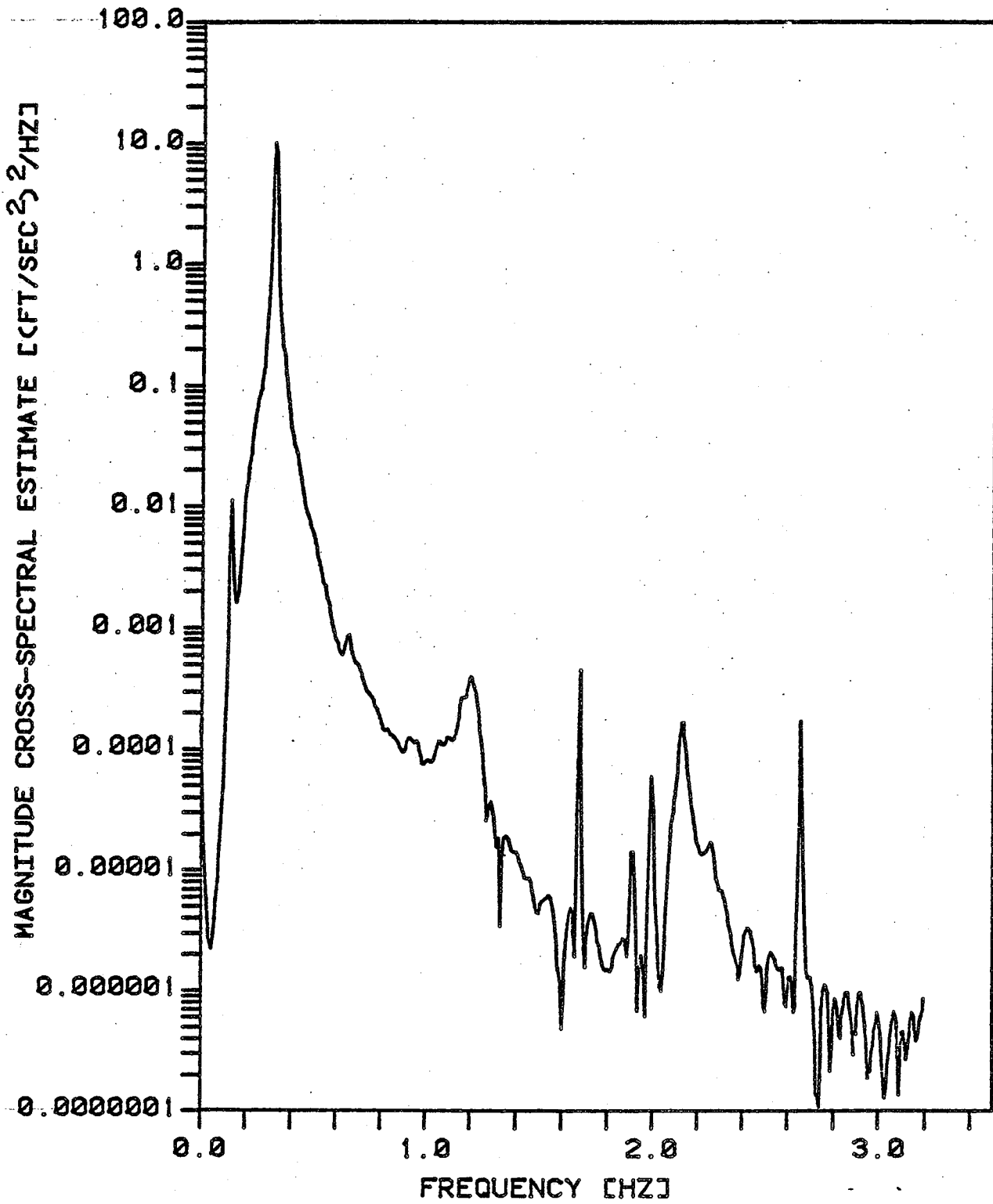


FIGURE NO. 7.7B
EFFECT OF AVERAGING ON MAGNITUDE CROSS-SPECTRUM
BRGMEM, NSEG = 9, M = 2048, NLAG = 80

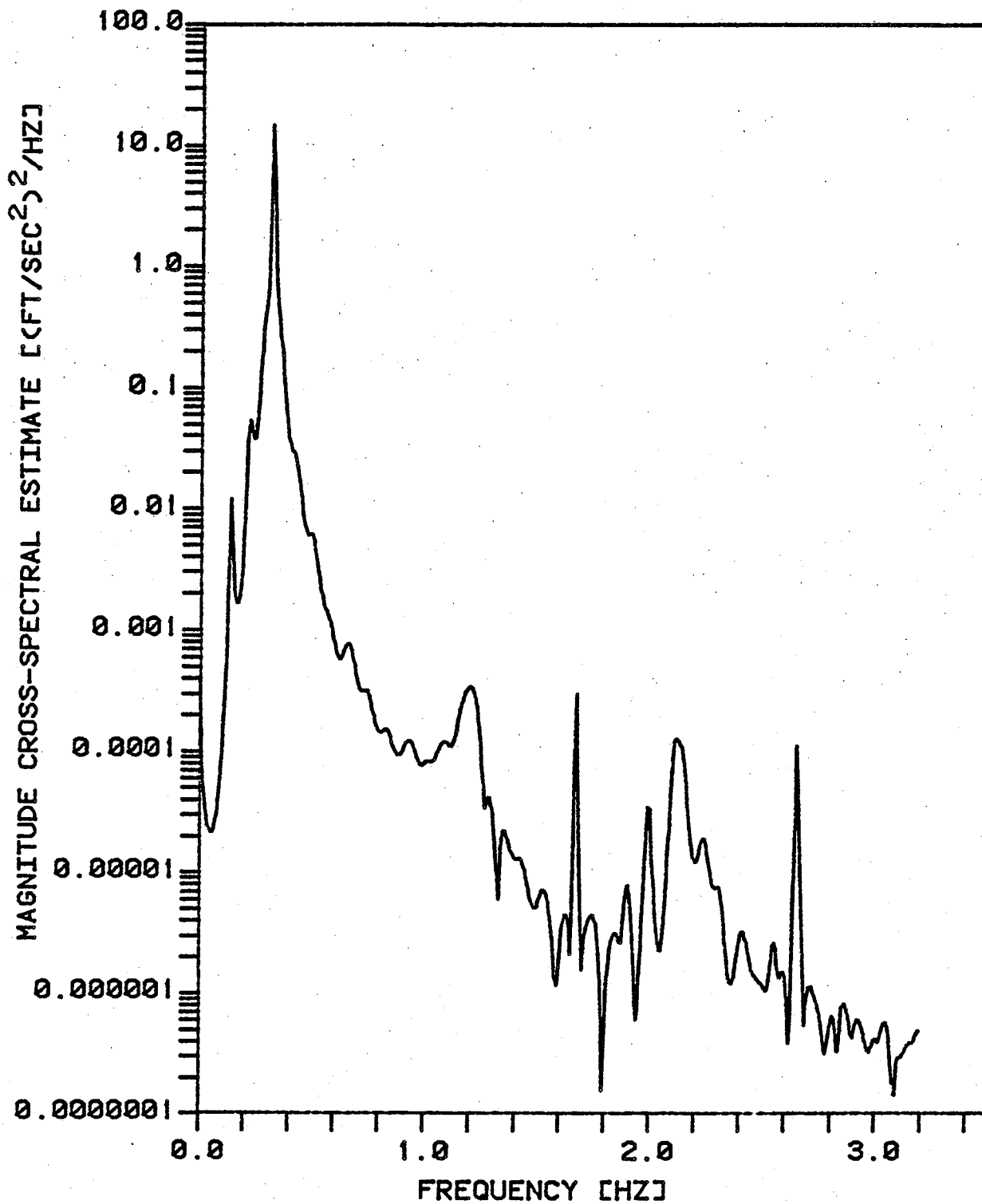


FIGURE NO. 7.7C
EFFECT OF AVERAGING ON MAGNITUDE CROSS-SPECTRUM
BRGMEM, NSEG = 1, N = 18432, NLAG = 80

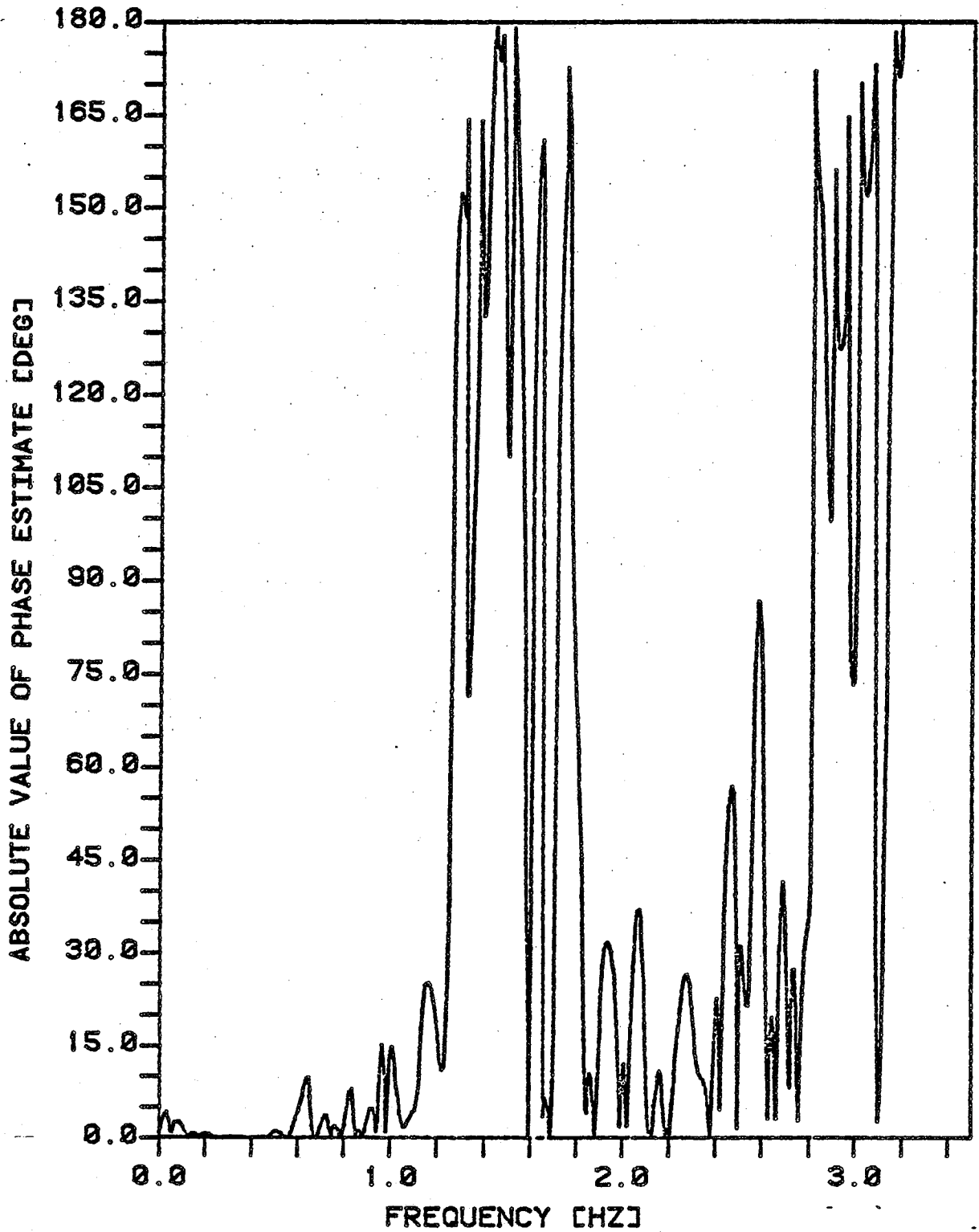


FIGURE NO. 7.8A
EFFECT OF AVERAGING ON PHASE ESTIMATES
BRGMEM, NSEG = 1, M = 2048, NLAG = 80

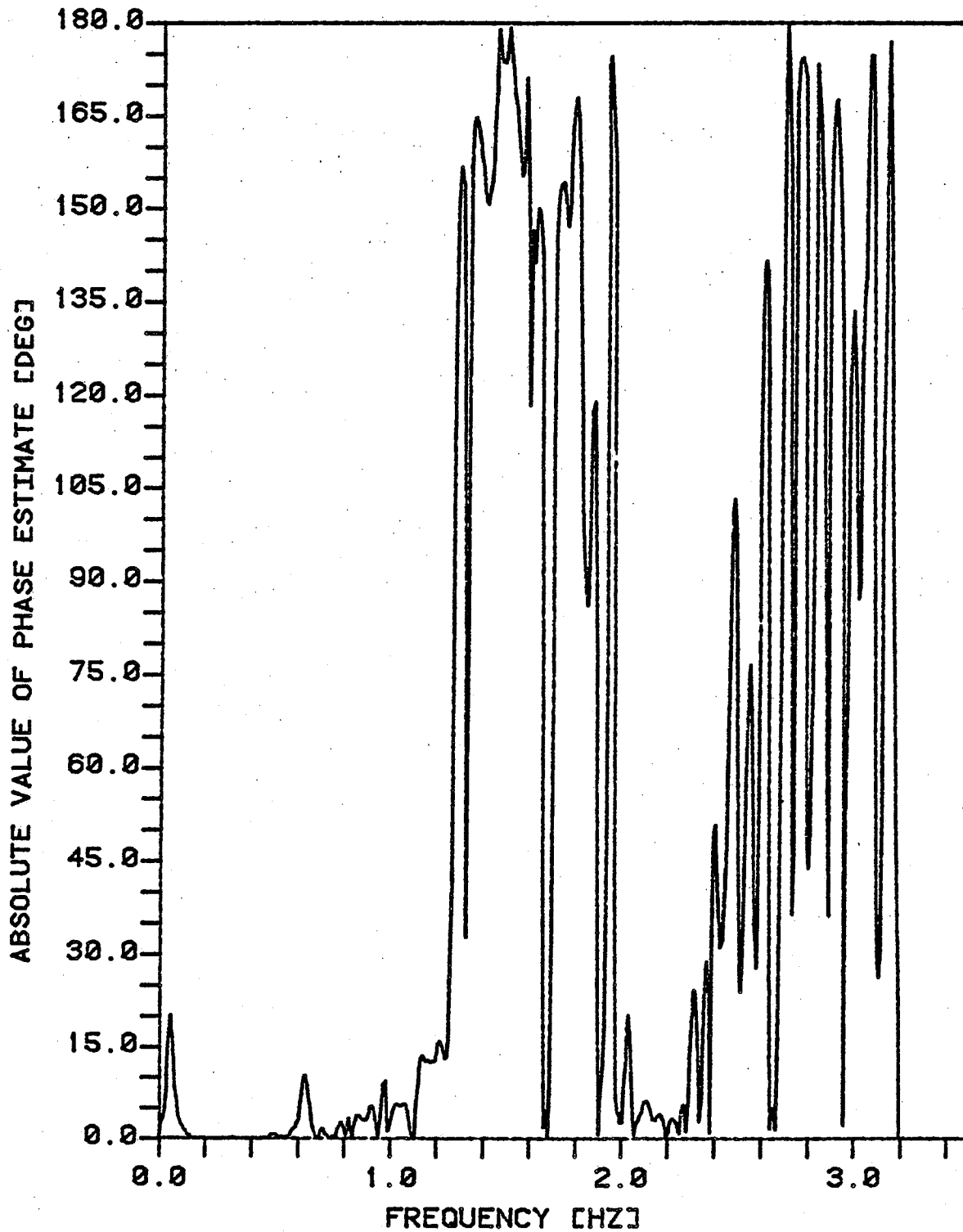


FIGURE NO. 7.8B
EFFECT OF AVERAGING ON PHASE ESTIMATES
BRGMEM, NSEG = 9, M = 2048, NLAG = 80

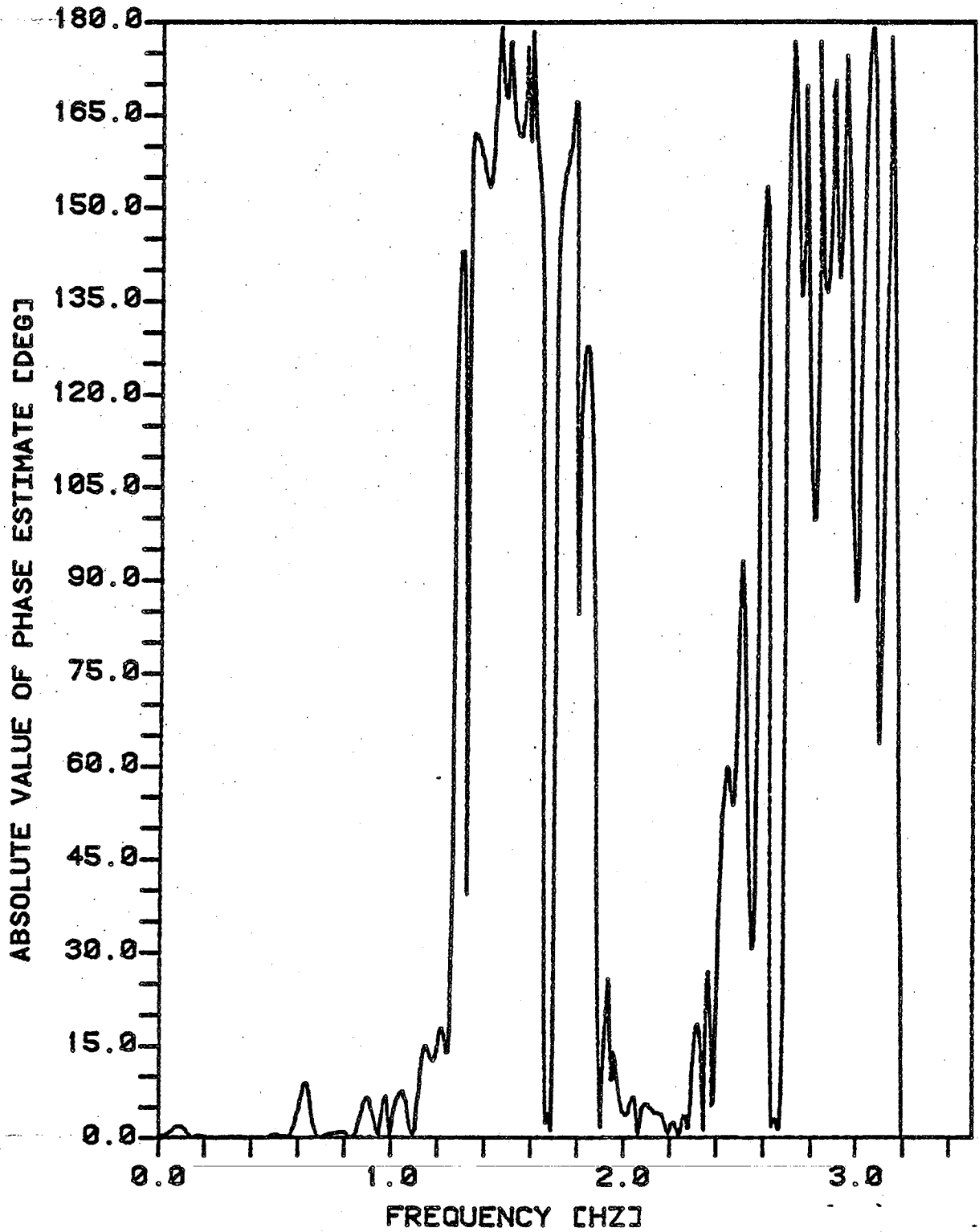


FIGURE NO. 7.8C
EFFECT OF AVERAGING ON PHASE ESTIMATES
BRGMEM, NSEG = 1, N = 18432, NLAG = 80

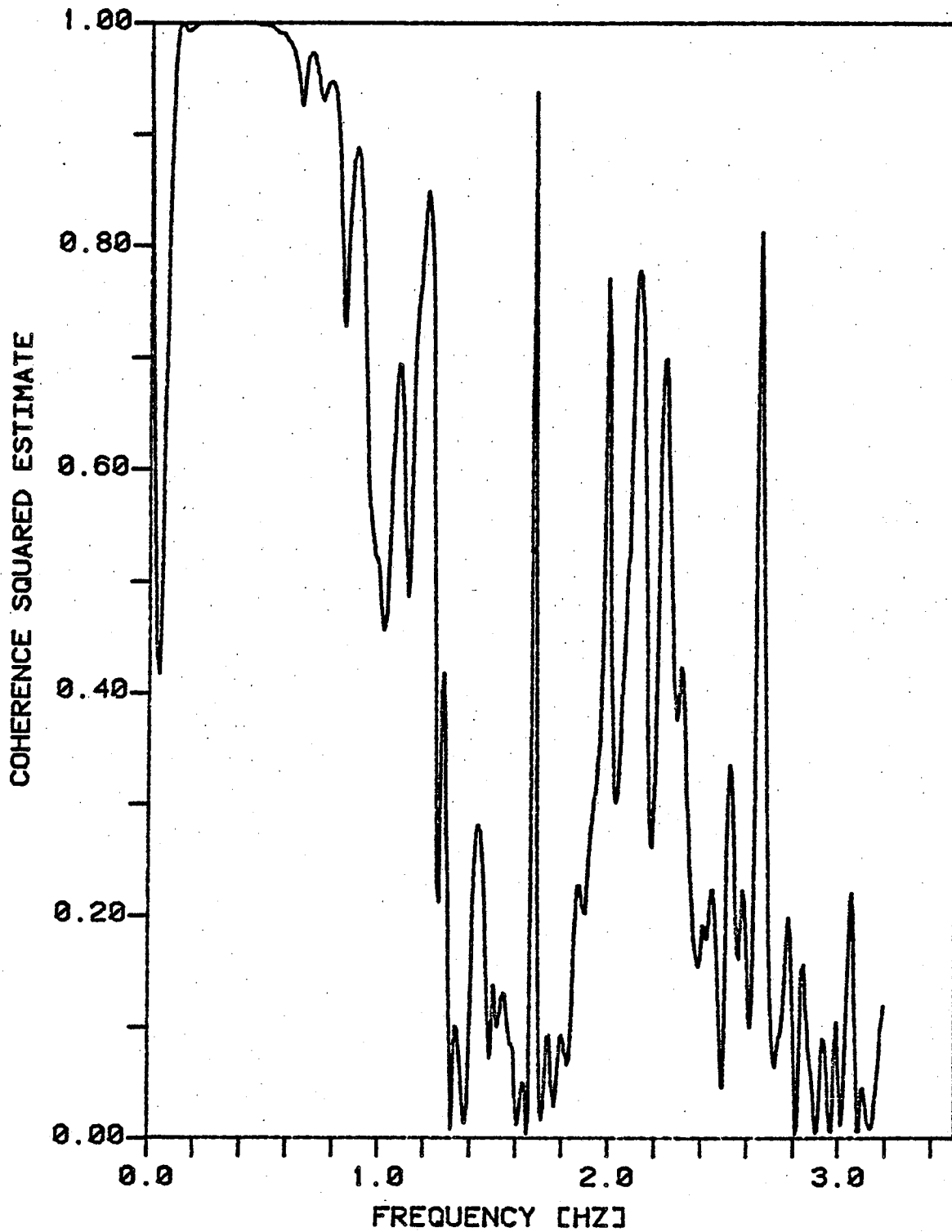


FIGURE NO. 7.9A
EFFECT OF AVERAGING ON COHERENCE ESTIMATES
BRGMEM, NSEG = 1, M = 2048, NLAG = 80

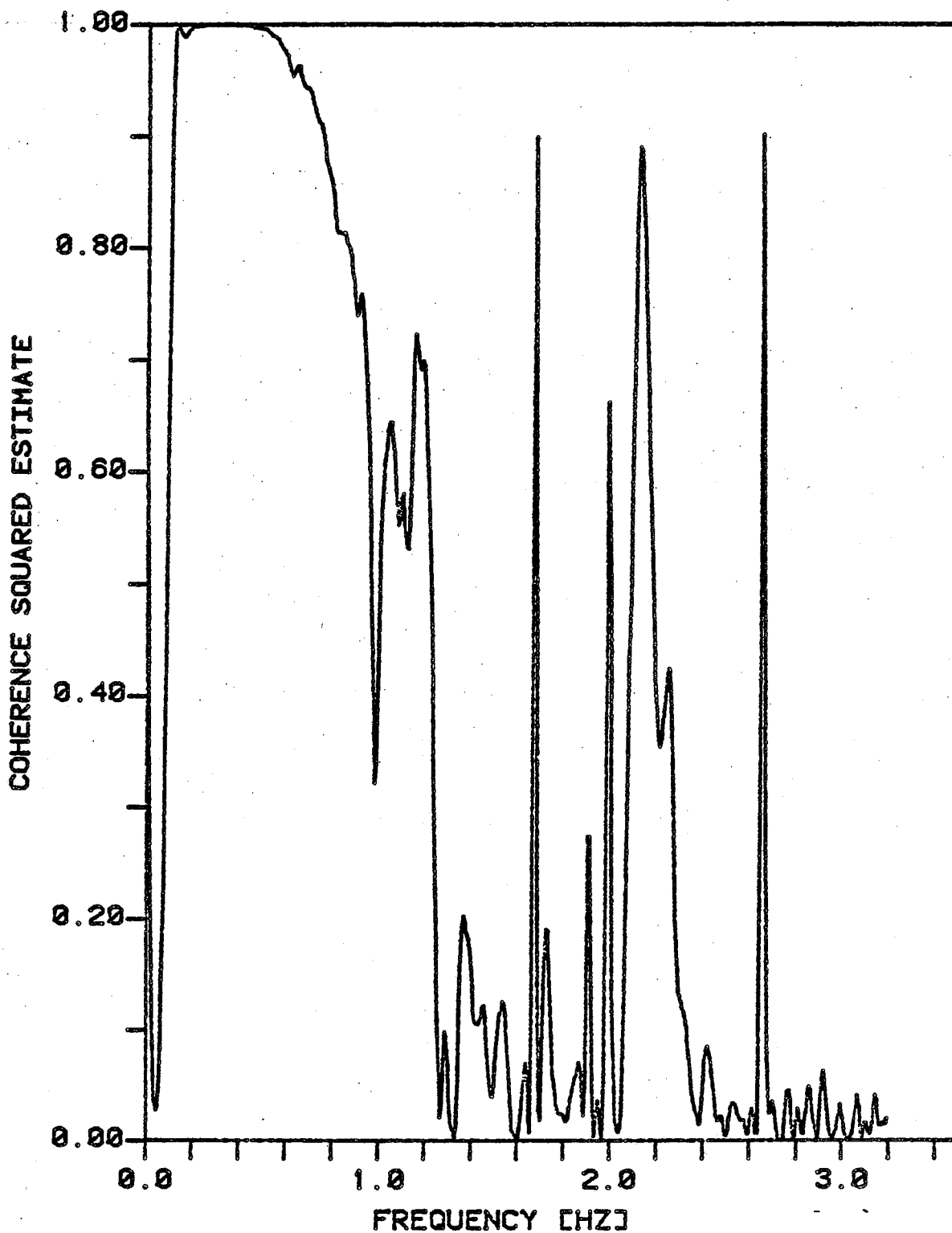


FIGURE NO. 7.9B
EFFECT OF AVERAGING ON COHERENCE ESTIMATES
BRGMEM, NSEG = 9, M = 2048, NLAG = 80

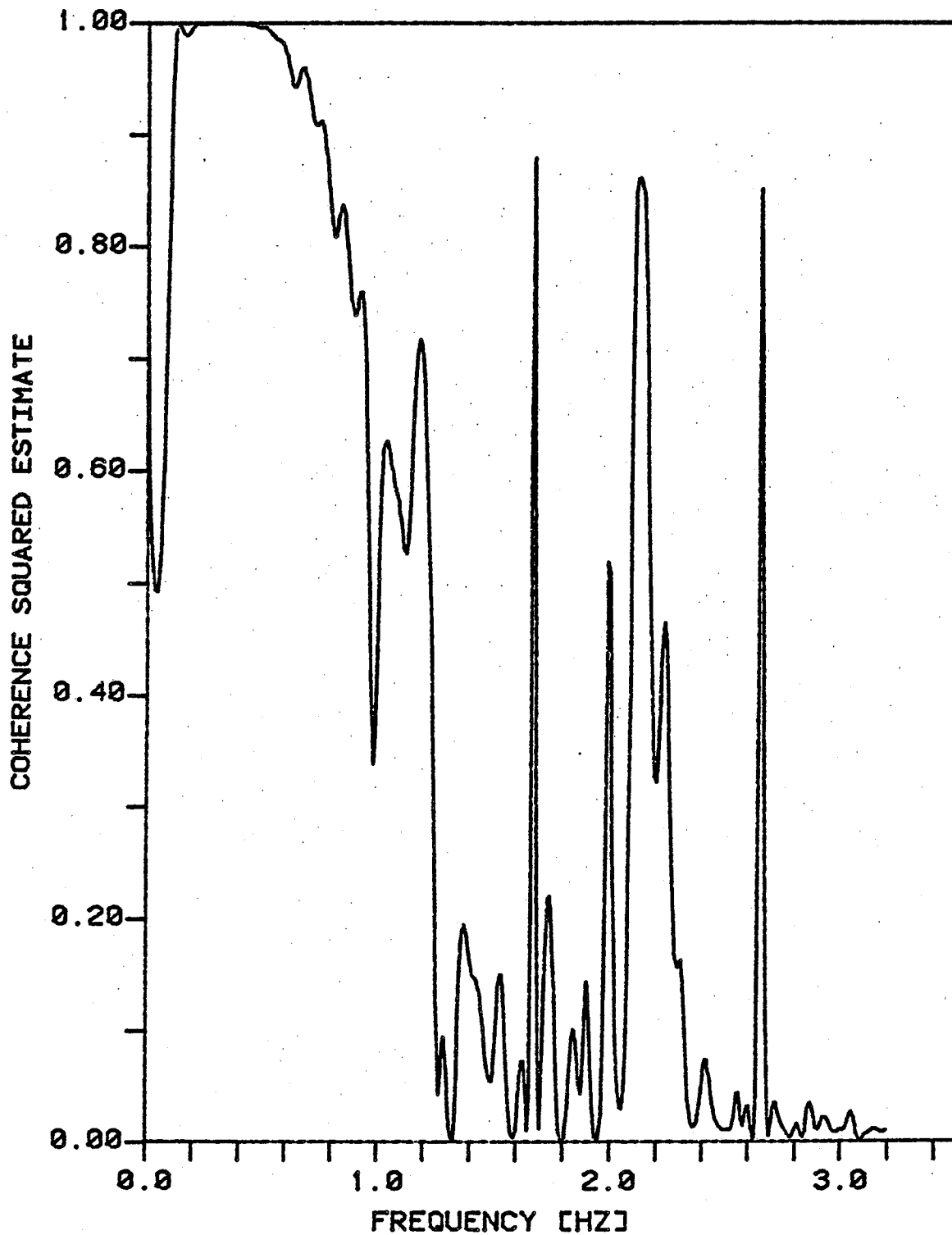


FIGURE NO. 7.9C
EFFECT OF AVERAGING ON COHERENCE ESTIMATES
BRGMEM, NSEG = 1, N = 18432, NLAG = 80

length) based on the multichannel Akaike's FPE model order criterion.

Based on the similarity of the shapes of the three curves in each figure, we can say the segmenting and averaging technique can be used with some degree of confidence where the analyst is faced with:

- (1) a restricted budget,
- (2) time constraint, and/or
- (3) small core (memory limited) computer.

Thus, even the use of only 2048 data points (320 seconds of data) gives satisfactory cross-spectral estimates.

7.3 COMPARISON OF THREE MULTICHANNEL METHODS

In this section, a comparison of the multichannel Blackman-Tukey and the two MEM methods is made. The Hanning window is used on the Blackman-Tukey method. The MEM direct on the data (BRGMEM) method is represented by the segment and average technique of 9 segments at 2048 data points per segment. Figures 7.10 - 7.12 represent the multichannel cross-spectral magnitude, phase, and coherence squared estimates respectively. Again, the phase estimates shown are the absolute value of the phase estimates. A series of three graphs for each estimate, numbered a, b, and c, are shown for the different multichannel spectral analysis methods listed below.

- (1) Graph a:
BTSPEC, Hanning window,

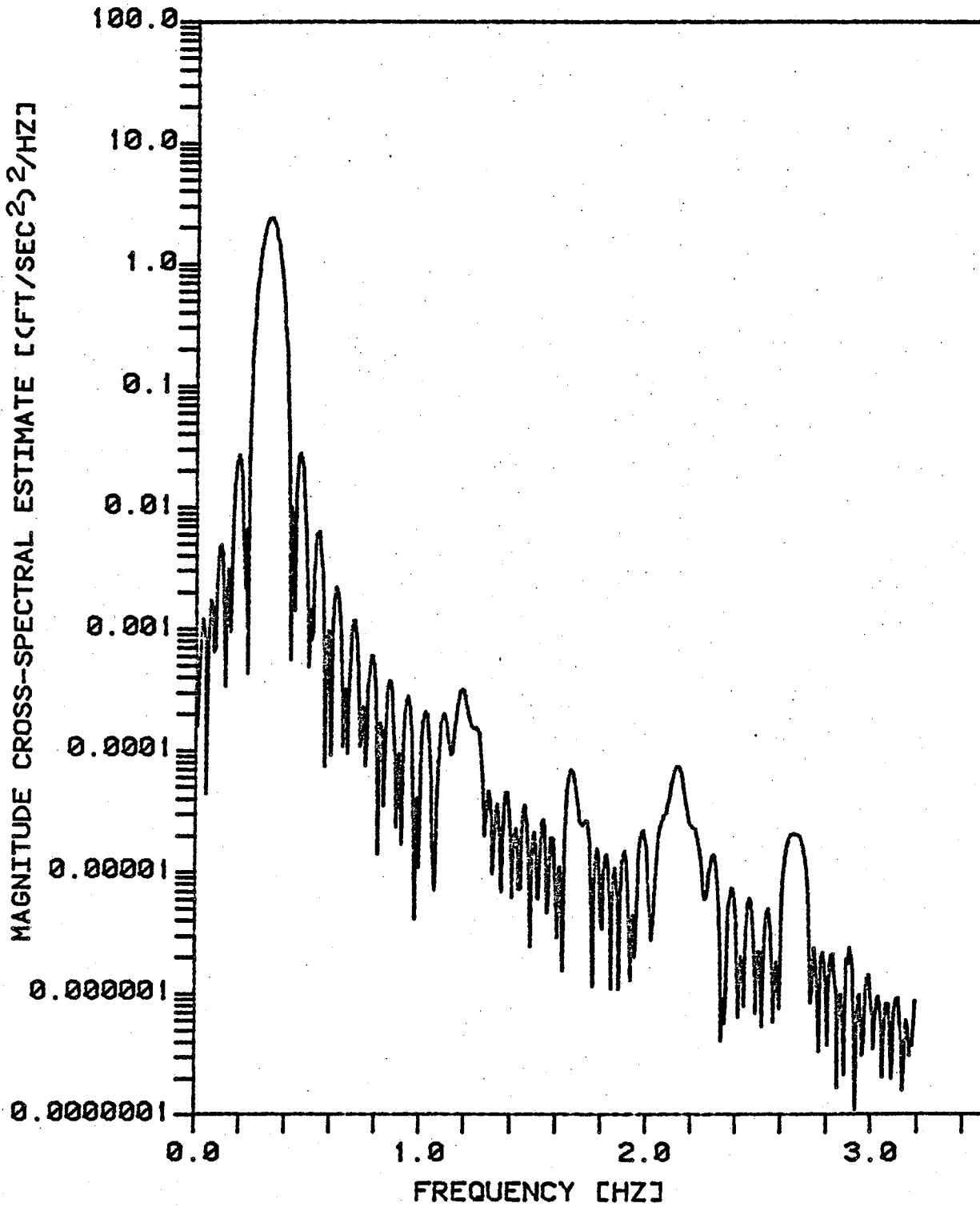


FIGURE NO. 7.10A
COMPARISON OF MAGNITUDE CROSS-SPECTRUM
BTSPEC, HANNING WINDOW, NLAG = 80

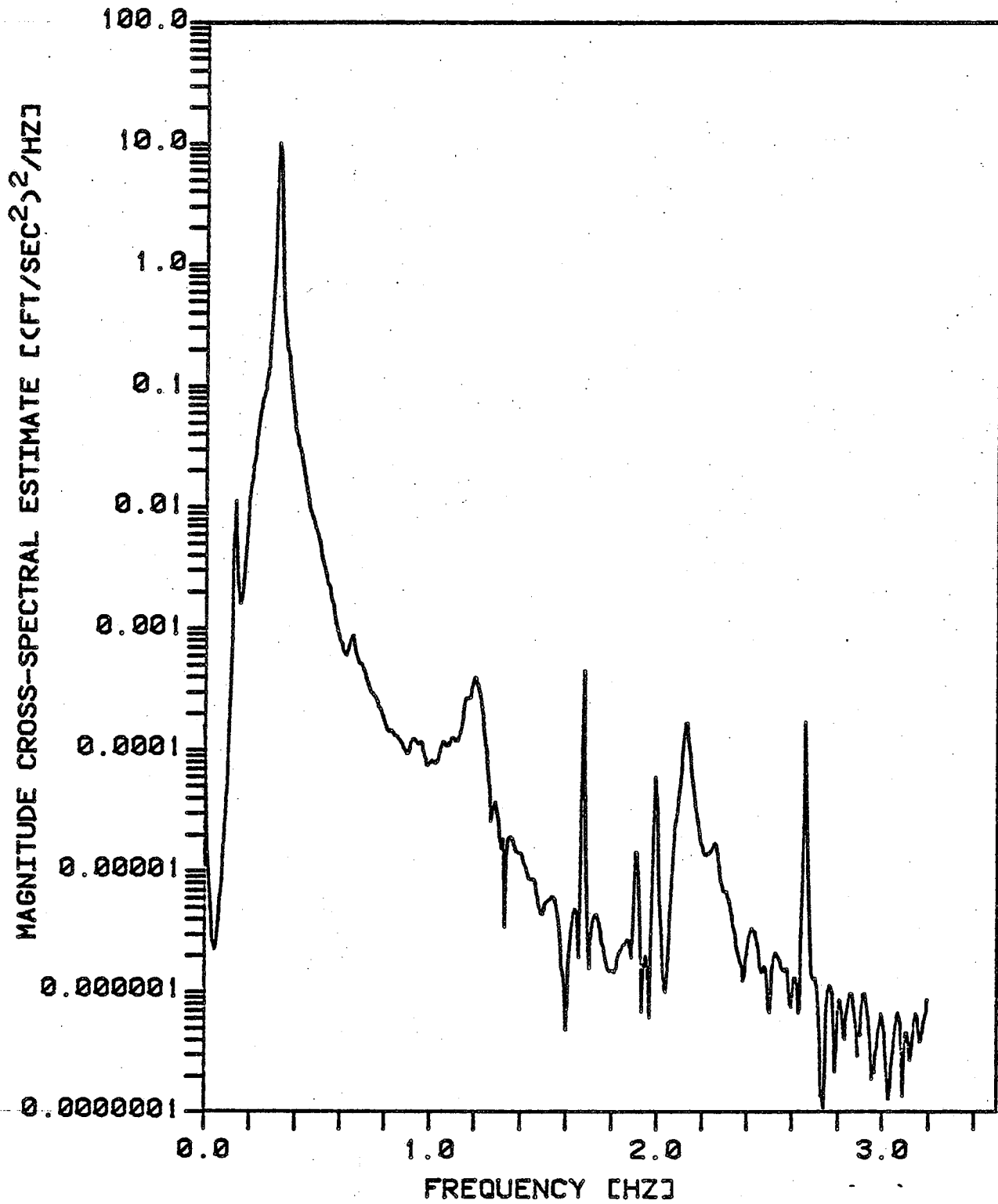


FIGURE NO. 7.10B
COMPARISON OF MAGNITUDE CROSS-SPECTRUM
BRGMEM, NSEG = 9, M = 2048, NLAG = 80

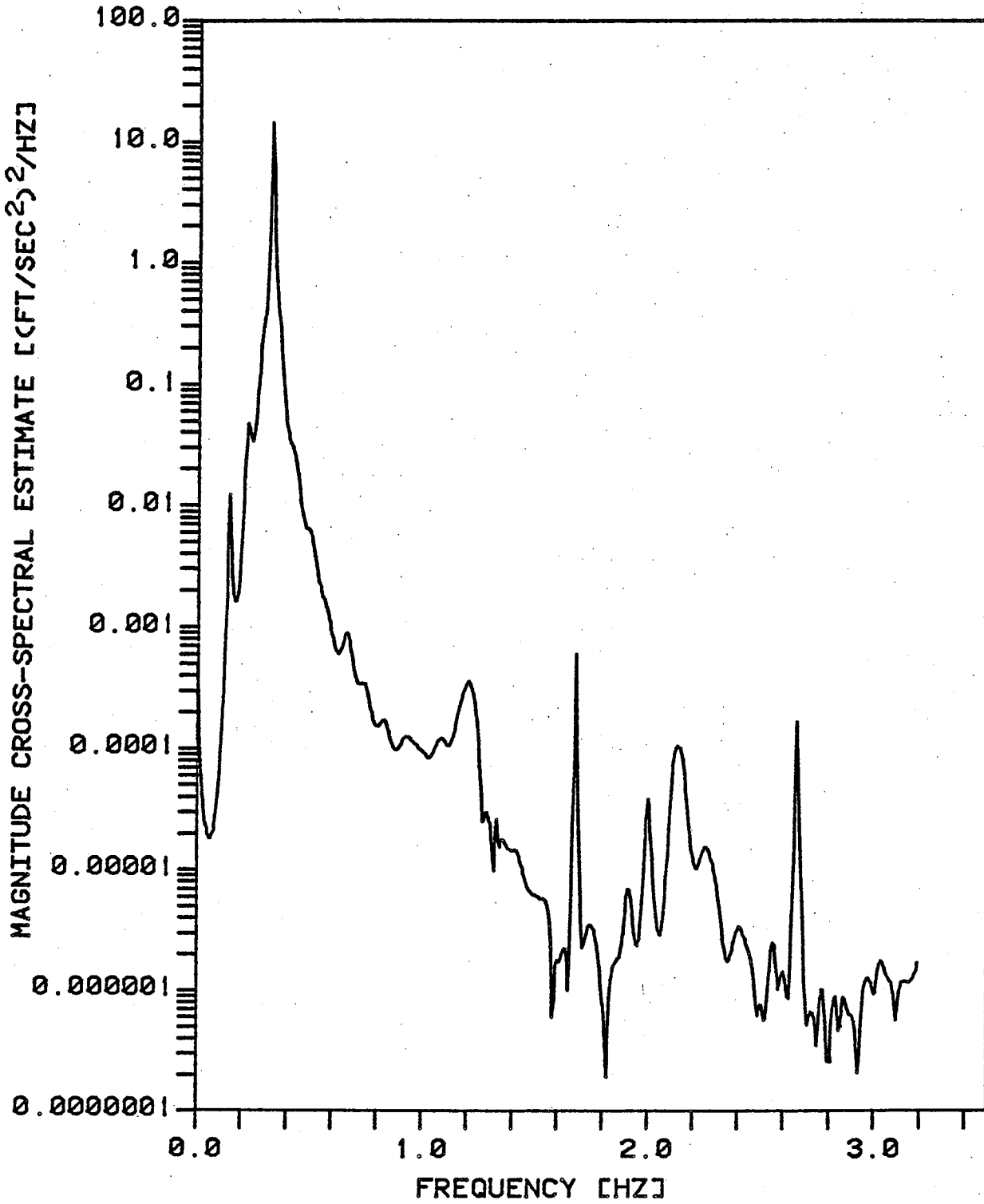


FIGURE NO. 7.10C
COMPARISON OF MAGNITUDE CROSS-SPECTRUM
RYWMEM, NLAG = 80

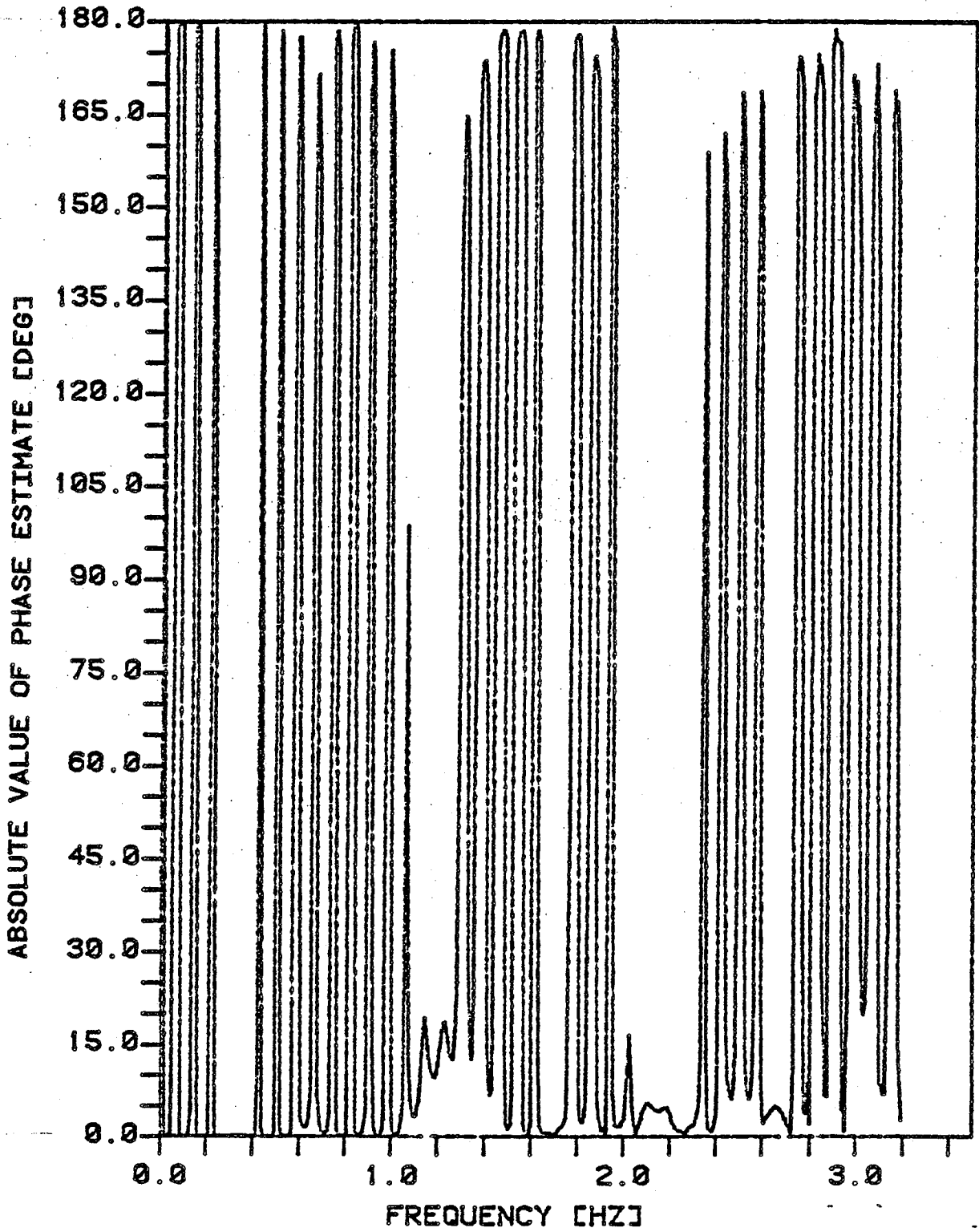


FIGURE NO. 7.11A
COMPARISON OF PHASE ESTIMATES
BTSPEC, HANNING WINDOW, NLAG = 80

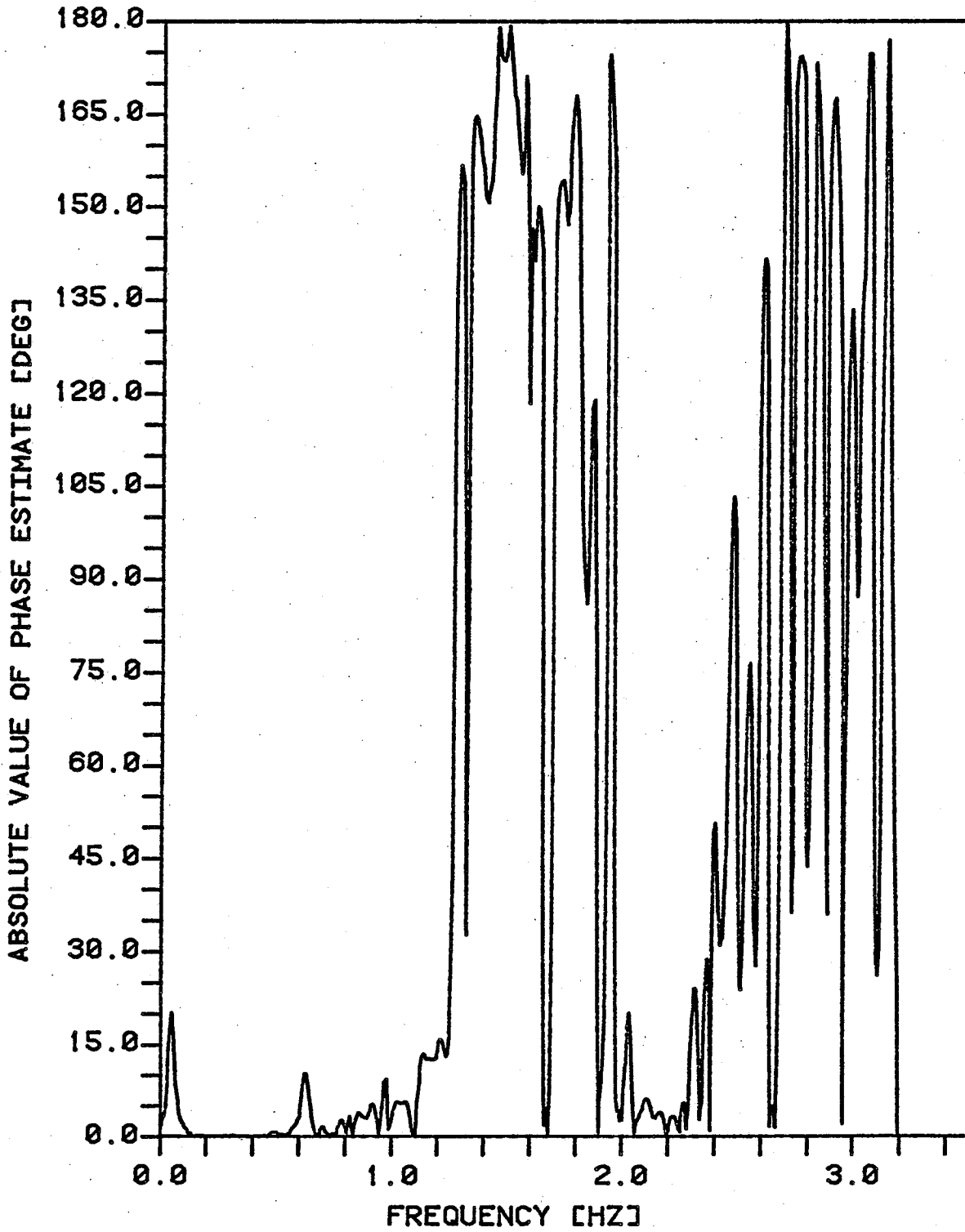


FIGURE NO. 7.11B
COMPARISON OF PHASE ESTIMATES
BRGMEM, NSEG = 9, M = 2048, NLAG = 80

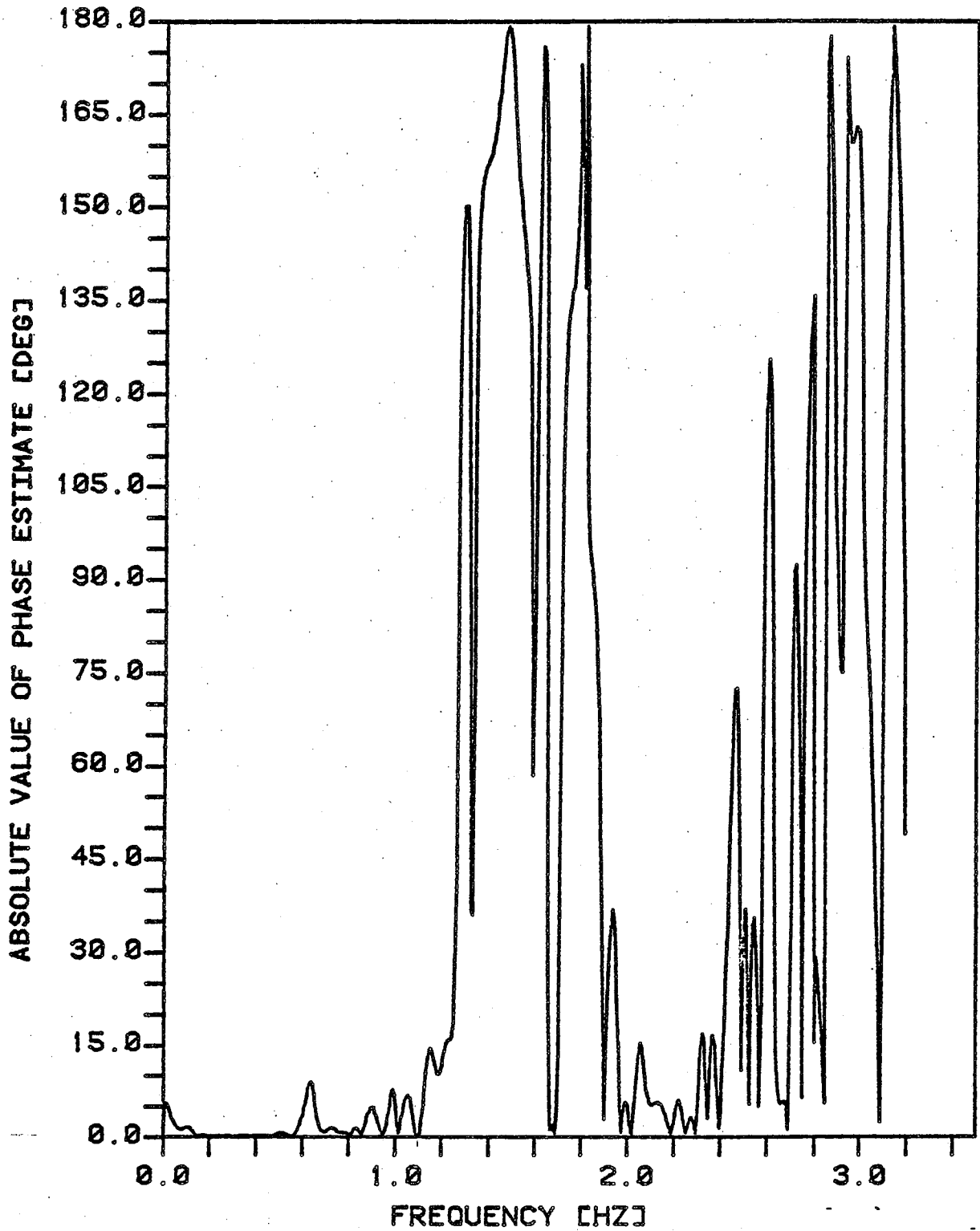


FIGURE NO. 7.11C
COMPARISON OF PHASE ESTIMATES
RYWMEM, NLAG = 80

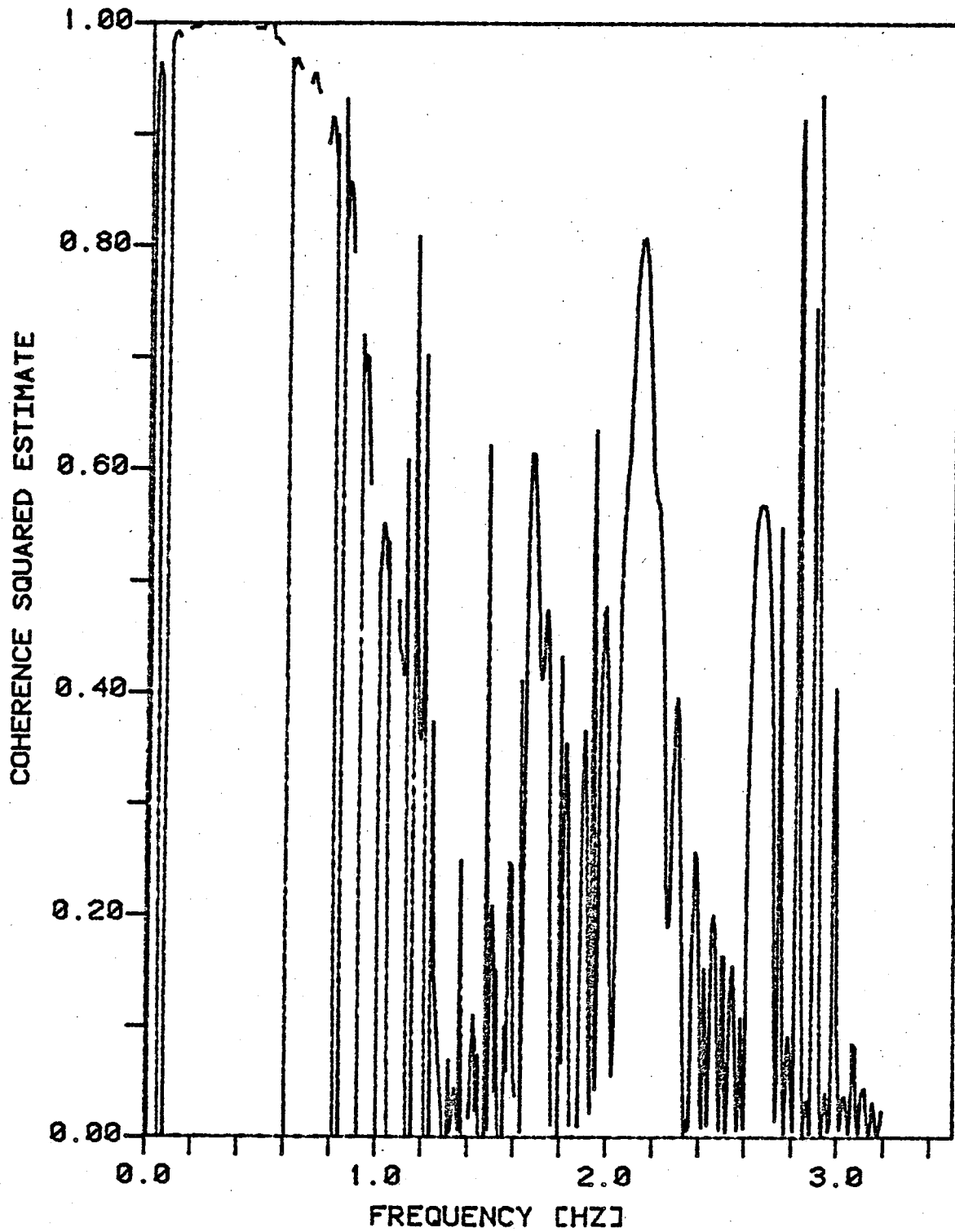


FIGURE NO. 7.12A
COMPARISON OF COHERENCE ESTIMATES
BTSPEC, HANNING WINDOW, NLAG = 80

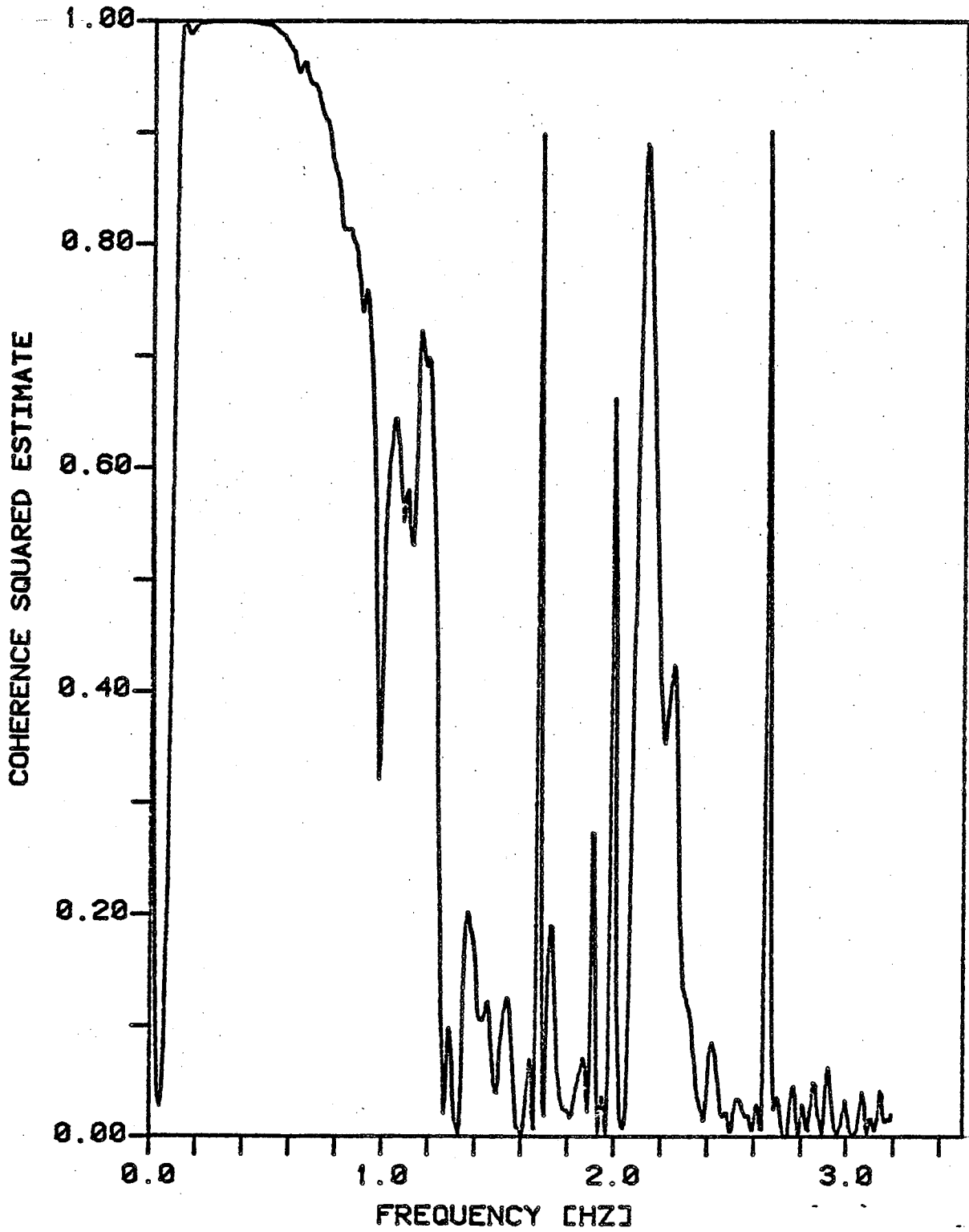


FIGURE NO. 7.12B
COMPARISON OF COHERENCE ESTIMATES
BRGMEM, NSEG = 9, M = 2048, NLAG = 80

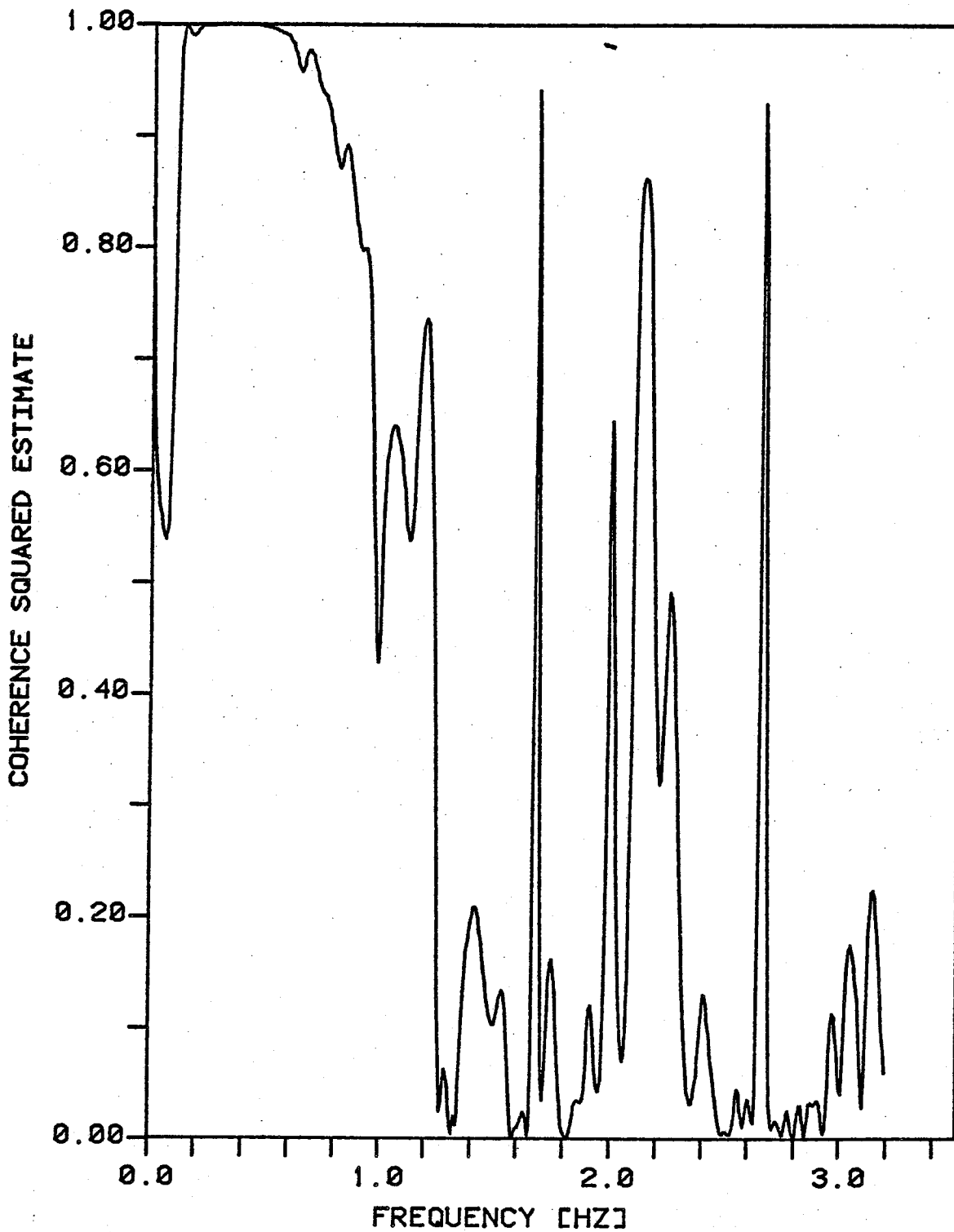


FIGURE NO. 7.12C
COMPARISON OF COHERENCE ESTIMATES
RYWMEM, NLAG = 80

- (2) Graph b:
BRGMEM, 9 segments @ 2048 points,
- (3) Graph c:
RYWMEM.

Each of the BTSPEC, BRGMEM, and RYWMEM methods is shown with a window duration or model order of 80, selected based on Akaike's Final Prediction Error (FPE) model order criterion.

Obviously, the BTSPEC curves don't even come close at this low a window duration of correctly calculating the cross-spectral estimates. A resolution bandwidth, B_e , of 0.1067 Hz was used. The effect of sidelobe leakage on the cross-spectral magnitude estimate is clearly seen in Figure 7.10a. Both multichannel MEM methods, however, give reasonable results. The RYWMEM results seem to be smoother overall than those calculated using the BRGMEM method. The cross-spectral magnitude estimates obtained using the RYWMEM method appear to somewhat more pronounced in the higher frequency range than the corresponding estimates obtained with the BRGMEM method. Also, the RYWMEM method gives phase estimates with less fluctuations than the BRGMEM method. When shorter data segments of 512 points each were averaged using the BRGMEM method (the same total number of data points), these fluctuations in the phase estimates were eliminated (graph not shown).

Thus, either of the multichannel MEM methods will give superior results relative to conventional multichannel spectral analysis methods. One of the reasons why the

Blackman-Tukey method gave such good comparative results is due to the large amount of data processed. The real time and cost saving of the MEM method is in its ability to calculate spectral estimates using only small amounts of data with low model orders or filter lengths. The BRGMEM method can be used to give reasonable spectral estimates where the segmenting and averaging technique is employed and large amounts of data are not processed. Otherwise, excessive amounts of computer storage and time are required relative to the RYWMEM method.

CHAPTER 8
APPLICATION OF MULTICHANNEL MEM METHODS
TO CAISSON RESPONSE RECORDS

In this chapter, the applications of multichannel spectral analysis methods to offshore structures are presented. Specifically, the time series accelerometer data collected on the caisson platform discussed in Chapter 6 is analyzed to determine (1) a dynamic frequency response (ie. transfer function) to wave excitation and (2) mode shape identification of the platform.

8.1 DYNAMIC RESPONSE TO WAVE EXCITATION

The dynamic frequency response to wave excitation is calculated using the wave height data and the north component of the biaxial pair of accelerometers (NAW) located in the center of the wellhead deck in Load Case 1. Figure 8.1 shows 80 seconds of the 4800 seconds (80 minutes) of wave height data collected with the wave staff. The time history has the distinctive characteristics of a Gaussian wide band random process. Figure 8.2 illustrates 80 seconds of the time history of the (NAW) accelerometer. Both time histories contain 512 data points sampled at 6.4 hz.

The two autocorrelations are shown in Figures 8.3 and 8.4 respectively. Both autocorrelations were calculated using the computer program ACORP employing the technique of Oppenheim and Schaffer [1975] of overlap and save FFT's. A

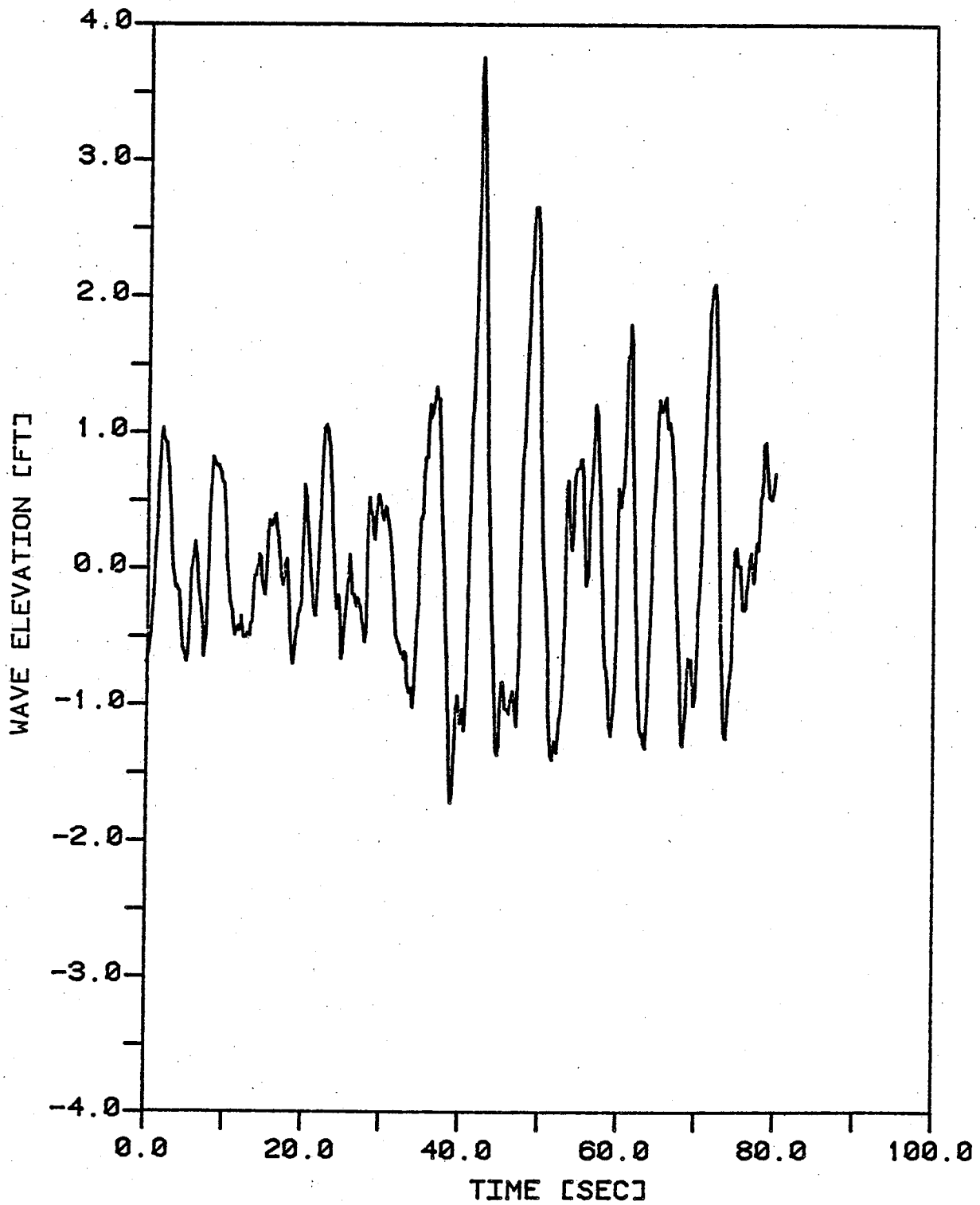


FIGURE NO. 8.1
WAVE HEIGHT TIME HISTORY
LOAD CASE 1

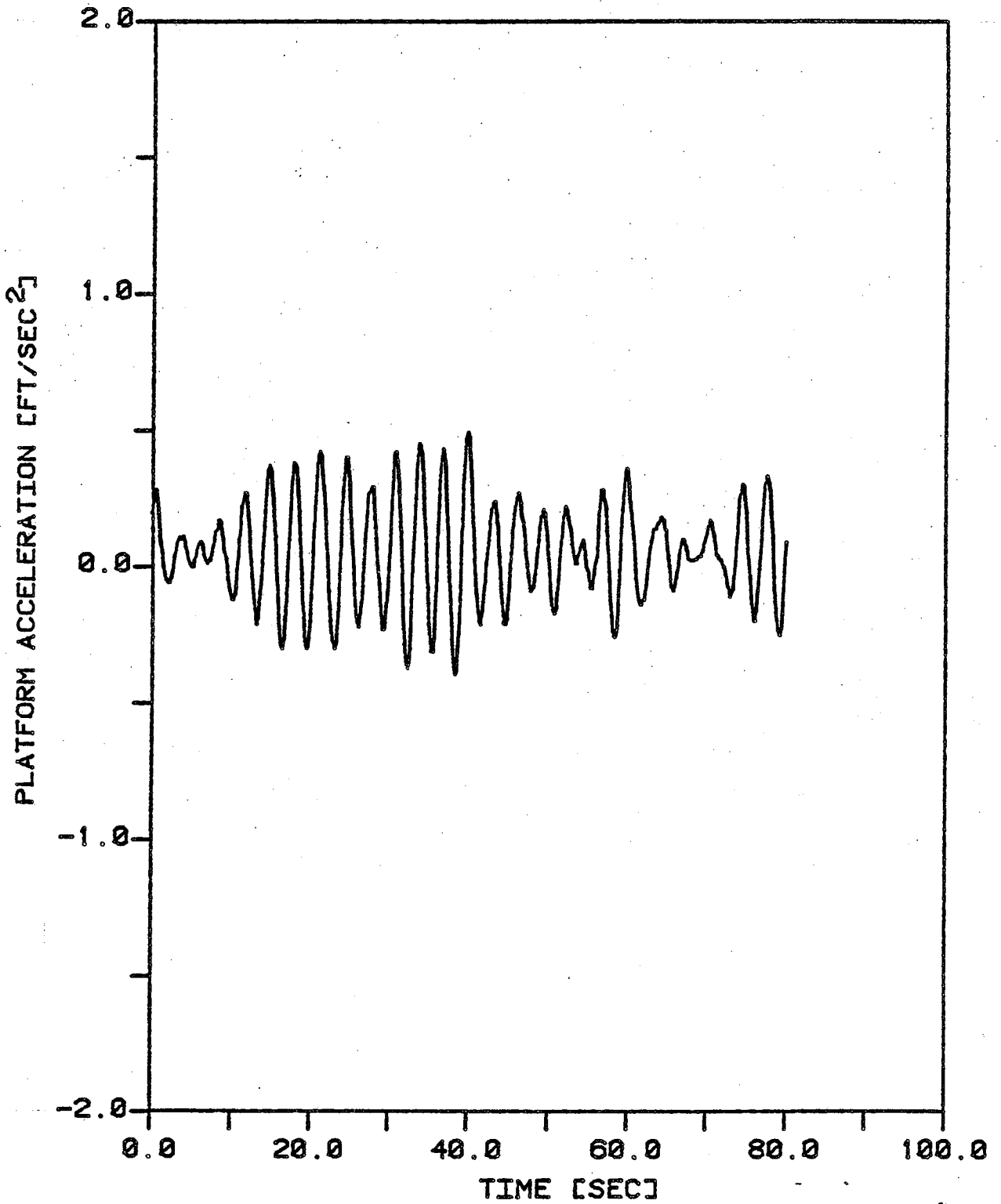


FIGURE NO. 8.2
NAW ACCELEROMETER TIME HISTORY
LOAD CASE 1

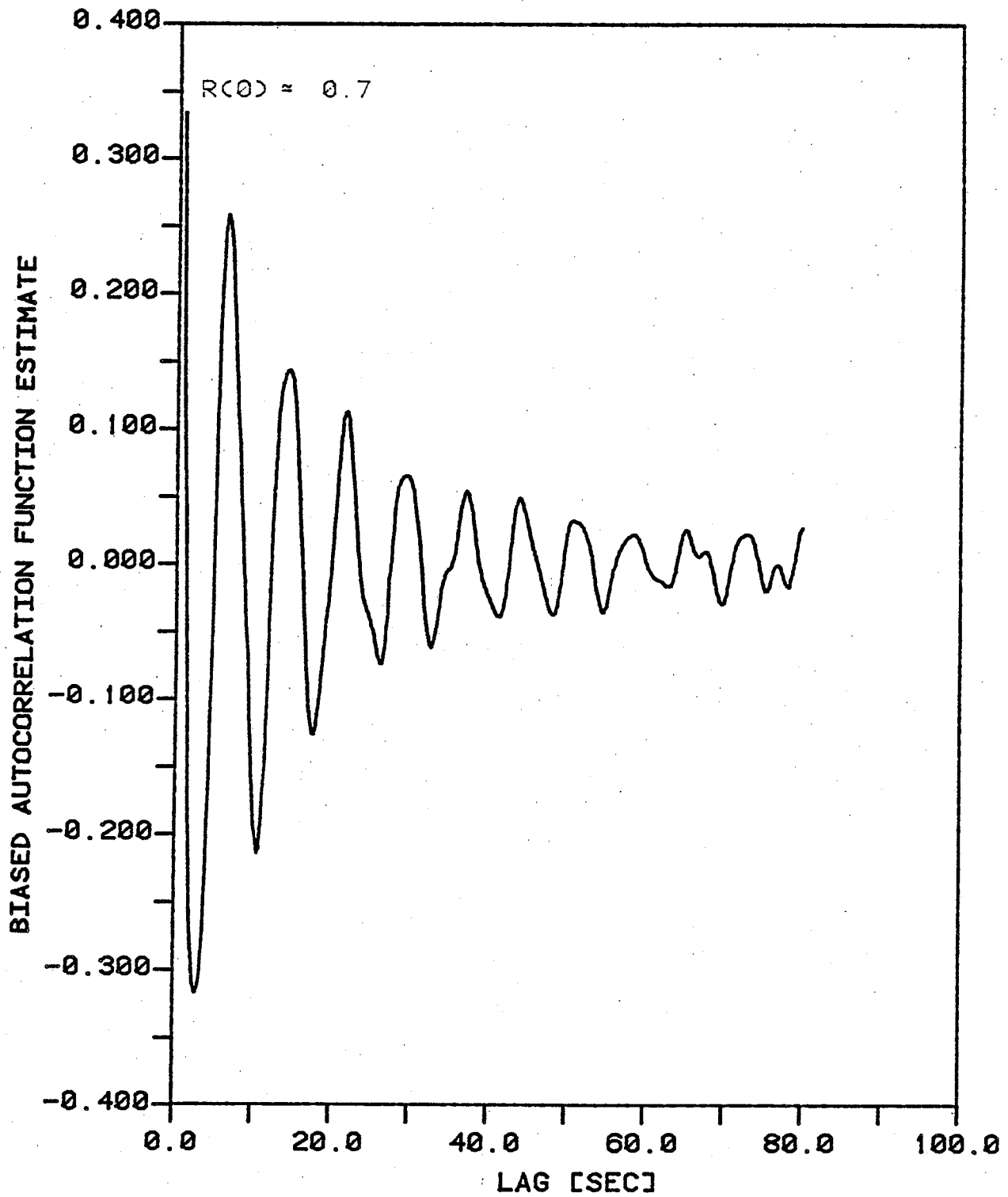


FIGURE NO. 8.3
WAVE HEIGHT AUTOCORRELATION
LOAD CASE 1, MAXLAG = 512, N = 29696

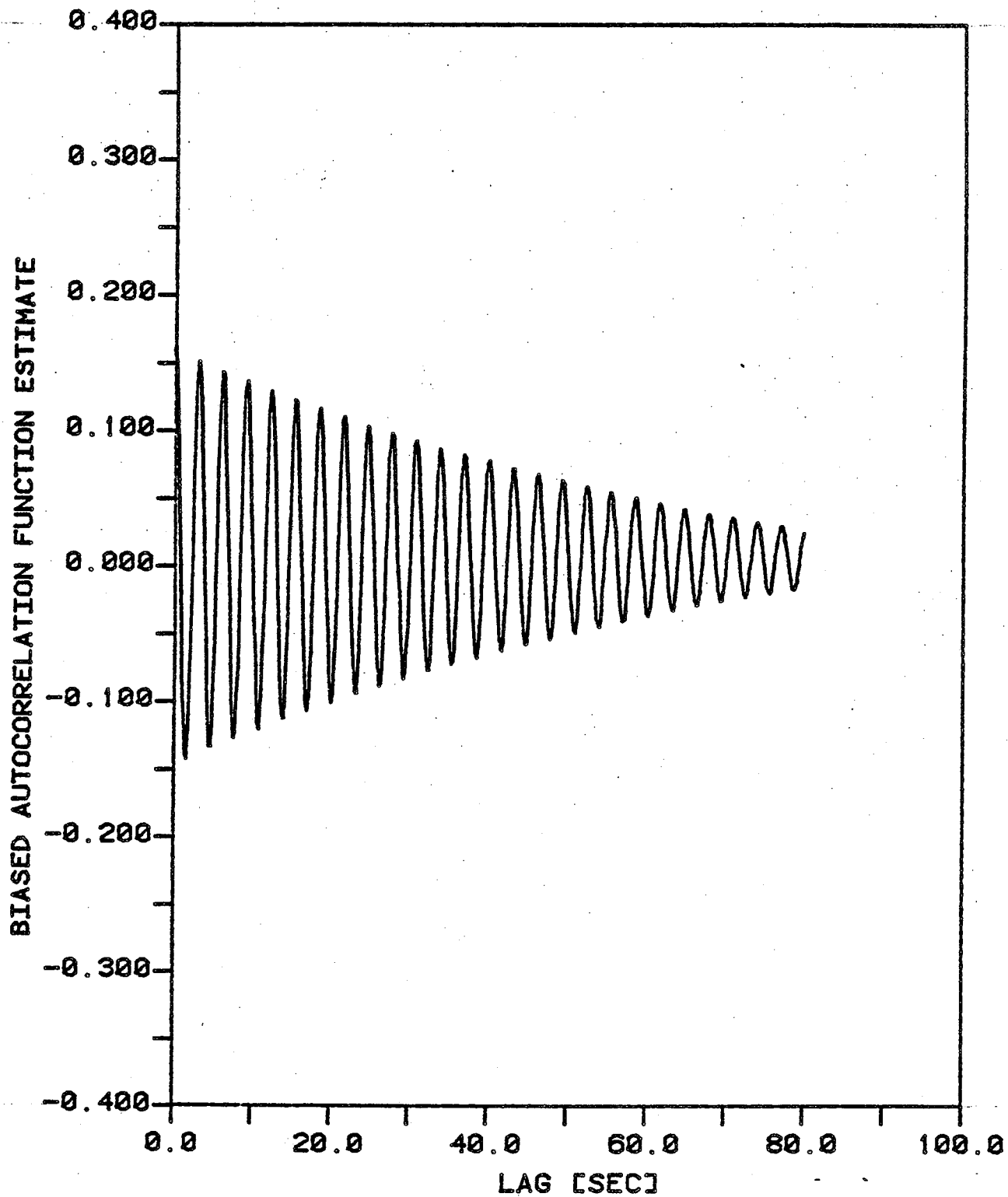


FIGURE NO. 8.4
NAW ACCELEROMETER AUTOCORRELATION
LOAD CASE 1, MAXLAG = 512, N = 29696

total of 58 segments of 512 data points each (29696 total data points) were used to give a DC removed, biased estimate. The autocorrelation of the NAW accelerometer exhibits the classical shape of a Gaussian narrow band random process as one would expect from a Gaussian input to a lightly-damped oscillator.

The cross-correlation is shown in Figure 8.5. The computer program XCOR was used to give a DC removed, biased estimate. The low values for negative lag values indicate that there is not much correlation for past values, which is as it should be for a causal process.

The autospectral estimates for the wave excitation and NAW accelerometer are shown in Figures 8.6 and 8.7 respectively. The auto and cross-spectral estimates were calculated to a model order of 60 lags according to Akaike's FPE model order criterion. The wave height spectrum has the typical "Pierson-Moskowitz" shape. The first or main peak at approximately 0.14 Hz is the predominant frequency of wave energy. The second peak at approximately 0.32 Hz represents a coupling between the wave staff and platform flexure (see Figure 8.7). As discussed in Section 6.4, the wave staff was attached rigidly from the wellhead deck. Therefore, the wave staff physically moved with the platform response.

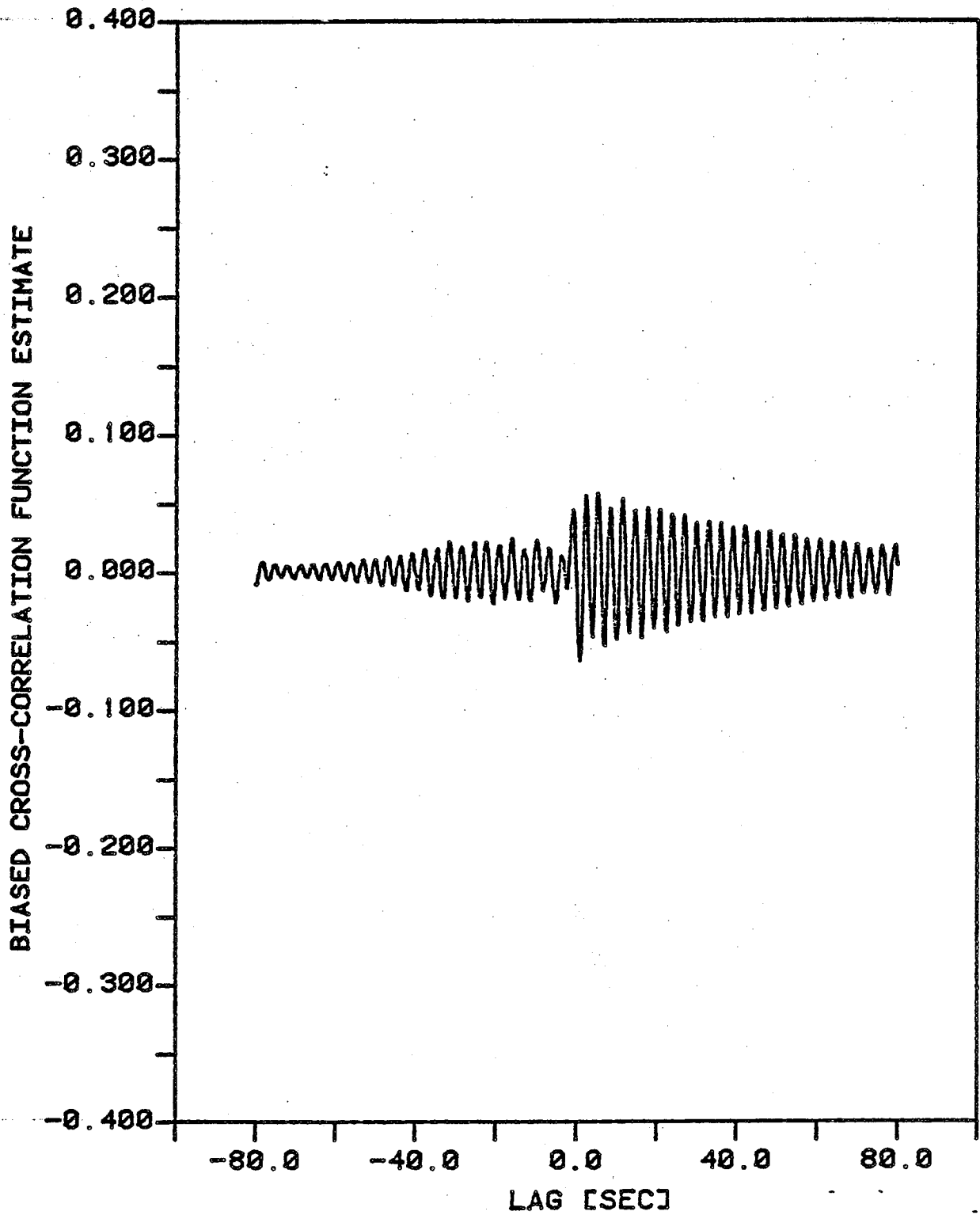


FIGURE NO. 8.5
WAVE AND NAW ACCELEROMETER CROSS-CORRELATION
LOAD CASE 1, MAXLAG = 512 (POS. SIDE), N = 29696

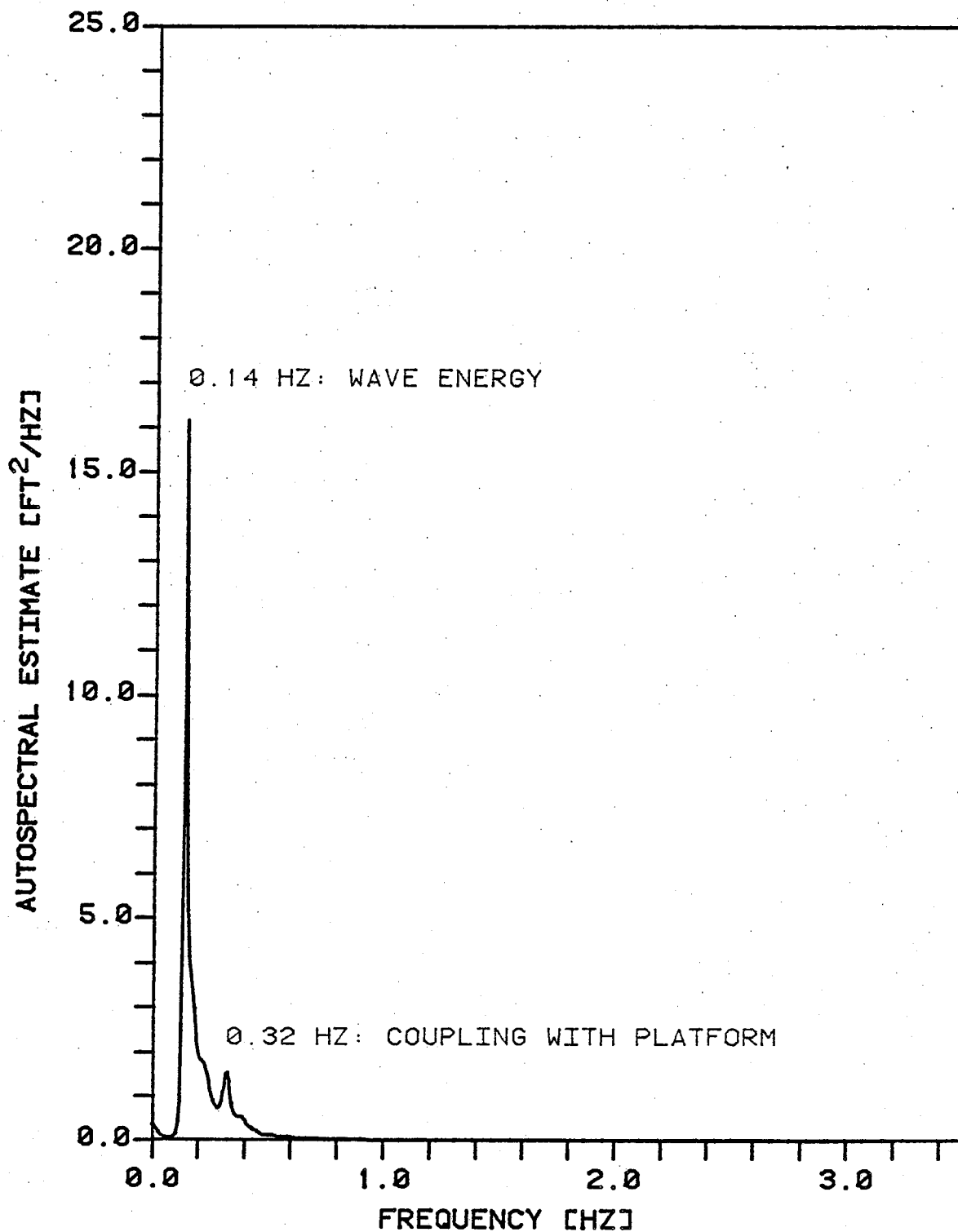


FIGURE NO. 8.6
WAVE HEIGHT AUTOSPECTRUM
LOAD CASE 1, NLAG = 60

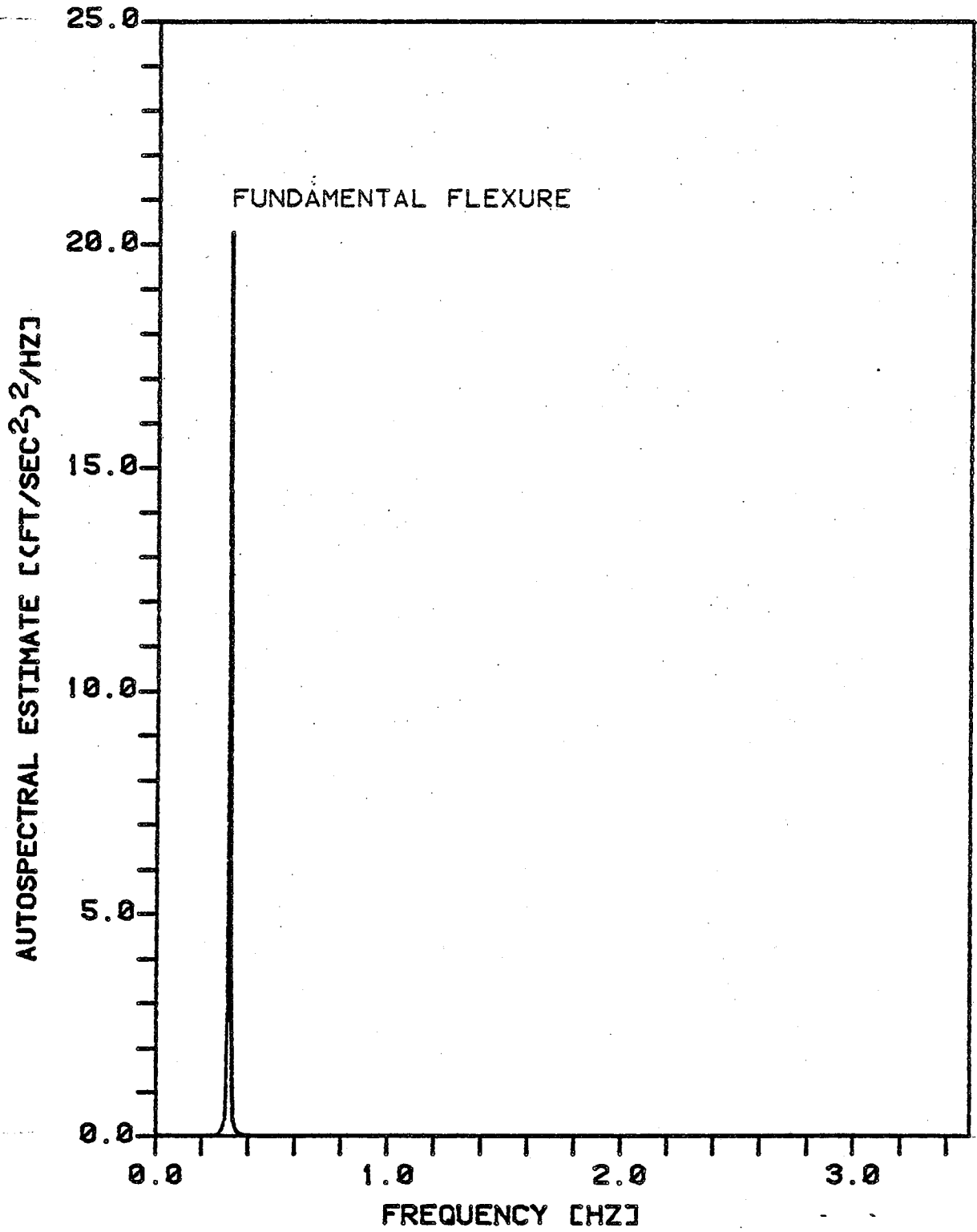


FIGURE NO. 8.7
NAW ACCELEROMETER AUTOSPECTRUM
LOAD CASE 1, NLAG = 60

The results of the cross-spectral analysis are shown in Figures 8.8 - 8.10 for the cross-spectral magnitude, coherence squared, and transfer function estimates respectively. The coherence shows a high degree of correlation (0.7) at 0.32 Hz. The transfer function estimate looks good except for the coupling problem. The second and third peaks at approximately 1.68 and 2.66 Hz are due to noise which shows up in all the time histories. These peaks are identified on all the plots as such. Causes of this noise will be discussed in Section 8.3.

8.2 MODE SHAPE IDENTIFICATION

In this section, the multichannel spectral analysis methods are applied to the caisson platform accelerometer data to determine mode shapes. The flexural and torsional mode shapes are evaluated using the transfer function estimates.

8.2.1 Flexural Modes

The helicopter (NAH) and wellhead (NAW) deck accelerometers of Load Case 2 are presented in this section as an example of the mode shape identification procedure. As discussed in Chapter 6, both had the same northerly orientation and were located in the same vertical plane through the center of the caisson platform. The NAH and NAW accelerometer time histories are shown in Figures 8.11 and

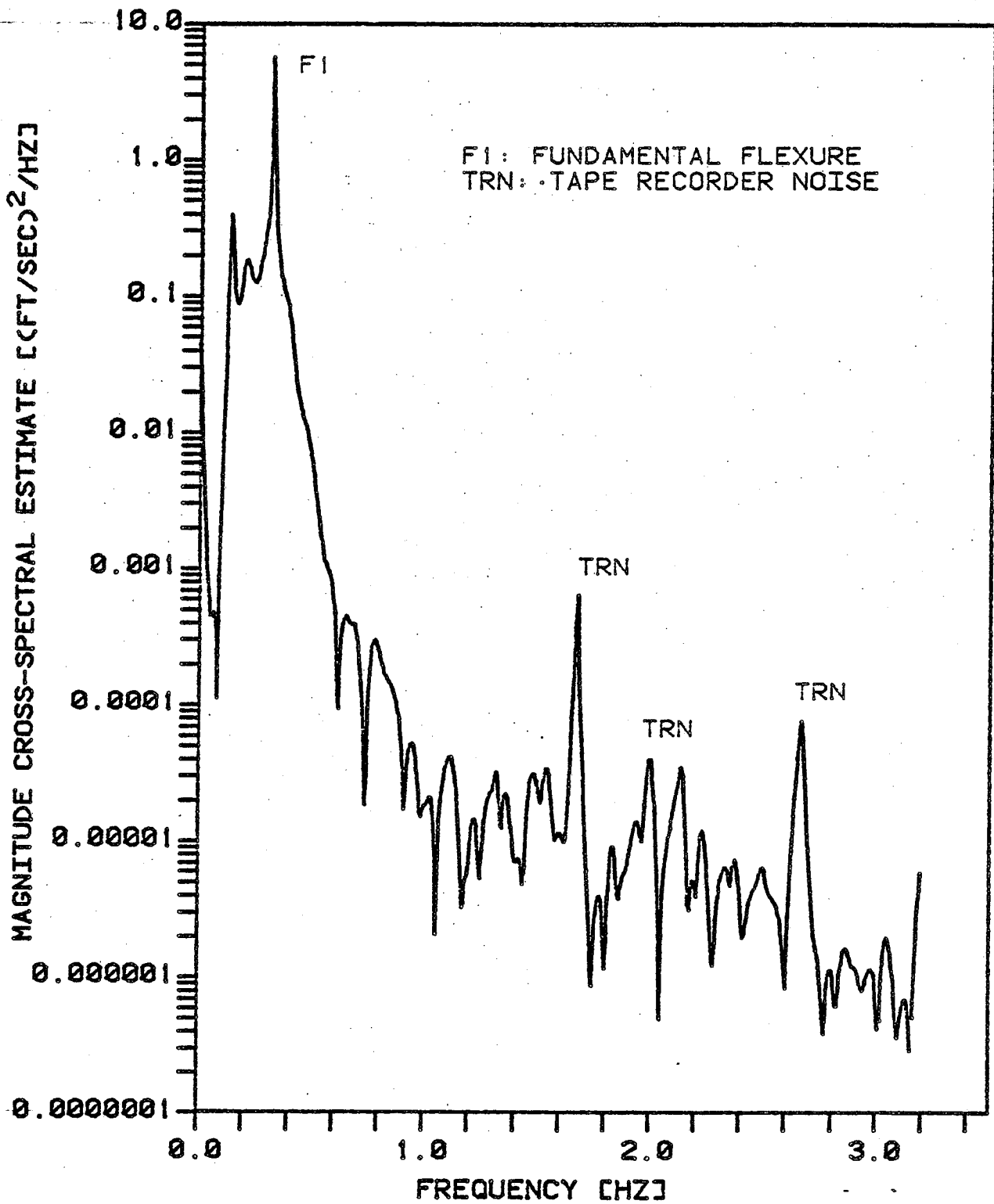


FIGURE NO. 8.8
WAVE HEIGHT AND NAW ACCELEROMETER MAGNITUDE
CROSS-SPECTRUM - LOAD CASE 1, NLAG = 60

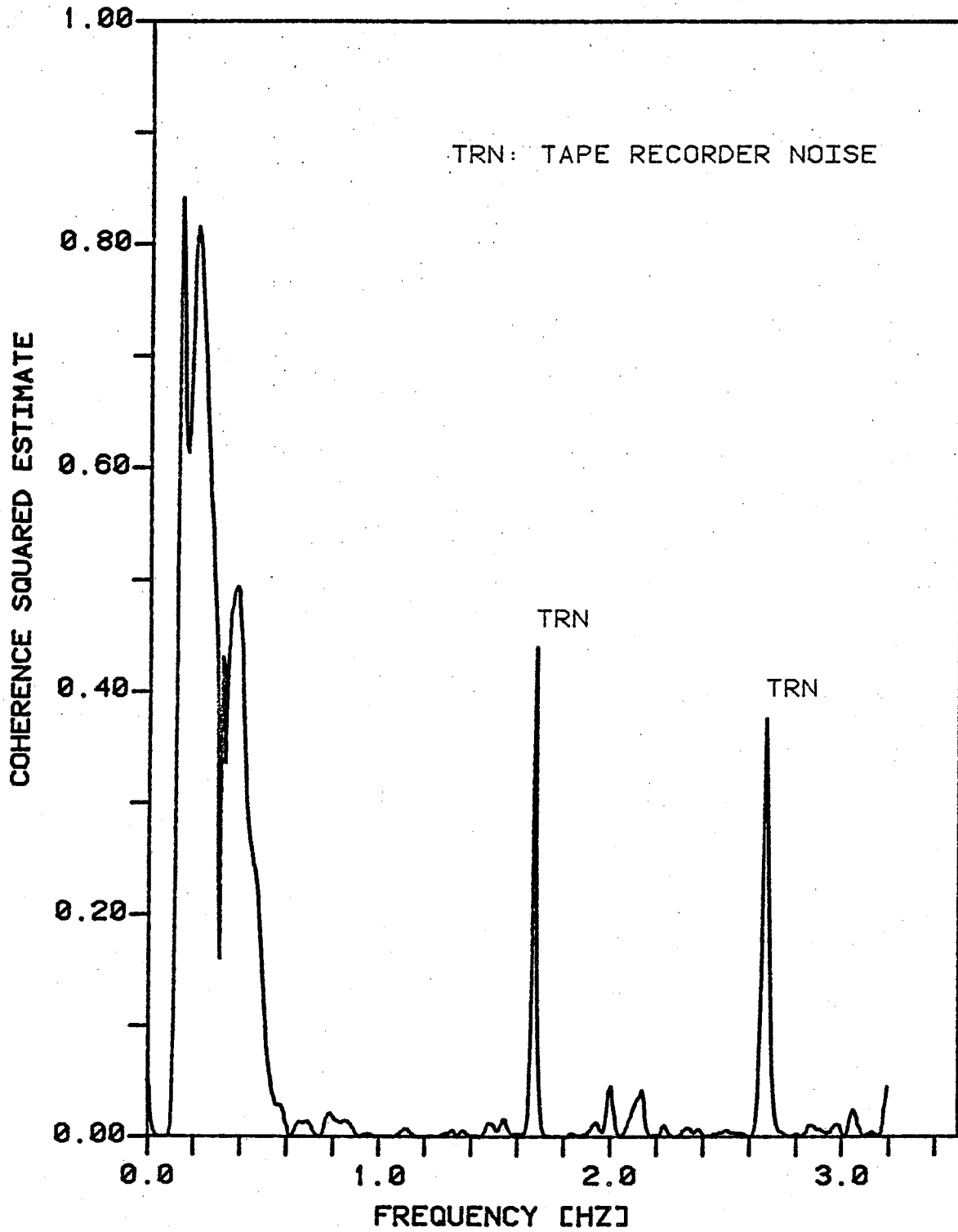


FIGURE NO. 8.9
WAVE HEIGHT & NAW ACCELEROMETER COHERENCE ESTIMATE
LOAD CASE 1, NLAG = 60

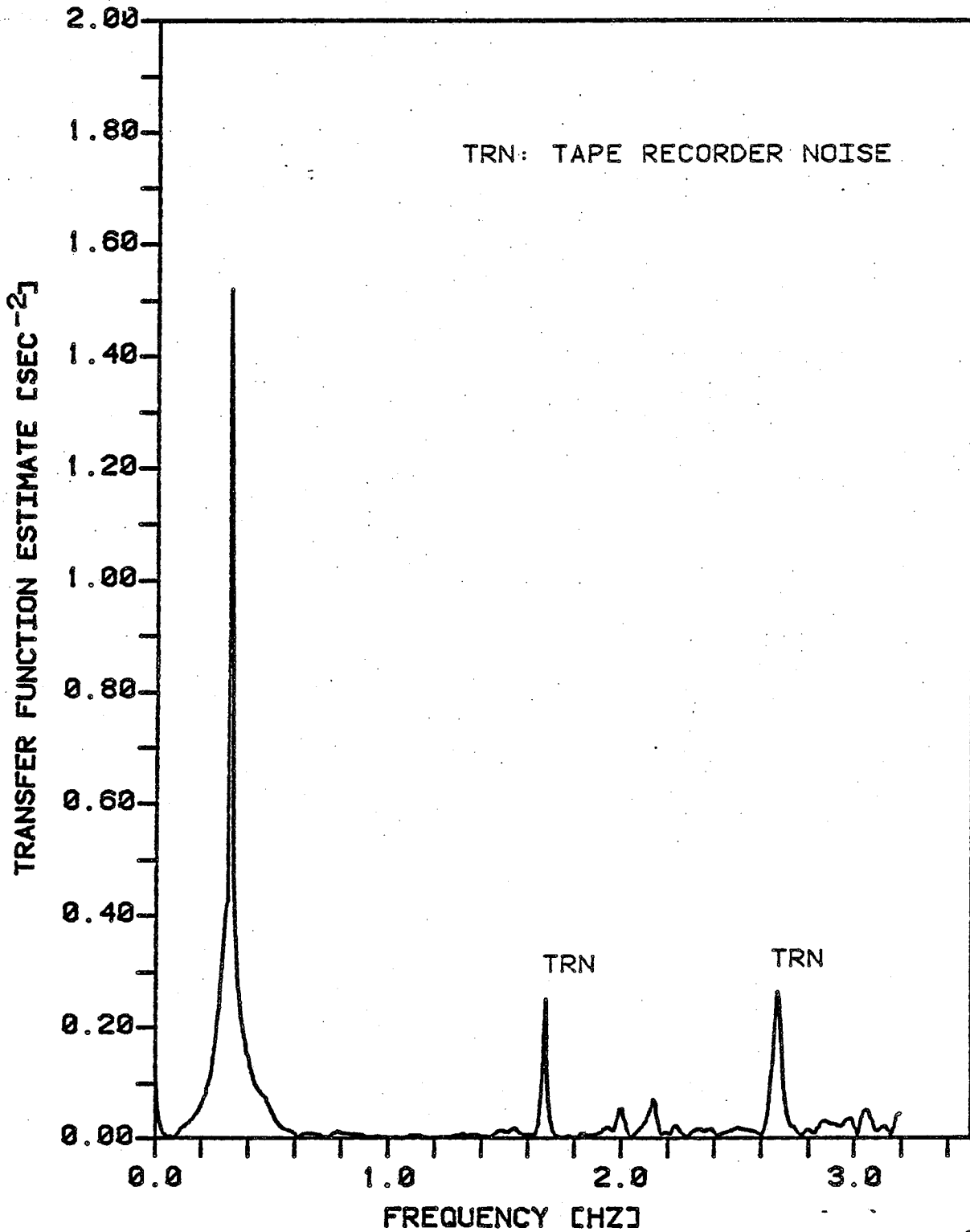


FIGURE NO. 8.10
WAVE HEIGHT & NAW ACCELEROMETER TRANSFER FUNCTION
ESTIMATE - LOAD CASE 1, NLAG = 60

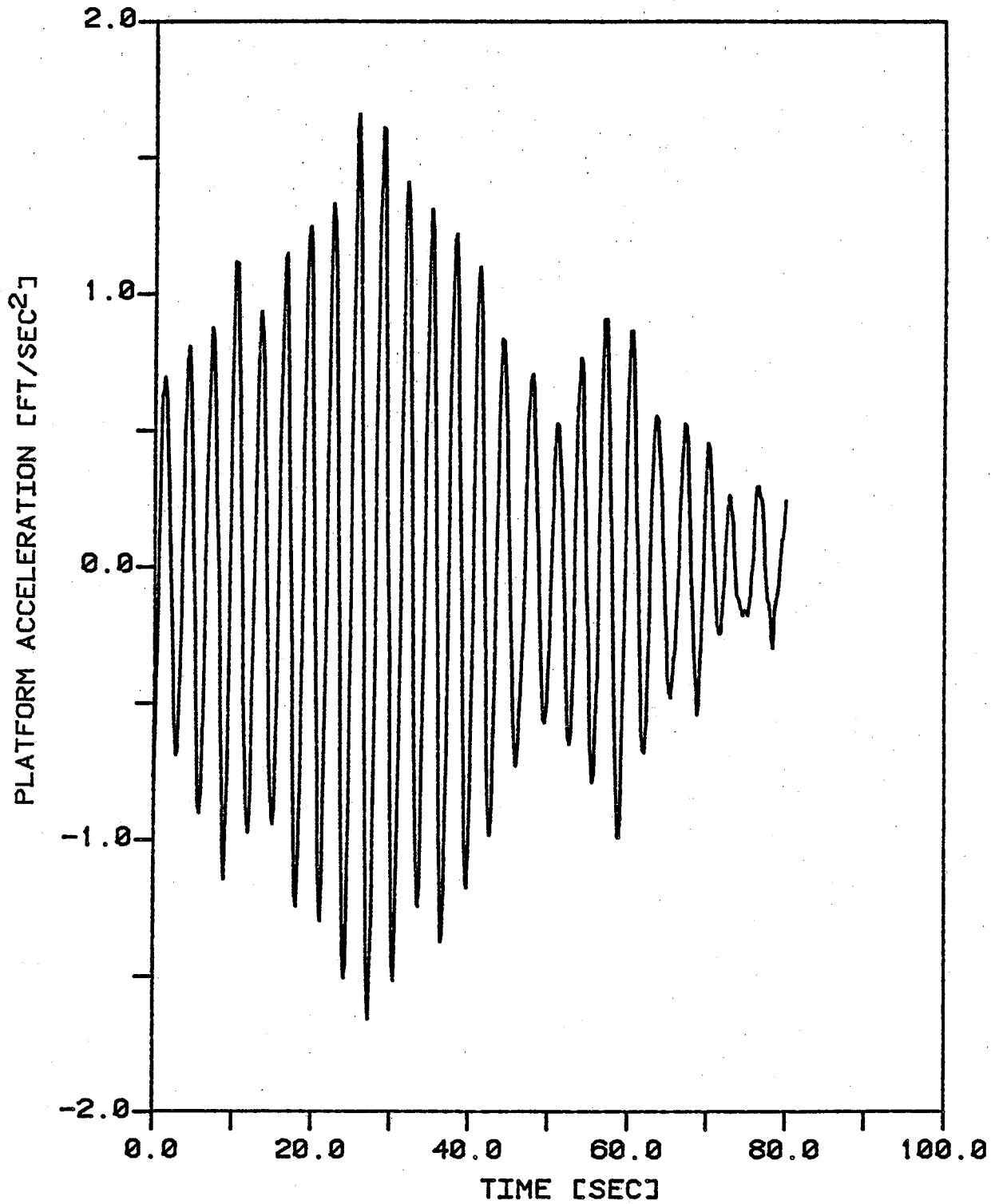


FIGURE NO. 8.11
NAH ACCELEROMETER TIME HISTORY
LOAD CASE 2

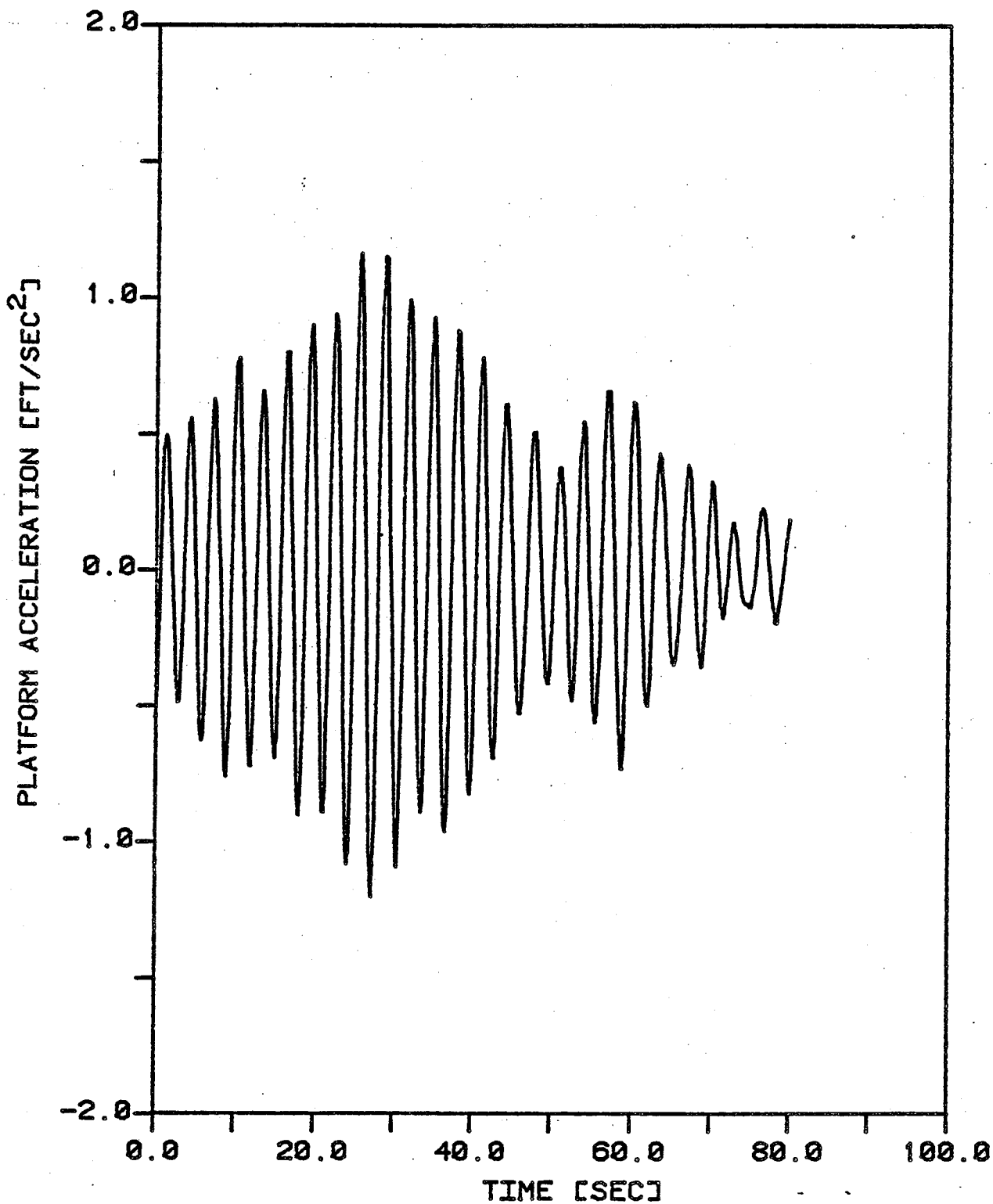


FIGURE NO. 8.12
NAW ACCELEROMETER TIME HISTORY
LOAD CASE 2

8.12 respectively. Again, each curve represents 80 seconds (512 data points) of data with a sampling frequency of 6.4 Hz. Both time histories have the same shape as they both have the same orientation. Note that the magnitude of the wellhead deck response is less than that of the helicopter deck.

The corresponding autocorrelations are shown in Figures 8.13 and 8.14. Again, the computer program ACORP was used with 58 segments of 512 data points each (29696 total data points) to obtain a DC removed, biased correlation function estimate. The maximum lag length is 80 seconds or 512 lags. Note that both curves have the same shape.

The cross-correlation is shown in Figure 8.15. Again, the computer program XCOR was used. The same input parameters used in the computer program ACORP were used here. Both auto and cross-correlations exhibit the classical shapes of a Gaussian narrow band random process.

Based on Akaike's FPE model order criterion for the BRGMEM direct on the data MEM method, an optimum value of 80 lags was used in the cross-spectral analysis. Figures 8.16 and 8.17 illustrate the autospectral estimates for the helicopter and wellhead decks respectively. Only the fundamental flexural peak can be discerned using linear plots as this peak at approximately 0.32 Hz possesses most of the spectral energy of the response spectra for both accelerometers.

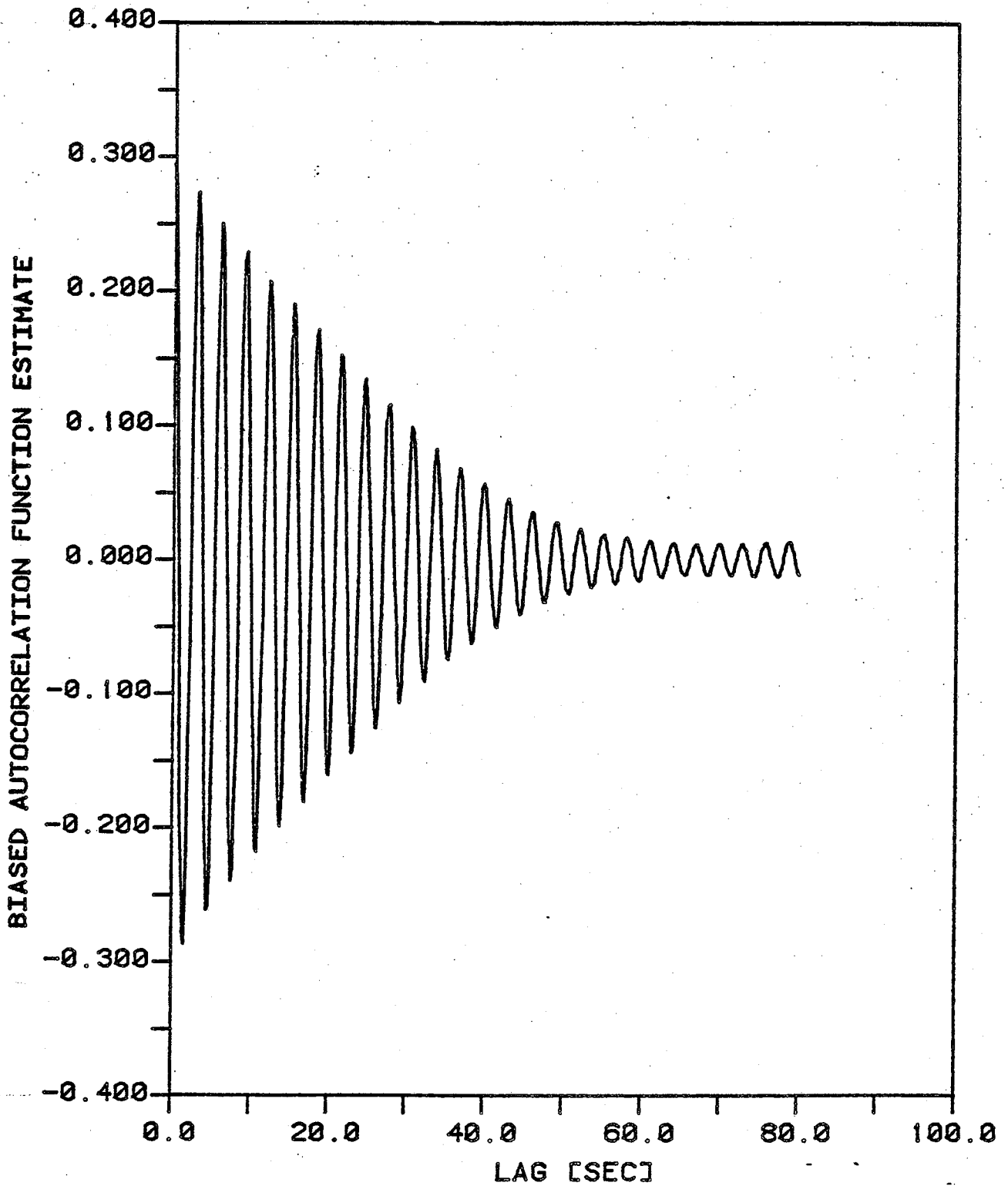


FIGURE NO. 8.13
NAH ACCELEROMETER AUTOCORRELATION
LOAD CASE 2, MAXLAG = 512, N = 29696

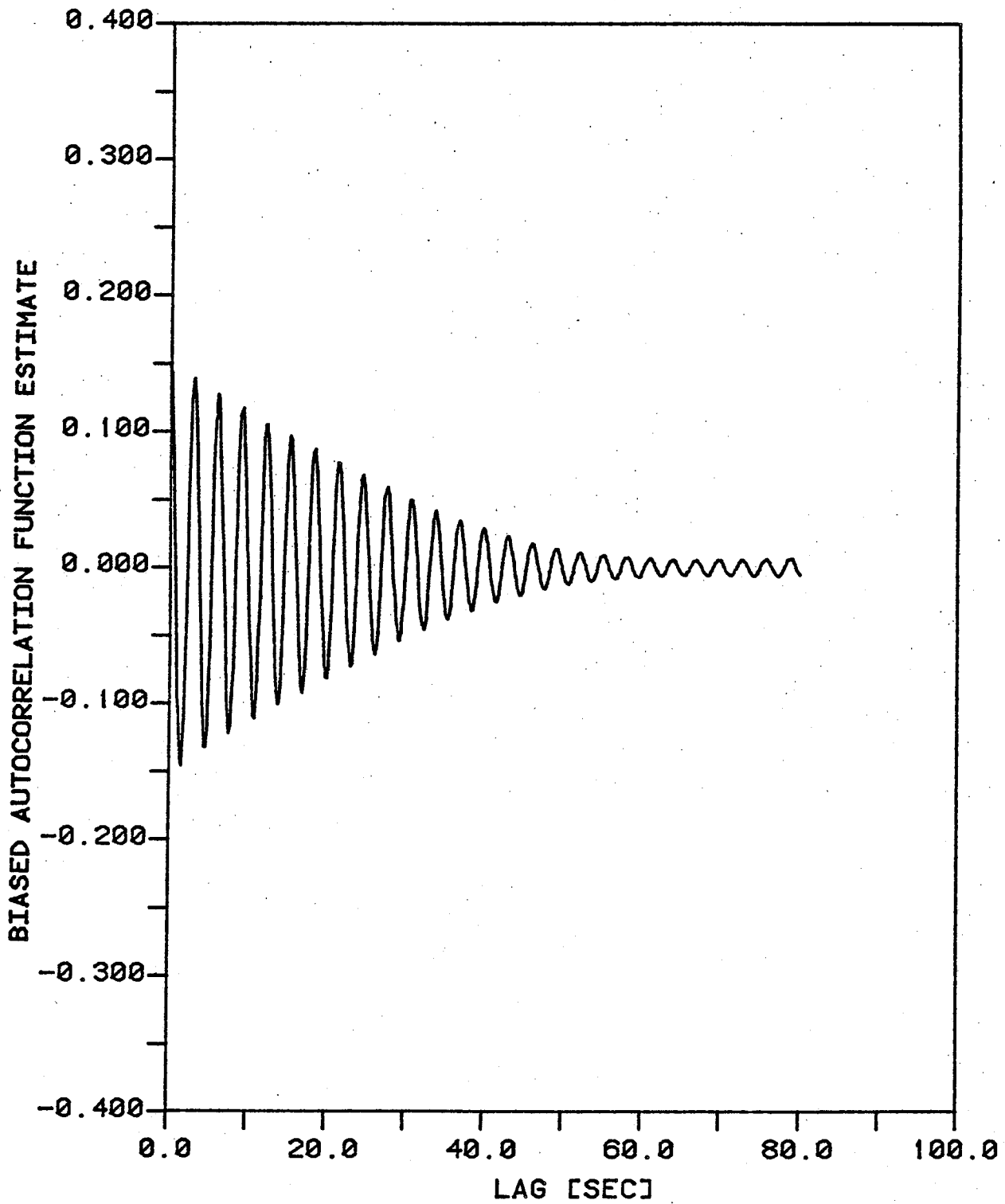


FIGURE NO. 8.14
NAW ACCELEROMETER AUTOCORRELATION
LOAD CASE 2, MAXLAG = 512, N = 29696

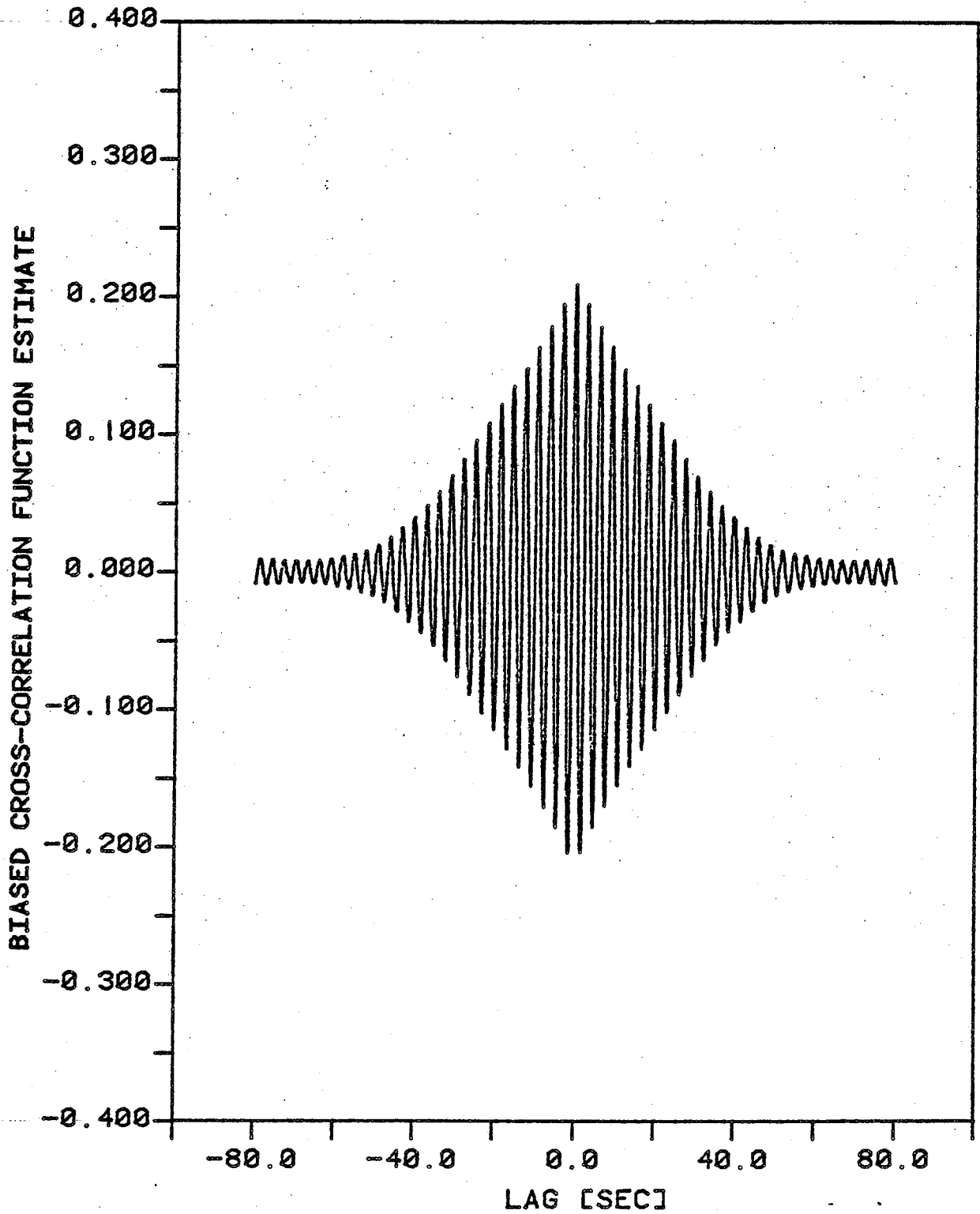


FIGURE NO. 8.15
NAH & NAW ACCELEROMETER CROSS-CORRELATION
LOAD CASE 2, MAXLAG =512 (POS. SIDE), N = 29696

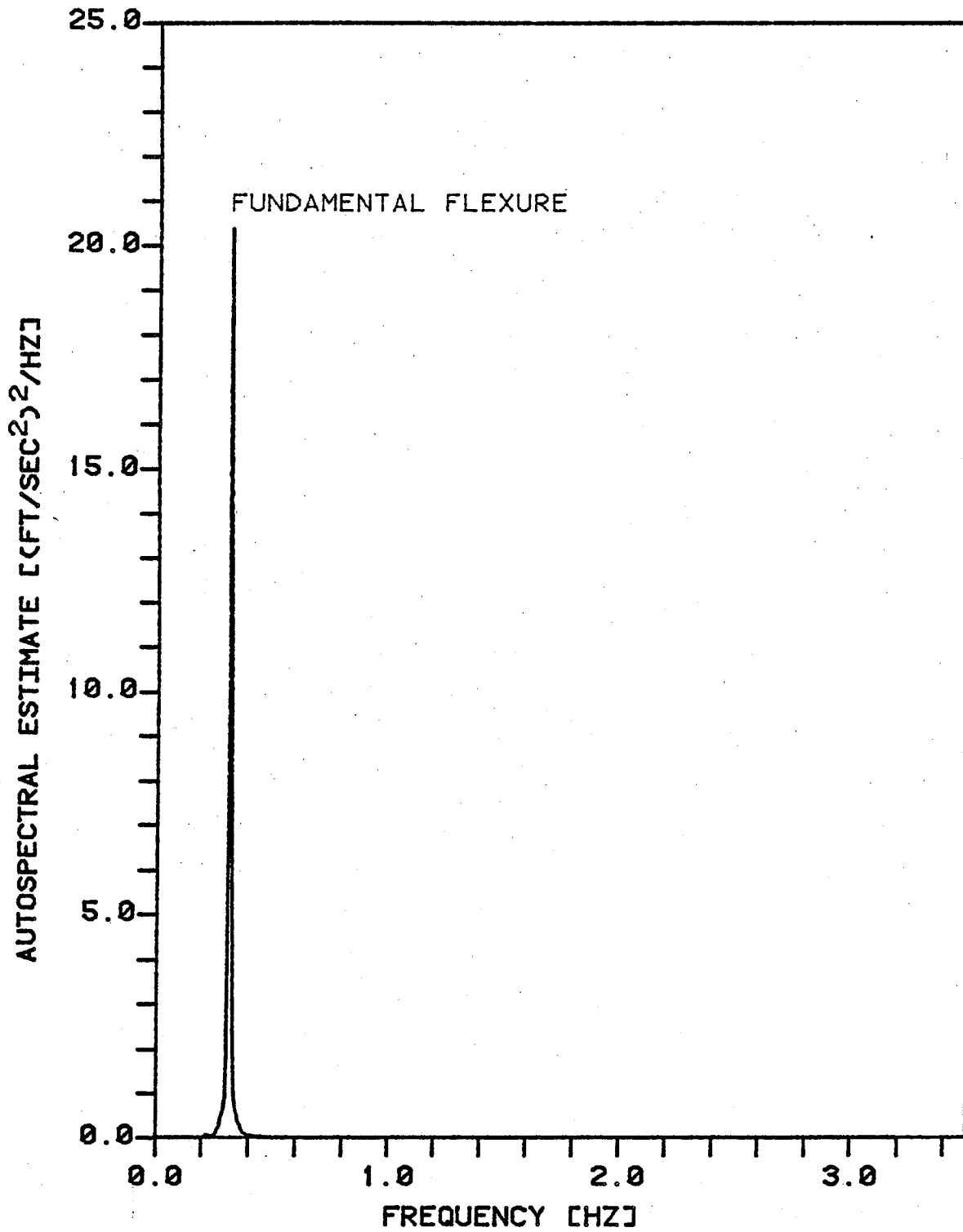


FIGURE NO. 8.16
NAH ACCELEROMETER AUTOSPECTRUM
LOAD CASE 2, NLAG = 80

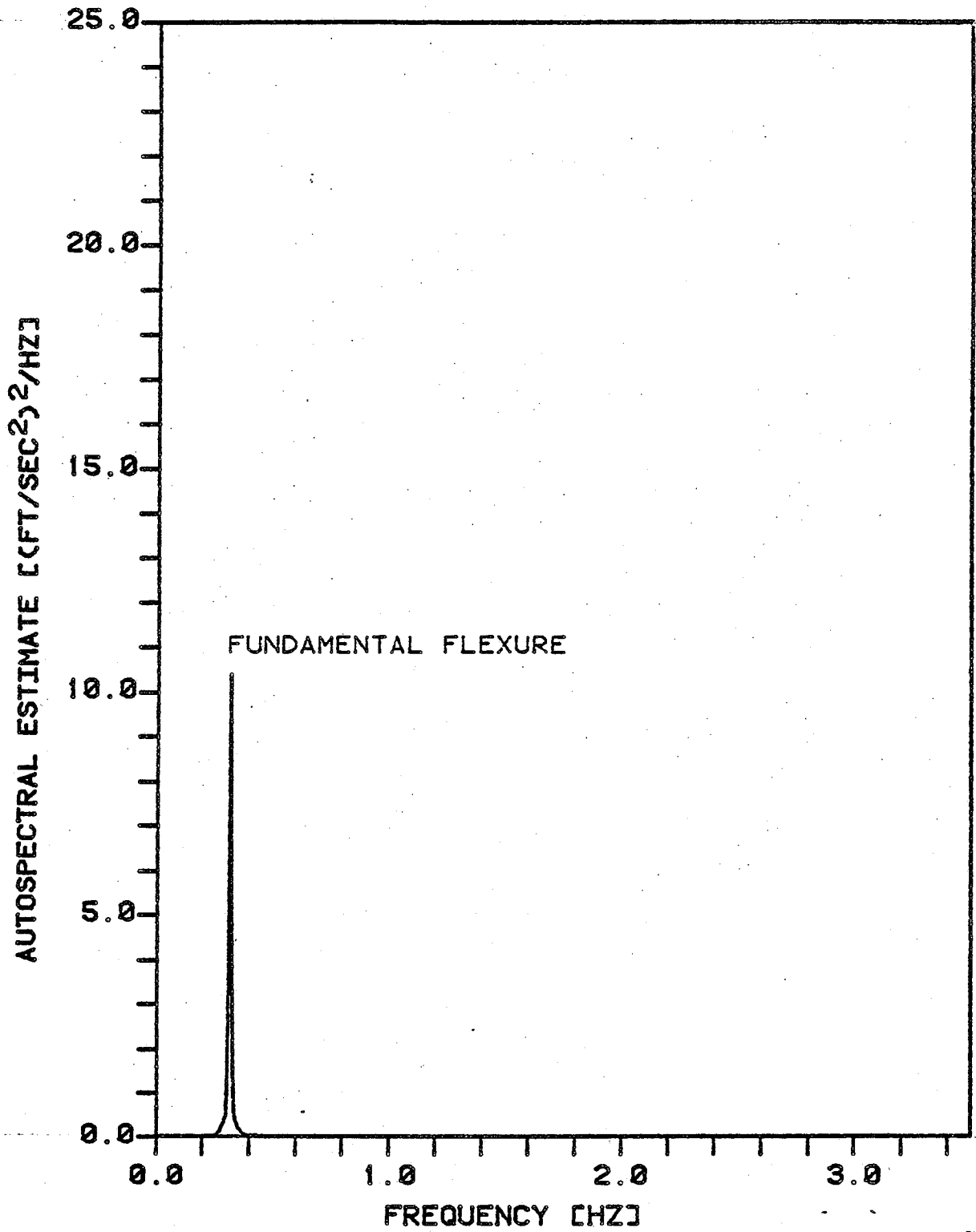


FIGURE NO. 8.17
NAW ACCELEROMETER AUTOSPECTRUM
LOAD CASE 2, NLAG = 80

Figures 8.18 - 8.20 show the cross-spectral estimates of magnitude, phase, and coherence squared respectively. Again, to prevent rapid crossovers between ± 180 degrees, the absolute value of the phase estimate has been plotted in all phase graphs. The semi-log plot of Figure 8.18 for the cross-spectral magnitude estimates shows the relative energy content among the first three flexural modes. Obviously, as illustrated in the autospectra, only the fundamental flexural mode contains any significant amount of energy. The first three flexural modes have been estimated to be located at 0.32, 1.20, and 3.06 Hz respectively. Only the first two modes are positively identified, however, because of the low coherence estimates for the third mode.

The transfer function estimates for the cross-spectral analysis between the helicopter deck and the production, wellhead, and boat landing accelerometer locations are shown in Figures 8.21 - 8.23 respectively. Table 8.1 lists a summary of the cross-spectral estimates for each of the first three flexural modes for each of these three combinations of accelerometer locations. These transfer function estimates were used with the helicopter deck as a psuedo-input to give relative acceleration magnitudes (ie. relative accelerometer location displacements if doubly integrated) between the decks for mode shape identification.

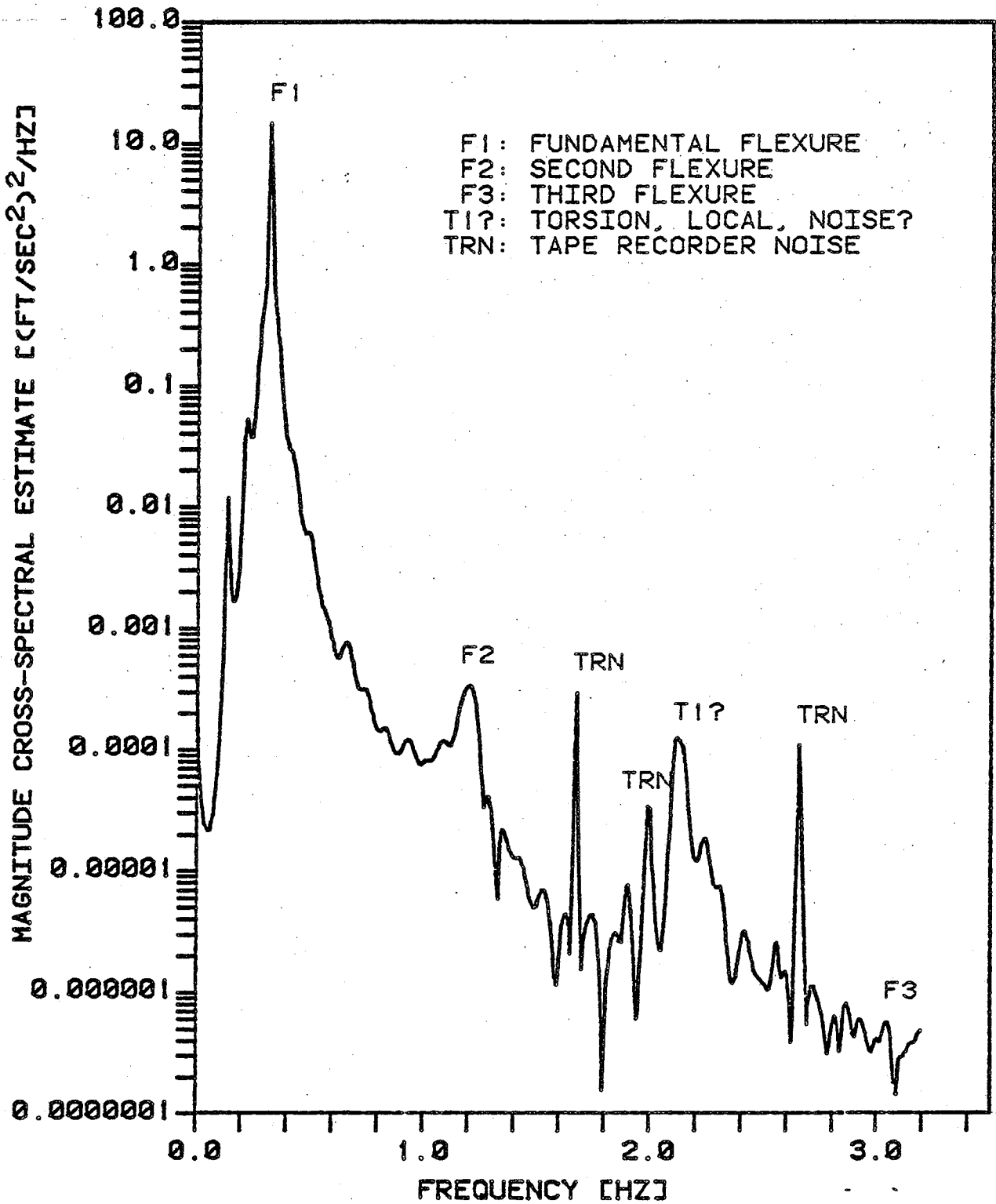


FIGURE NO. 8.18
NAH & NAW ACCELEROMETER MAGNITUDE CROSS-SPECTRUM
LOAD CASE 2, NLAG = 80

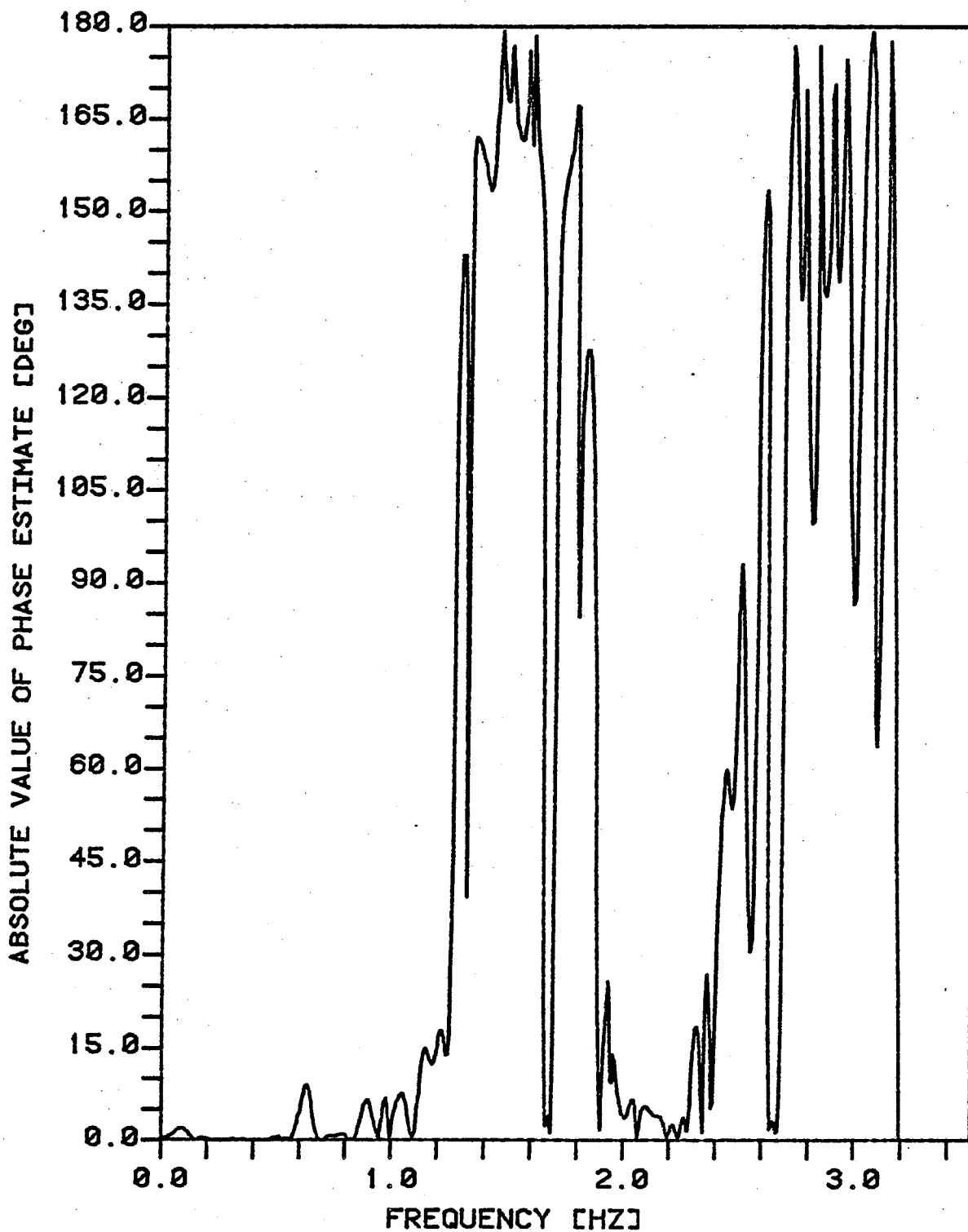


FIGURE NO. 8.19
NAH & NAW ACCELEROMETER PHASE ESTIMATES
LOAD CASE 2, NLAG = 80

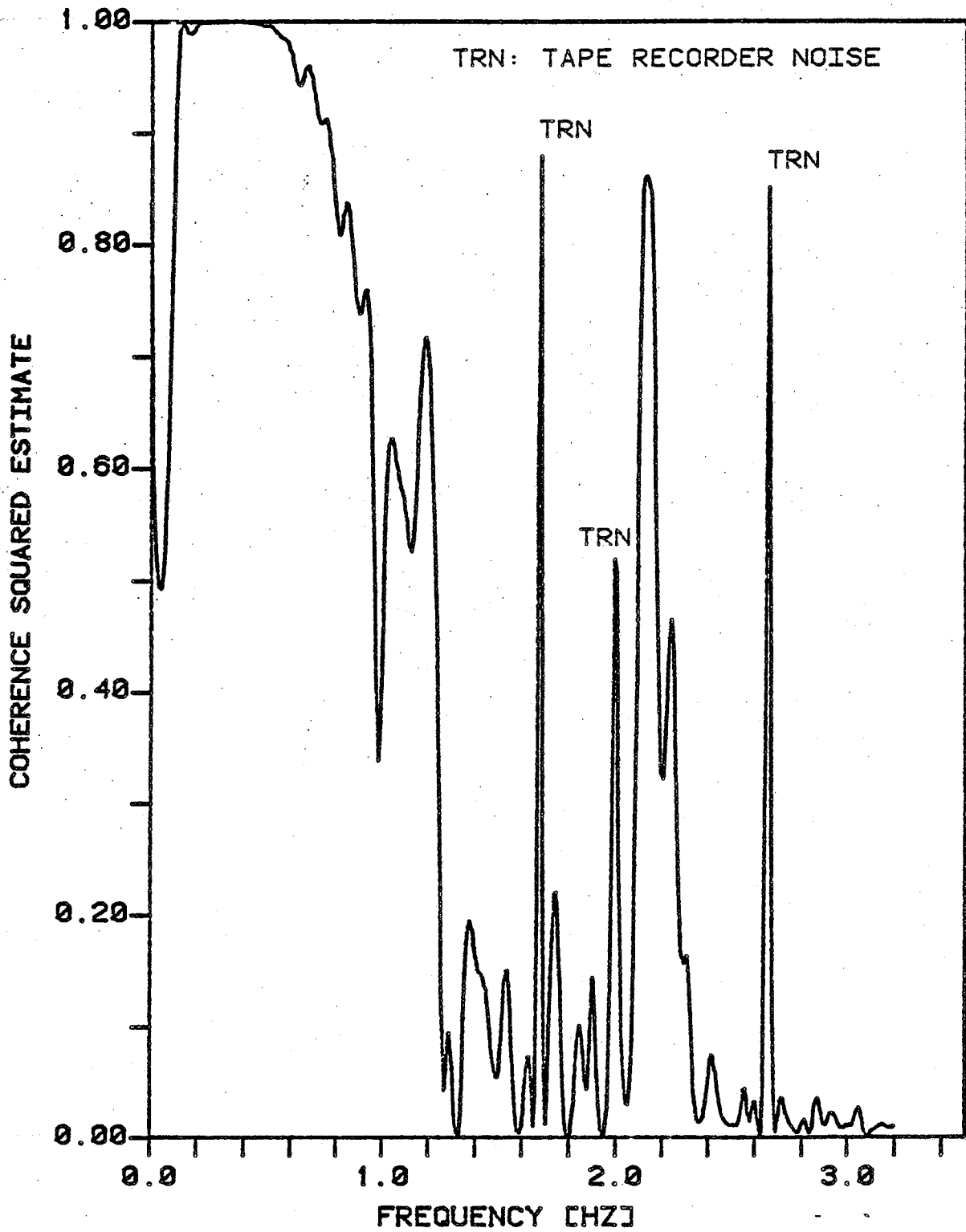


FIGURE NO. 8.20
NAH & NAW ACCELEROMETER COHERENCE ESTIMATES
LOAD CASE 2, NLAG = 80

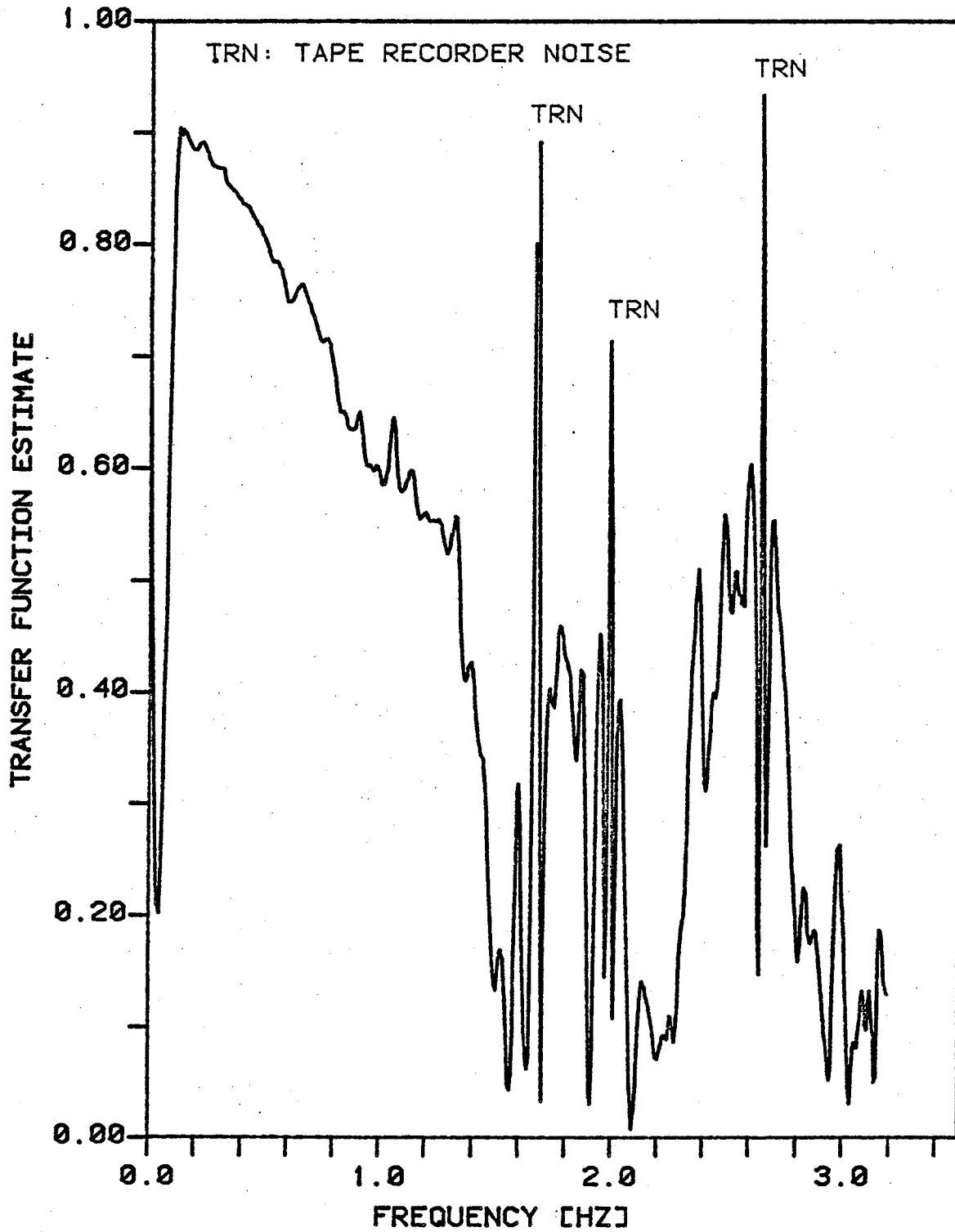


FIGURE NO. 8.21
NAH & NAP ACCELEROMETER TRANSFER FUNCTION ESTIMATES
LOAD CASE 2, NLAG = 80

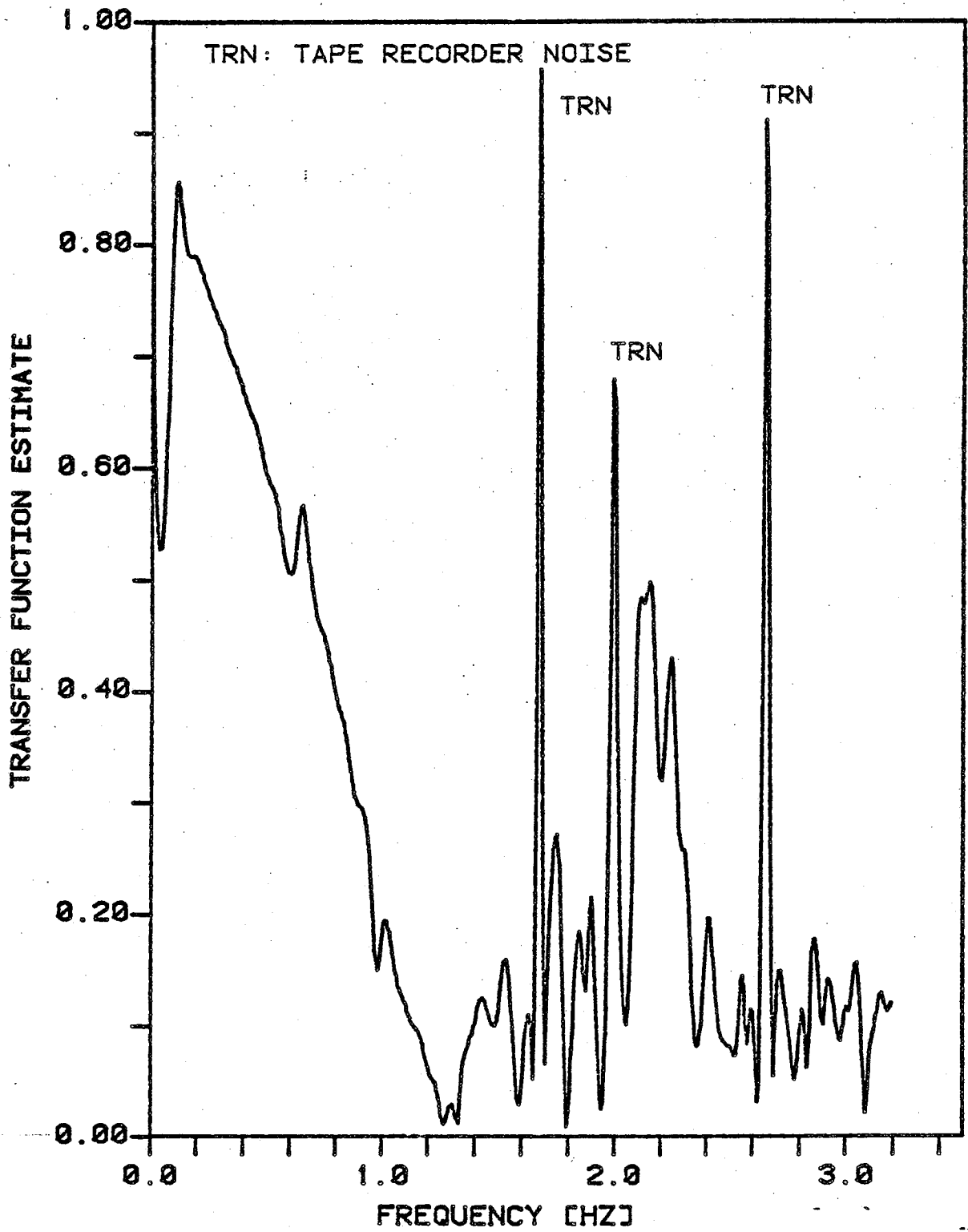


FIGURE NO. 8.22
NAH & NAW ACCELEROMETER TRANSFER FUNCTION ESTIMATES
LOAD CASE 2, NLAG = 80

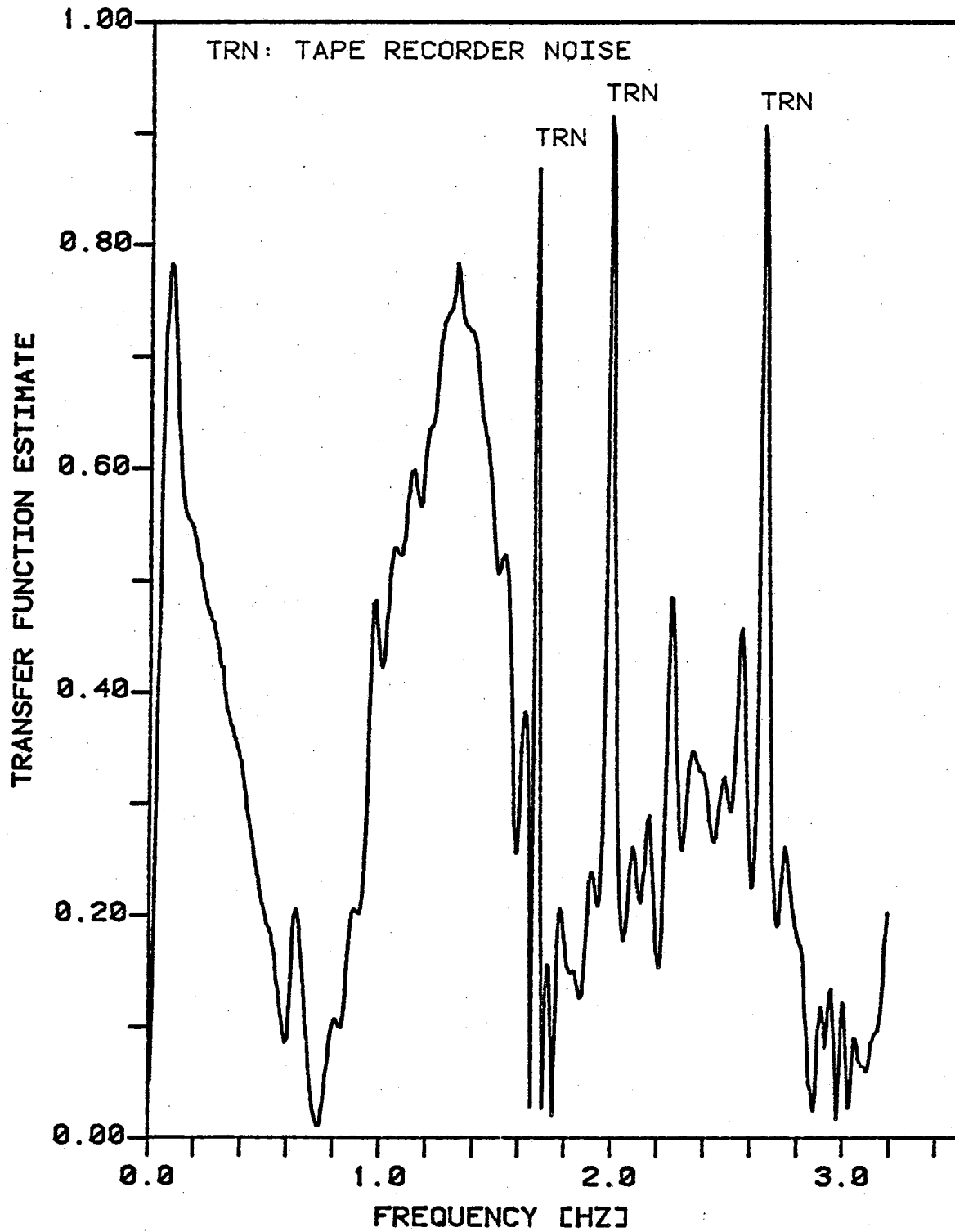


FIGURE NO. 8.23
NAH & NAB ACCELEROMETER TRANSFER FUNCTION ESTIMATES
LOAD CASE 2, NLAG = 80

TABLE 8.1
SUMMARY OF CROSS-SPECTRAL ESTIMATES
FIRST THREE FLEXURAL MODES

<u>Accelerometers</u>	<u>Phase [Deg]</u>	<u>Coherence Sq.</u>	<u>Transfer Function</u>
Fundamental Flexure = 0.32 Hz			
NAH and NAP	0	1.00	0.85
NAH and NAW	0	1.00	0.70
NAH and NAB	0	1.00	0.40
Second Flexure = 1.20 Hz			
NAH and NAP	0	1.00	0.57
NAH and NAW	12	0.70	0.07
NAH and NAB	180	0.95	0.65
Third Flexure = 3.06 Hz			
NAH and NAP	15	0.00	0.15
NAH and NAW	180	0.05	0.15
NAH and NAB	180	0.00	0.10

TABLE 8.2
COMPARISON OF CALCULATED NATURAL FREQUENCY ESTIMATES


<u>Description</u>	<u>Mode 1, Hz</u>	<u>Mode 2, Hz</u>	<u>Mode 3, Hz</u>
Finite Element Model	0.33	1.12	3.3
Multichannel Spectral Analysis	0.32	1.20	3.06

A two-dimensional model incorporating geometrical, mass, and stiffness properties of the caisson platform as well as soil conditions was used to perform a finite element analysis [Cook, 1981]. The model, consisting of two DOF beam and truss elements (translational and rotational), is shown in Figure 8.24. Concentrated masses for the deck weights, and added mass equal to the displaced volume of the caisson in the water column were used in the modeling. The soil properties were approximated with linear springs. The natural frequencies and mode shapes of the three lowest flexural modes were calculated.

A comparison of the first three estimated flexural mode natural frequencies with those calculated using Cook's finite element model is shown in Table 8.2. Hong [1976] calculated a value of 0.30 Hz for the fundamental flexural mode. A comparison of the first two relative mode shapes is given in Figure 8.25. Thus, the natural frequencies and mode shapes estimated using the MEM multichannel spectral analysis techniques compare favorably with other reported results. As mentioned previously, the third flexural mode is suspect due to the low coherence squared values.

8.2.2 Torsional Mode Shape

In this section, an attempt is made to identify the fundamental torsional mode shape using the two east oriented accelerometers located on the wellhead deck in Load Case 1.


 CONCENTRATED NODAL MASS
 NODE POINTS
 TRANSLATIONAL DOF
 ROTATIONAL DOF

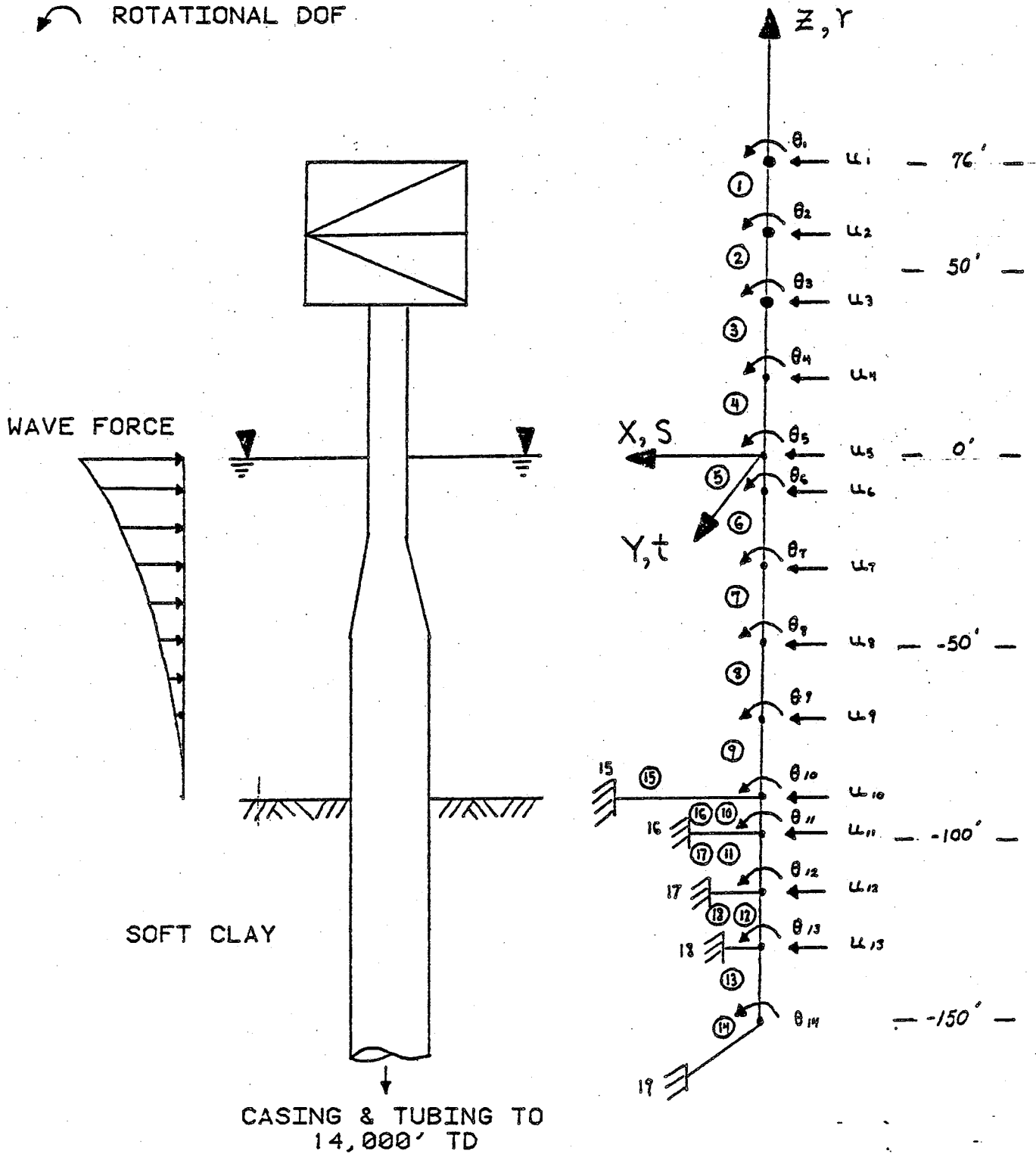


FIGURE NO. 8.24
 FINITE ELEMENT MODEL OF OFFSHORE CAISSON PLATFORM
 (AFTER COOK, 1981)

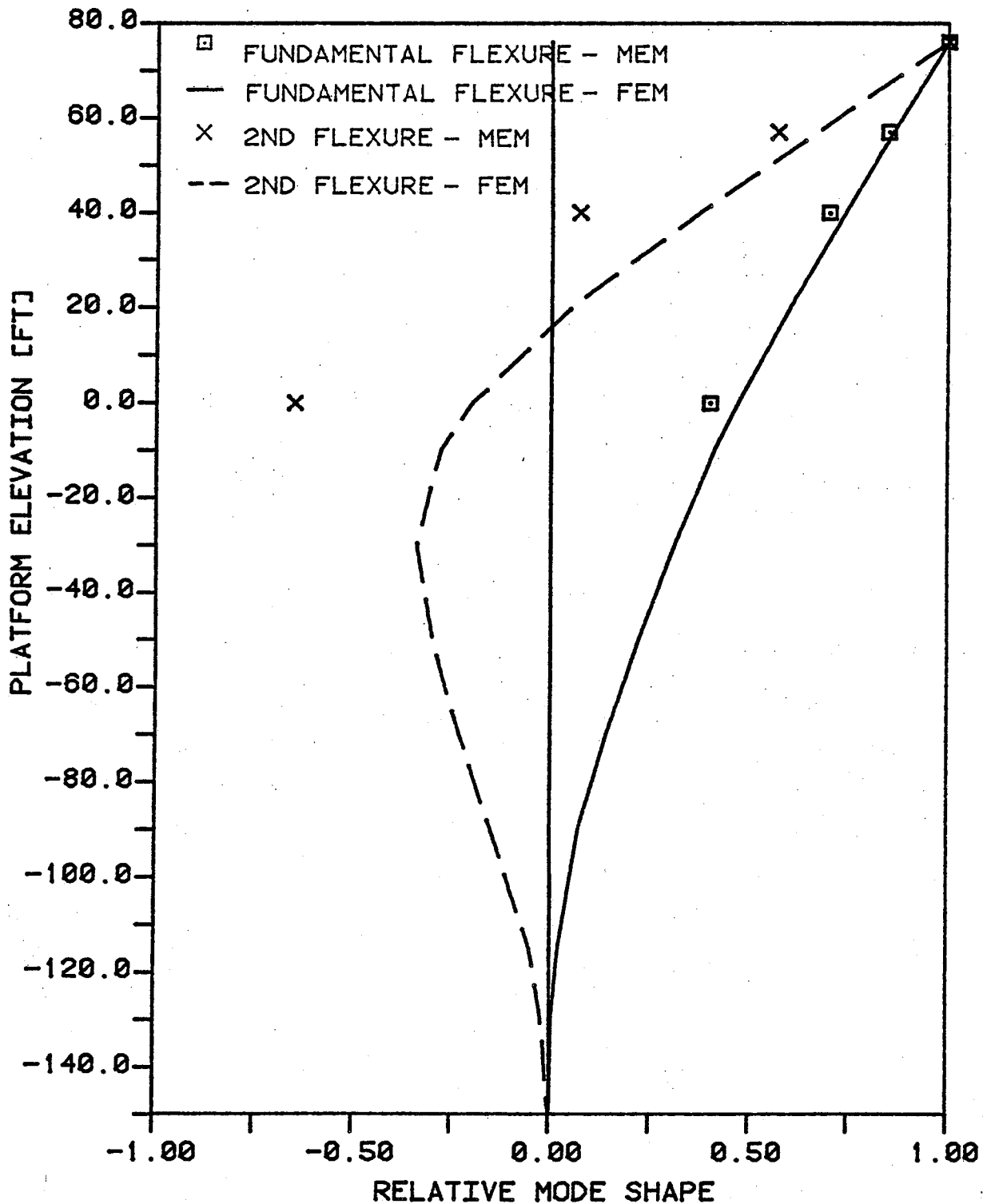


FIGURE NO. 8.25
COMPARISON OF CALCULATED MODE SHAPES USING MEM SPECTRAL ANALYSIS & FINITE ELEMENT METHODS - LOAD CASE 2

These accelerometers are the east component of the biaxial pair in the center of the wellhead deck (EAW) and the east accelerometer located on the northern edge of the wellhead deck (EAT). The EAW accelerometer is used as the input signal in the hopes that the relatively small torsional response of this accelerometer (due to its location in the center of the deck) will produce a large transfer function estimate at the natural frequency in torsion.

The time history for the EAW accelerometer is shown in Figure 8.26. It is identical to that of the EAT accelerometer. The auto and cross-correlation function estimates are shown in Figures 8.27 and 8.28 respectively.

Figure 8.29 is a linear plot of the autospectral estimates for the EAW accelerometer. Again, the autospectrum for the EAT accelerometer is identical. Estimates of cross-spectral magnitude, phase, coherence squared, and transfer function are shown in Figures 8.30 - 8.33 respectively. The large peak at approximately 2.13 Hz was initially believed to be an aliased or folded replica of the actual fundamental torsional natural frequency. Aliased frequencies are given by the formula

$$2 * n * f_c \pm f \quad (8.1)$$

where,

- n : even integer 1, 2, 3, ...
- f_c : cutoff or Nyquist frequency, Hz
- f : aliased frequency of interest, Hz

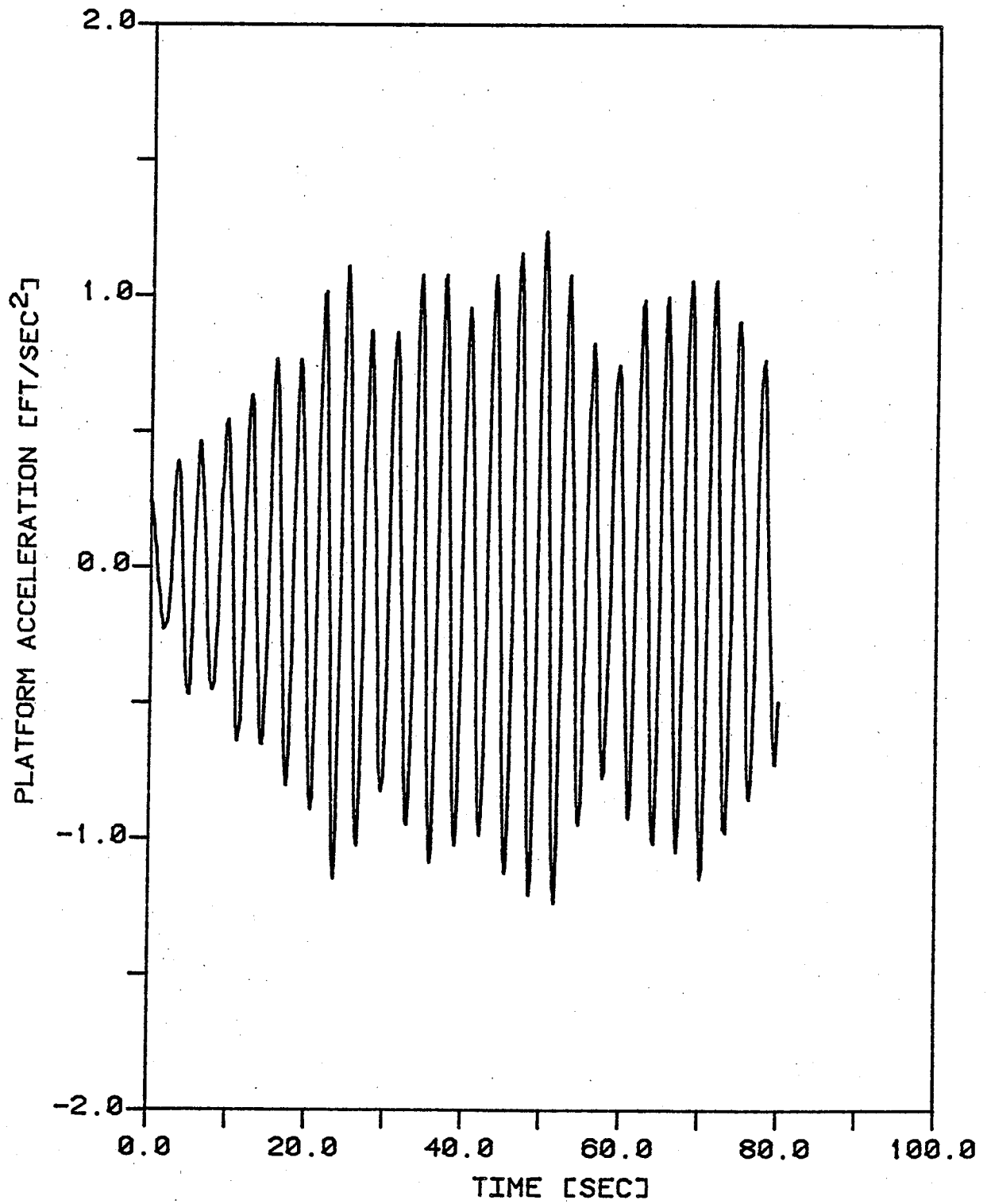


FIGURE NO. 8.26
EAW ACCELEROMETER TIME HISTORY
LOAD CASE 1

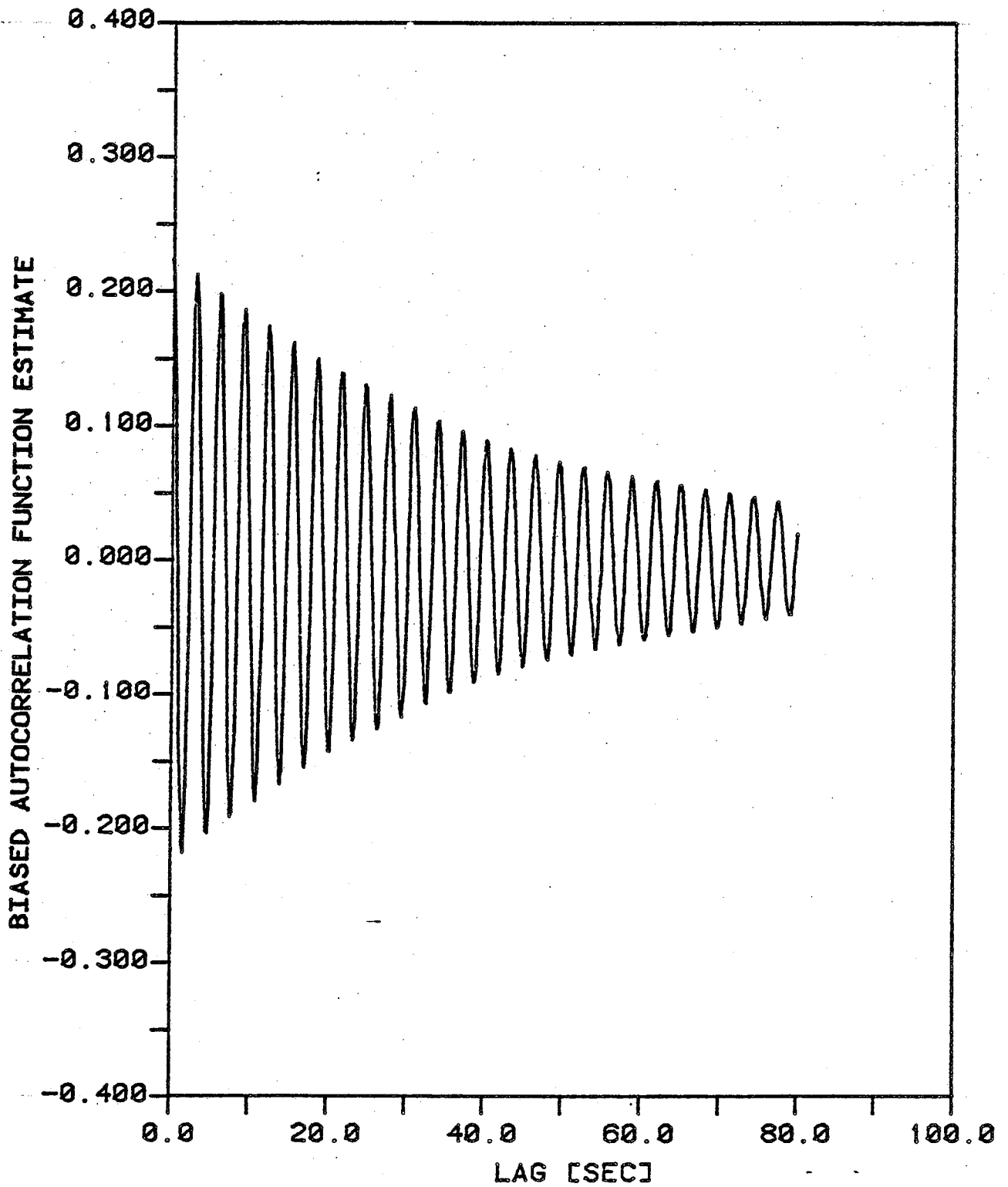


FIGURE NO. 8.27
EAW ACCELEROMETER AUTOCORRELATION
LOAD CASE 1, MAXLAG = 512, N = 29696

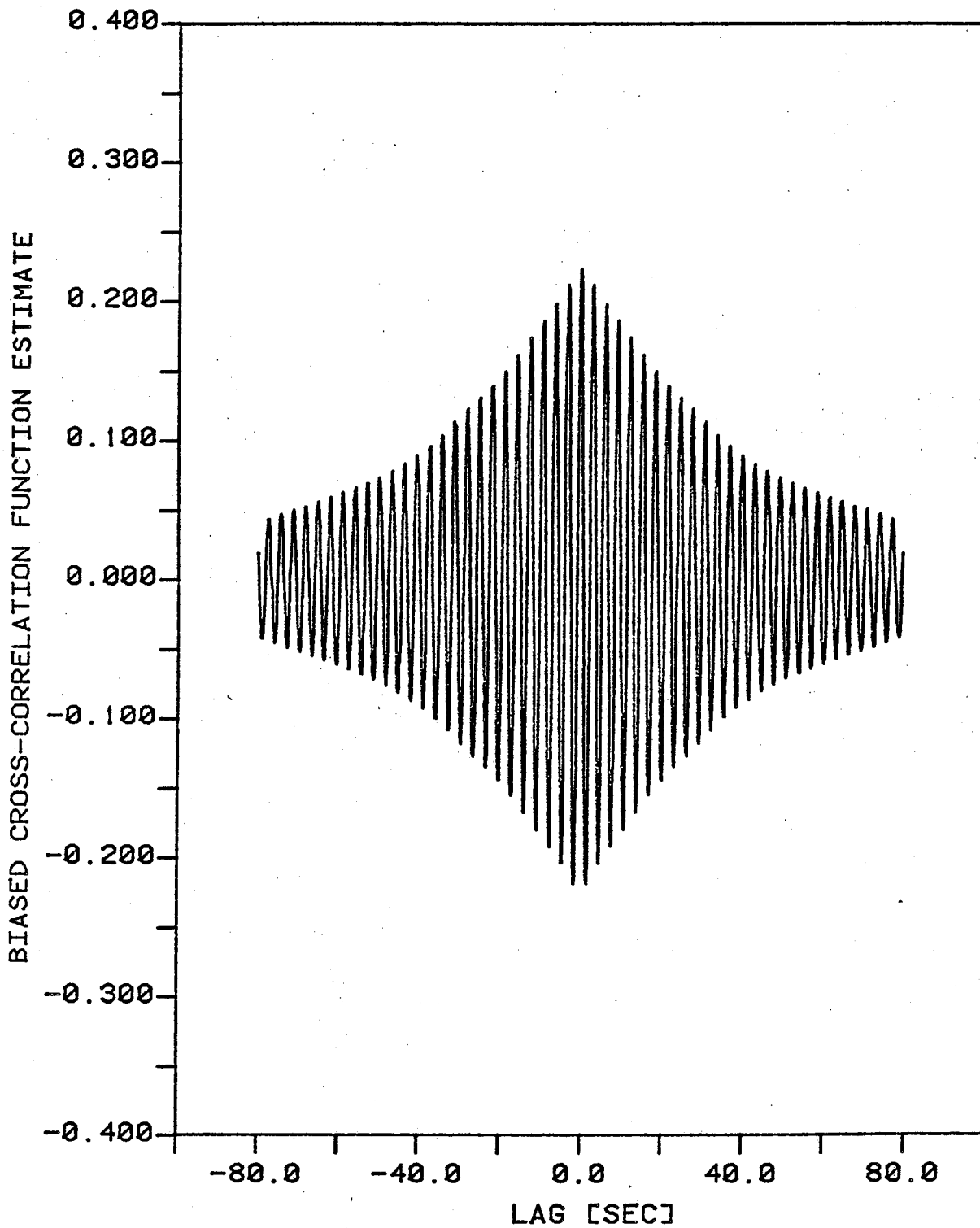


FIGURE NO. 8.28
EAW & EAT ACCELEROMETER CROSS-CORRELATION
LOAD CASE 1, MAXLAG = 512 (POS. SIDE), N = 29696

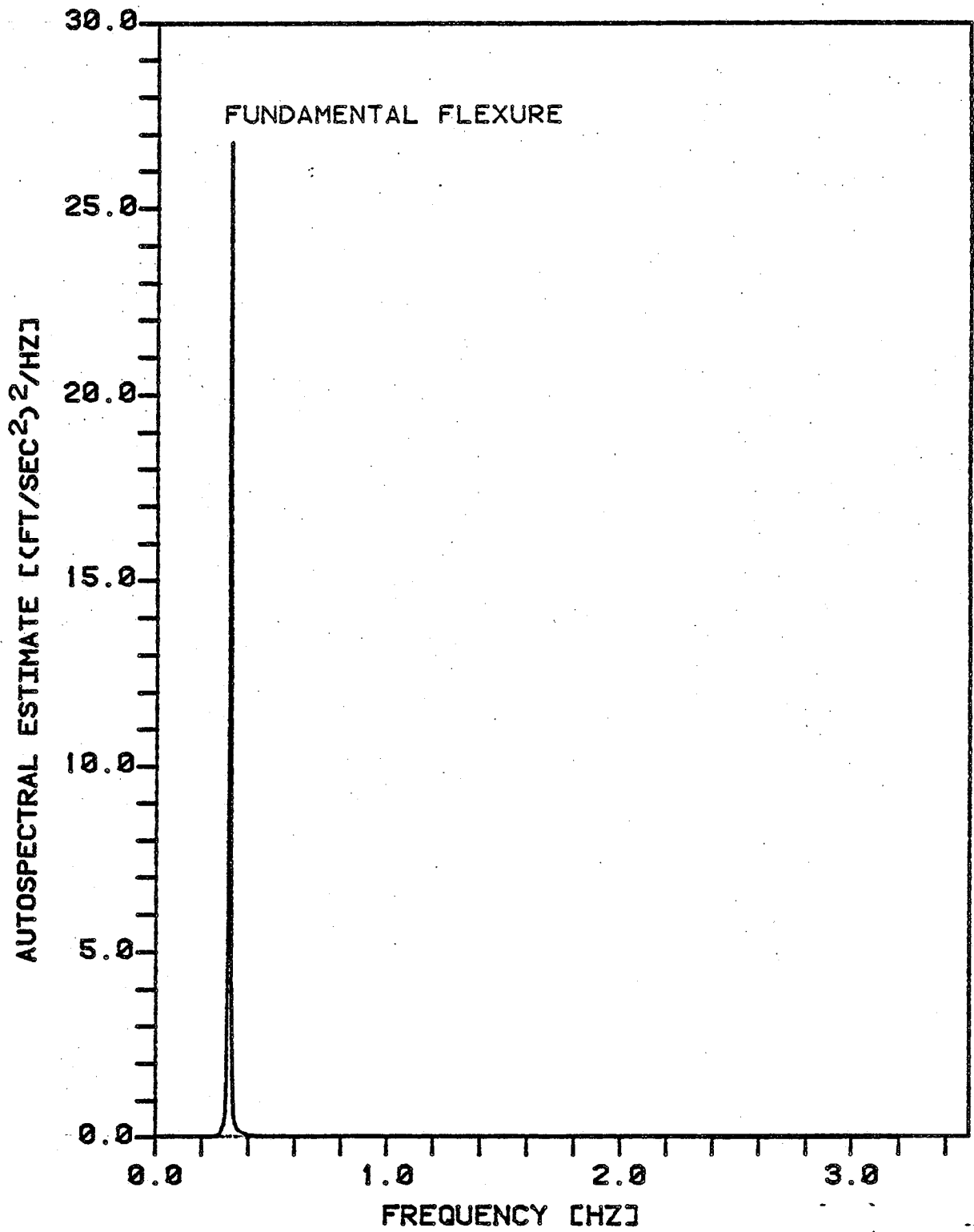


FIGURE NO. 8.29
EAW ACCELEROMETER AUTOSPECTRUM
LOAD CASE 1, NLAG = 60

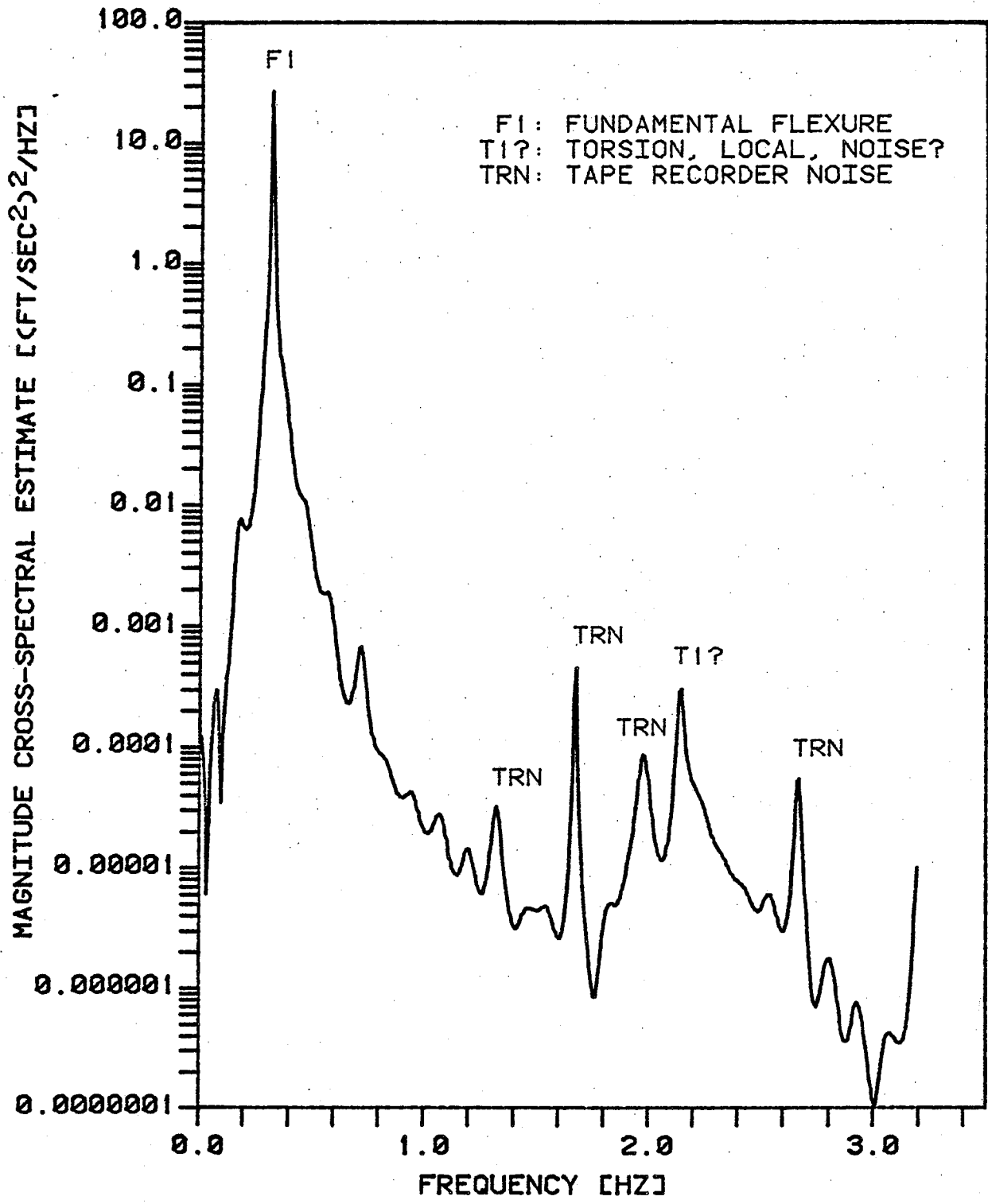


FIGURE NO. 8.30
EAW & EAT ACCELEROMETER MAGNITUDE CROSS-SPECTRUM
LOAD CASE 1, NLAG = 60

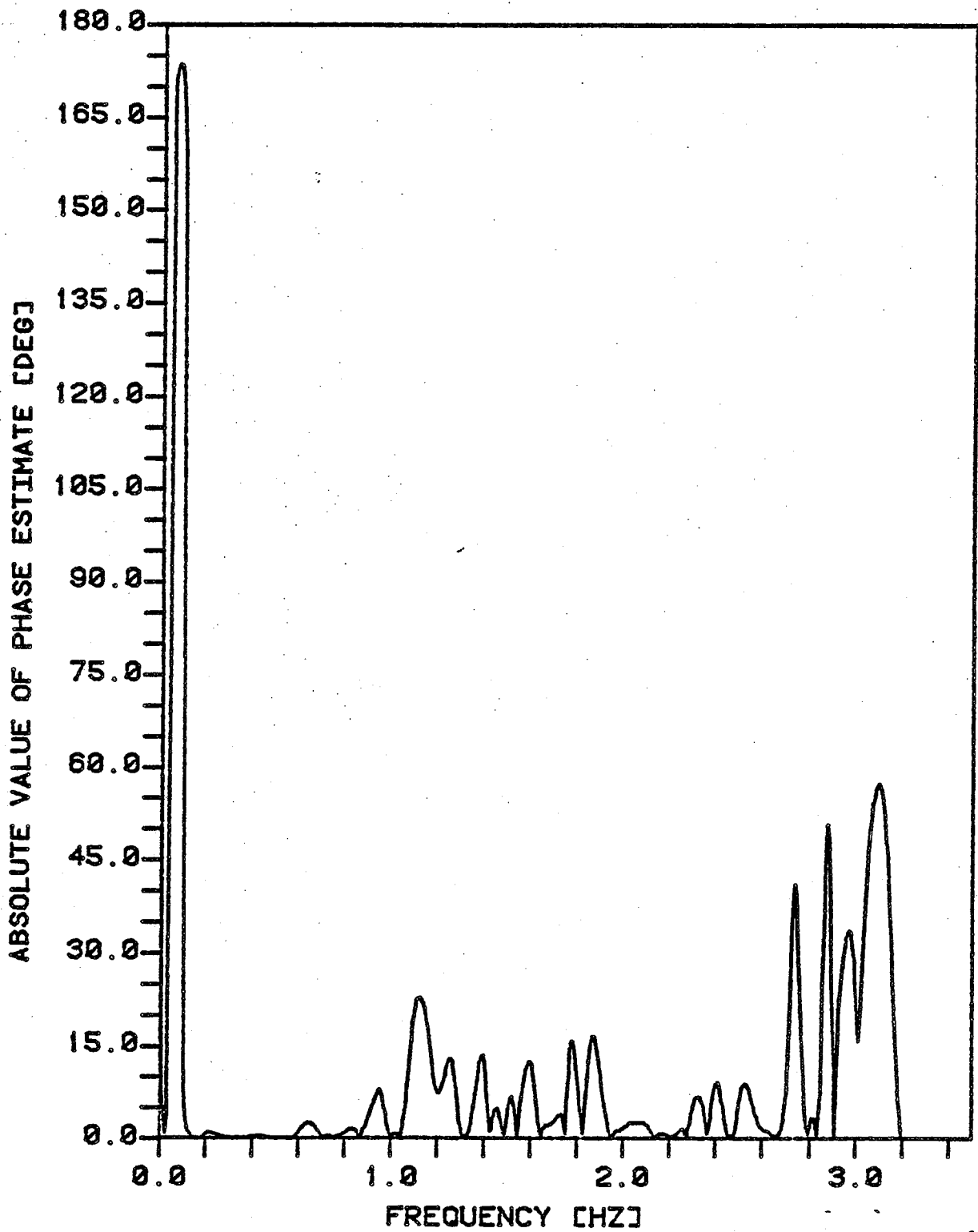


FIGURE NO. 8.31
EAW & EAT ACCELEROMETER PHASE ESTIMATES
LOAD CASE 1, NLAG = 60

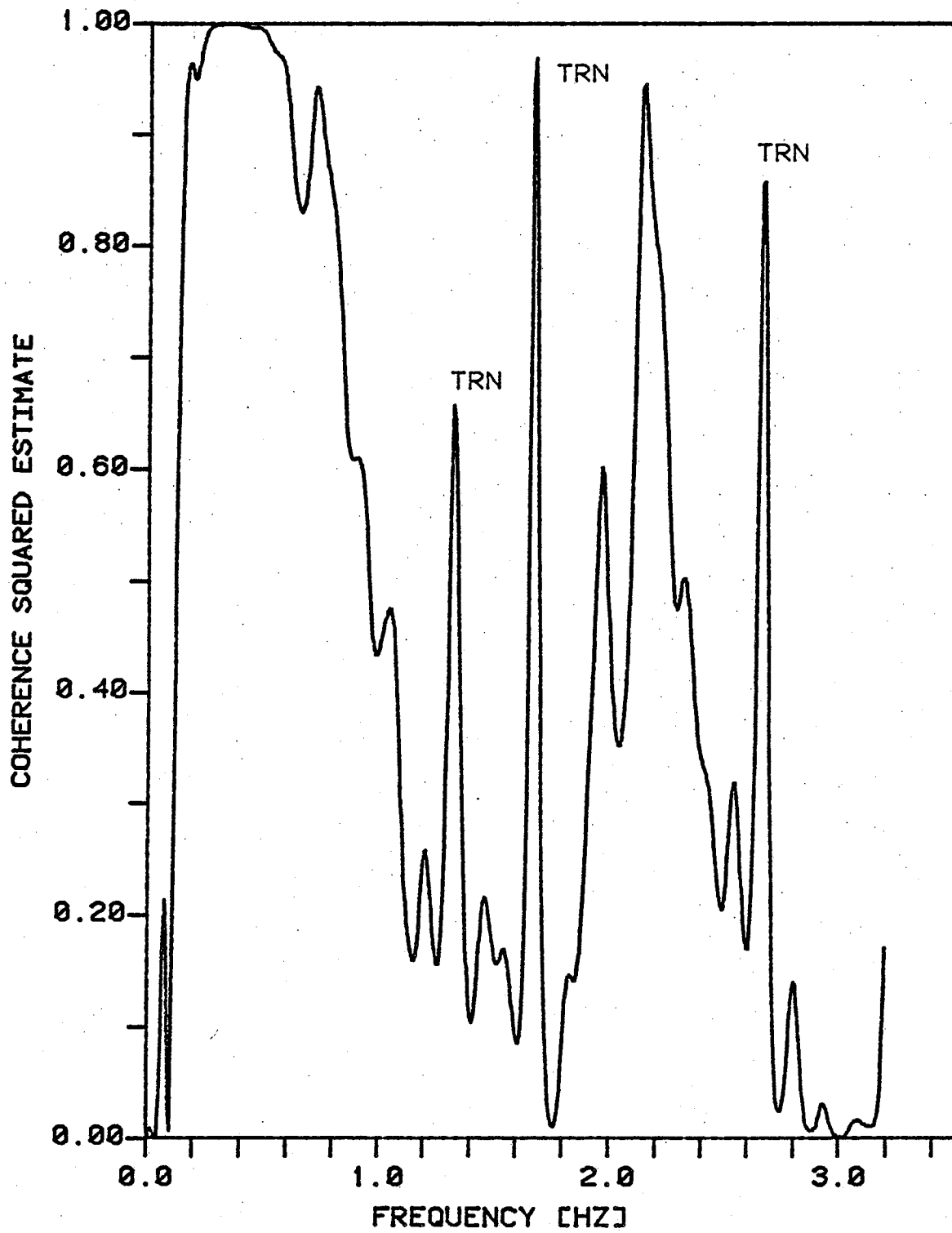


FIGURE NO. 8.32
EAW & EAT ACCELEROMETER COHERENCE ESTIMATES
LOAD CASE 1, NLAG = 60

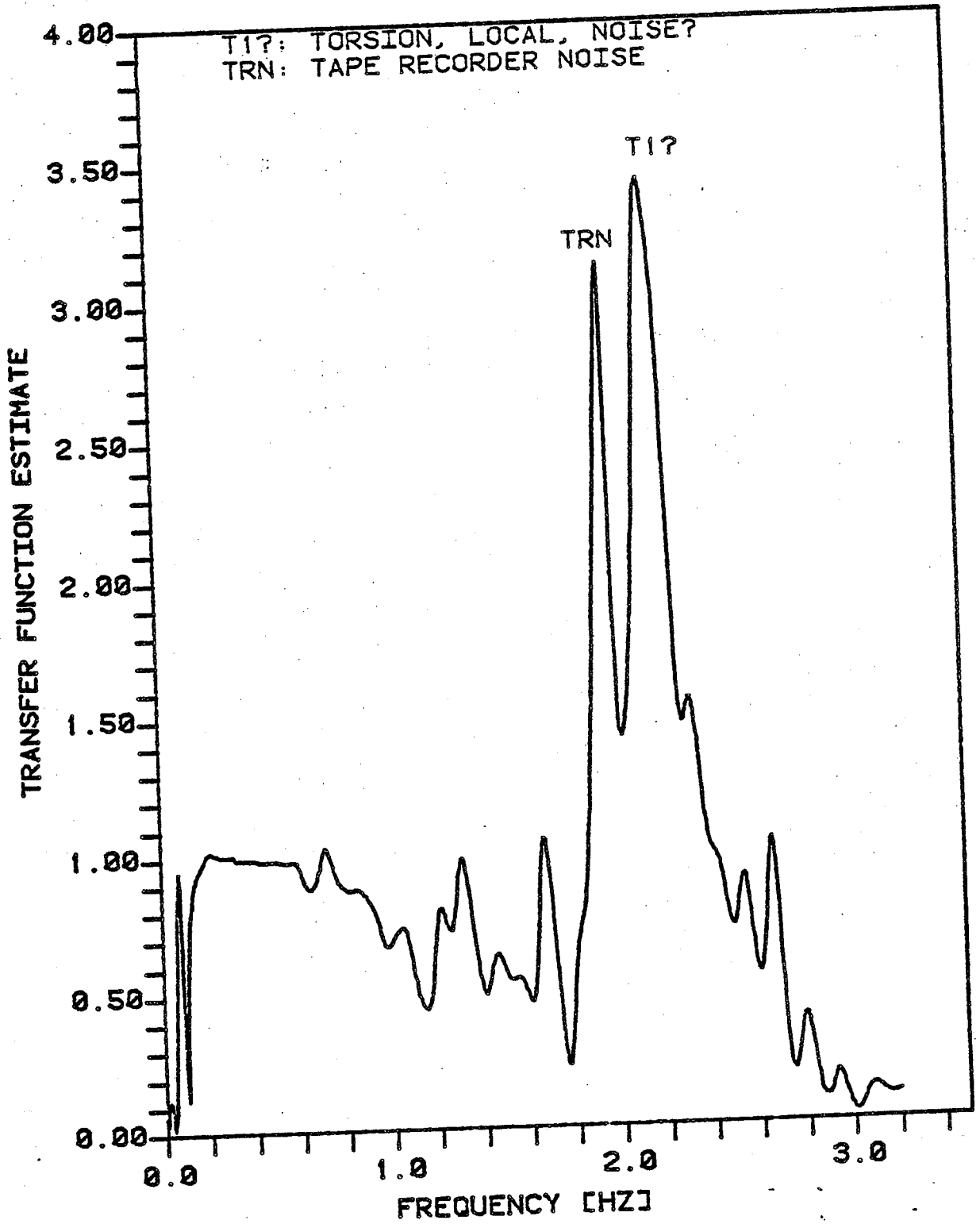


FIGURE NO. 8.33
EAW & EAT ACCELEROMETER TRANSFER FUNCTION ESTIMATES
LOAD CASE 1, NLAG = 60

A crude estimate of 4.3 Hz for the fundamental natural frequency in torsion was calculated using

$$f_{\theta} = (1/2\pi) * \text{SQRT}[K_{\theta} / I] \quad (8.2)$$

where,

f_{θ} : fundamental natural frequency in torsion, Hz

K_{θ} : equivalent torsional spring for the caisson,
ft-lb/rad

I : mass moment of inertia for the caisson,
slugs-ft²

As an additional check, the EAW and EAT data records were re-digitized at a higher sampling frequency of 12.8 Hz. The expected torsional peak at 4.3 Hz was not obtained in the cross-spectral magnitude estimates. The best explanation for the cause of this peak is other sources of noise on the platform which have not yet been positively identified, or some local platform mode.

8.3 SPURIOUS NOISE PEAKS

Appearing in every auto and cross-spectral estimate plot are spikes or peaks located at approximately 1.68 and 2.66 Hz. Based on the phase and coherence estimates, these peaks do not represent true energy content of the response spectra. Rather they are due to noise. To test if the noise was due to the tape recorder, one channel of the tape recorder was grounded and an empty data record was recorded and digitized at a sampling frequency of 6.4 Hz. Figure 8.34 shows a plot of the biased autocorrelation function estimates to 512 lags. A MEM autospectral estimate

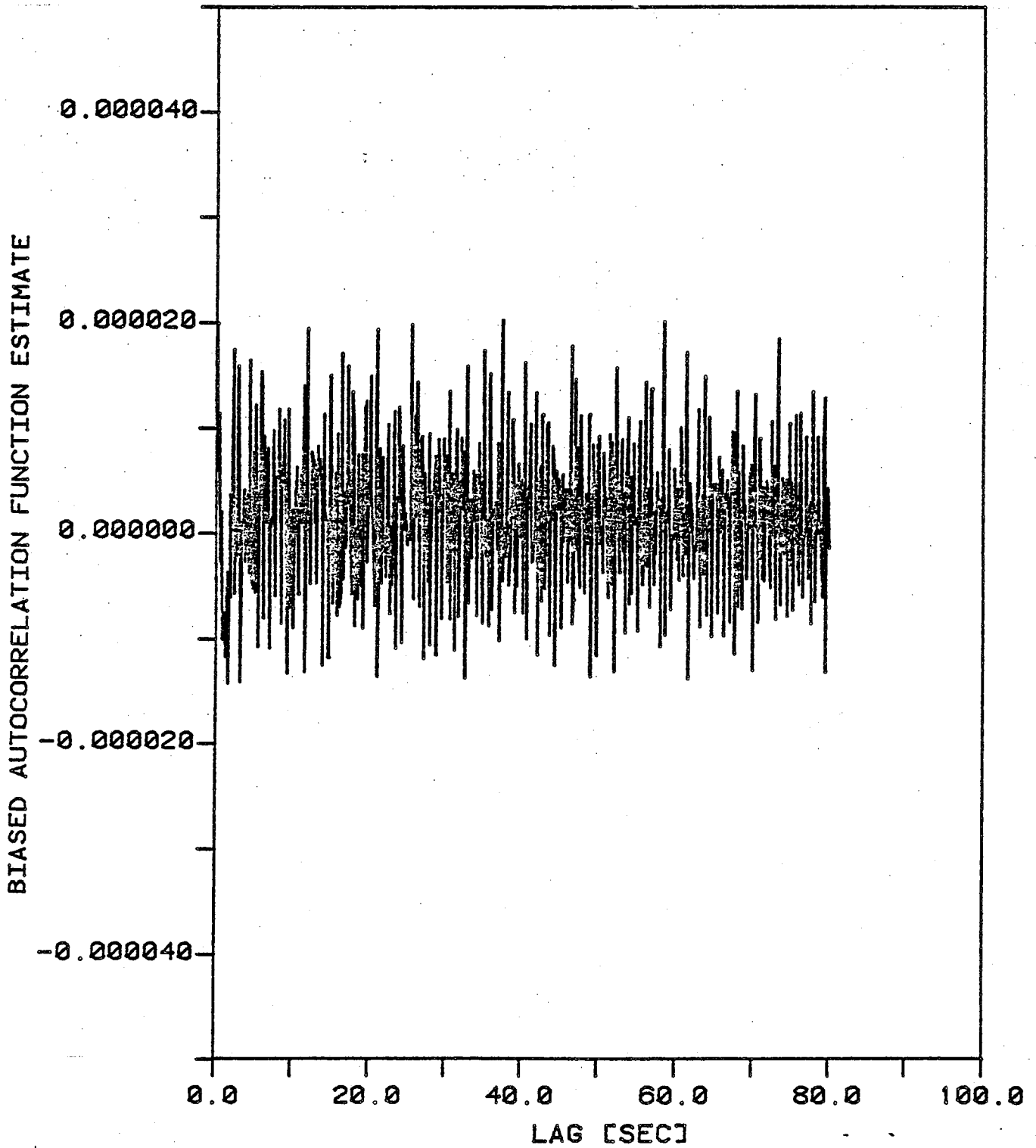


FIGURE NO. 8.34
TAPE RECORDER NOISE AUTOCORRELATION
MAXLAG = 512, N = 25600

for 80 lags is shown in Figure 8.35. Again, the same procedure as discussed in Section 6.5, was used to calculate these estimates. Based on the results of this test, the noise peaks located at 1.68 and 2.66 Hz are definitely attributable to tape recorder noise, probably caused by transport flutter. In addition, other noise peaks at 1.34, 2.01, and 2.20 Hz were also identified. None of these peaks corresponded to the suspected torsional peak at 2.13 Hz.

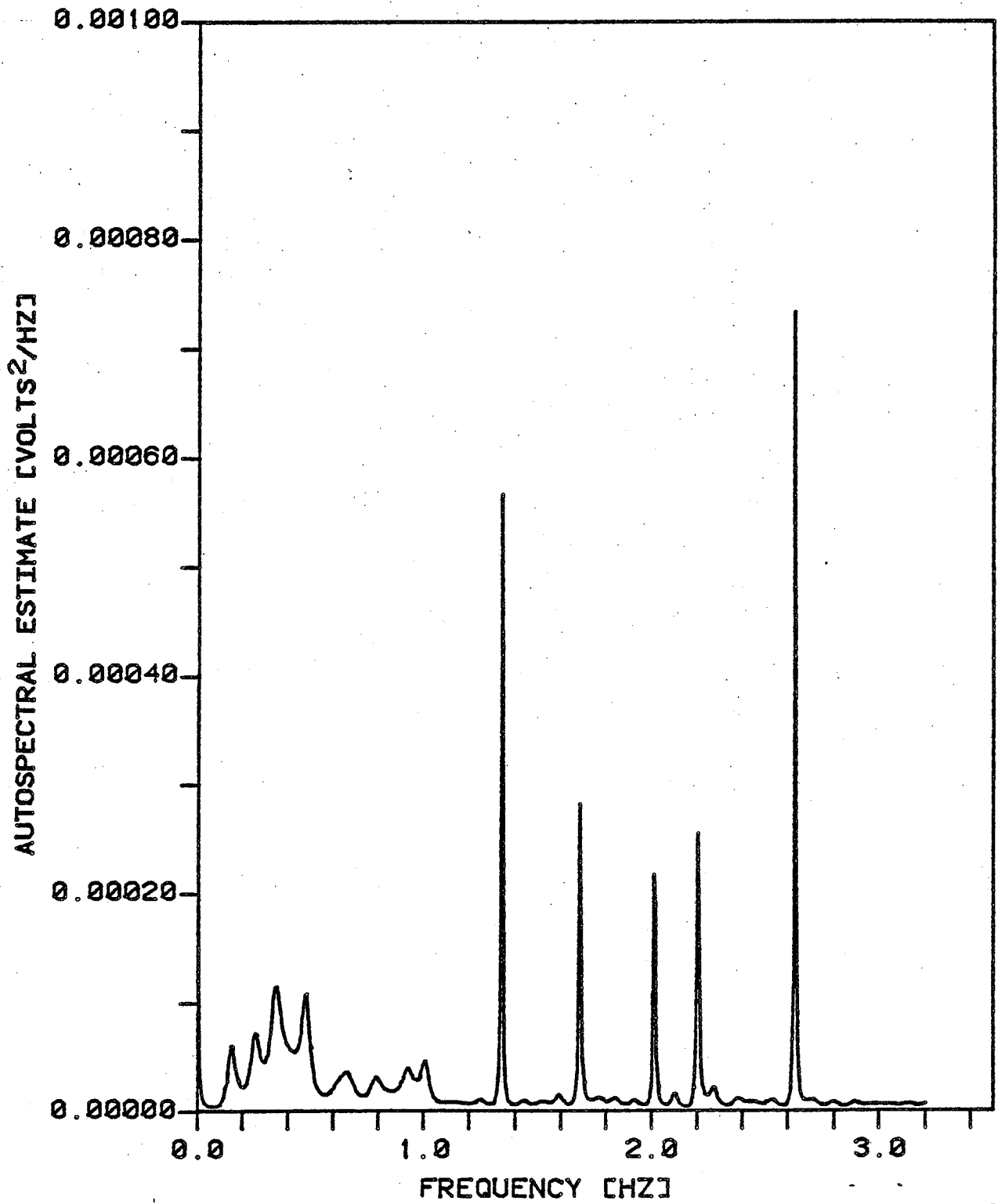


FIGURE NO. 8.35
TAPE RECORDER NOISE AUTOSPECTRUM
NLAG = 60

CHAPTER 9
SUMMARY AND CONCLUSIONS

Two different versions of the multichannel Maximum Entropy Method of spectral analysis have been implemented and compared with a multichannel version of the Blackman-Tukey method. The two MEM multichannel computer programs are a direct on the data method of Burg (BRGMEM) and a correlation extension or Yule-Walker method (RYWMEM), both originally formulated by Strand. The BRGMEM method employs a least squares estimate of the reflection coefficients with inverse power weighting to guarantee a positive-definite covariance matrix and a resulting stable spectral estimate. The RYWMEM method is based on the triangular decomposition of the correlation matrix using an algorithm developed by Rissanen. The multichannel Blackman-Tukey code gives the user the choice of four different windows: (1) Boxcar, (2) Bartlett, (3) Hanning, and (4) Parzen. Both multichannel MEM methods gave superior results relative to the Blackman-Tukey method. The RYWMEM spectral estimates seemed to be smoother than those calculated using the BRGMEM method. This was especially evident in the phase estimates. Where large amounts of data are to be processed, the user may want to use the RYWMEM method to avoid the large computer storage and time requirements.

The BRGMEM method was implemented in a form that allowed segmenting and averaging of the data, much like periodogram spectral estimates are calculated to minimize the variance. For comparison, one segment at 2048 data points, nine segments at 2048 data points each, and one segment at 18432 data points were analyzed. The two shorter, segmented data records gave satisfactory cross-spectral estimates relative to the longer data record of 18432 data points (48 minutes). Therefore, where the analyst is faced with time, budget, and/or computer memory storage constraints; the segmenting and averaging technique using the multichannel BRGMEM computer program has merit.

A transfer function estimate using the multichannel methods of spectral analysis was used in mode shape identification of an offshore caisson platform located in 89 ft. of water. Transfer function estimates obtained from multichannel spectral analysis are known to be superior to those estimates obtained using autospectral methods in terms of their relative insensitivity to input and output noise. These transfer function estimates, using accelerometers as psuedo-inputs, give relative acceleration amplitudes (which, if doubly integrated, would be relative displacement amplitudes) between two accelerometers. Comparison of these relative acceleration magnitudes with the relative displacement amplitudes obtained from a finite element model of the caisson platform gave reasonable agreement. The third flexural mode values were not useable, however,

because of low coherence values. Thus, this technique can be a useful tool (in conjunction with the cross-spectral estimates of magnitude, phase, and coherence) in mode shape identification.

Future research can go in several different directions. One is to implement the multichannel MEM methods for three or more channels of inputs and outputs on the larger VAX 11/780 computer. This will enable the calculation of partial correlation and cross-spectral estimates which consider the effect of multiple inputs on a particular output. The current MEM versions only consider the influence of one input or channel on the other channel or output.

Several different modifications to the Burg algorithm have been proposed to alleviate the problems of spontaneous line splitting, frequency shifting, and rounding errors of the Levinson recursion which sometimes affect this method. Notable among these are the papers by (1) Barrodale and Erickson [1980] which presents a least squares Cholesky algorithm for short data records which avoids the shortcomings inherent with the Toeplitz form, and (2) Fougere [1976] which presents a modification to the Burg algorithm to prevent spontaneous tone splitting and frequency shifting. Their ideas should be investigated further to determine their usefulness in multichannel spectral analysis of offshore structures.

Another area of future research involves the development and implementation of an ARMA (Autoregressive, Moving Average) model for single and multichannel spectral analysis. The ARMA model utilizes zeros as well as poles and therefore requires smaller model orders or filter lengths to achieve the same degree of resolution. The MEM method is more prone to introduce spurious peaks in the spectral estimates due to its all pole nature. Thus, substantial savings in computer time and more accurate spectral estimates may be possible over the all pole MEM methods.

LIST OF REFERENCES

- Andersen, N. 1974 "On the Calculation of Filter Coefficients for Maximum Entropy Spectral Analysis," *Geophysics*, Vol. 39, No. 1, February, 1974, pp. 69-72.
- Baggeroer, A.B. 1976 "Confidence Intervals for Regression Maximum Entropy Spectral Estimates," *IEEE Transactions on Information Theory*, Vol. IT-22, No. 5, 1976, pp. 534-545.
- Baggeroer, A.B. 1979 "Recent Signal Processing Advances in Spectral and Frequency Wavenumber Function Estimation and their Application to Offshore Structures," BOSS '79, Second International Conference on Behavior of Offshore Structures, Imperial College, London, England, August, 1979.
- Barrodale, I. 1980 "Algorithms for Least-Squares Linear Prediction and Maximum Entropy Spectral Analysis -- Part I: Theory," *Geophysics*, Vol. 45, No. 3, March, 1980, pp. 420-432.
- Erickson, R.E.
- Barrodale, I. 1980 "Algorithms for Least-Squares Linear Prediction and Maximum Entropy Spectral Analysis -- Part II: Fortran Program," *Geophysics*, Vol. 45, No. 3, March, 1980, pp. 433-446.
- Erickson, R.E.
- Begg, R.D. 1976 "Structural Integrity Monitoring Using Digital Processing of Vibration Signals," OTC 2549, Houston, Texas, May, 1976.
- Mackenzie, A.C.
- Dodds, C.J.
- Loland, O.
- Bellman, R. 1970 Introduction to Matrix Analysis, Second Edition, McGraw-Hill, New York.
- Bendat, J.S. 1971 Random Data: Analysis and Measurement Procedures, Wiley-Interscience, New York.
- Piersol, A.G.
- Bendat, J.S. 1980 Engineering Applications of Correlation and Spectral Analysis, Wiley-Interscience, New York.
- Piersol, A.G.

LIST OF REFERENCES (Cont.) -170-

- Blackman, R.B. 1958 The Measurement of Power Spectra,
Tukey, J.W. Dover, New York.
- Bloomfield, P. 1976 Fourier Analysis of Time Series:
An Introduction, Wiley and Sons,
New York.
- Bracewell, R.N. 1978 The Fourier Transform and Its
Applications, McGraw-Hill, New York.
- Burg, J.P. 1967 "Maximum Entropy Spectral Analysis,"
37th Society of Exploration Geologists
Winter Meeting, Oklahoma City,
Oklahoma, 1967.
- Burg, J.P. 1972 "Relationship between Maximum Entropy
Method and Maximum Likelihood Method,"
Geophysics, Vol. 27, No. 2,
1972, pp. 375-376.
- Burke, B.G. 1980 "Characterization of Ambient Vibration
Sundararajan, C. Data by Response Shape Vectors,"
Safaie, F.M. OTC 3862, Houston, Texas, May, 1980.
- Campbell, R.B. 1979 "The Estimation of Natural Frequencies
and Damping Ratios of Offshore
Structures," Ph.D. Thesis, Massachusetts
Institute of Technology, January, 1979.
- Campbell, R.B. 1980 "The Estimation of Natural Frequencies
and Damping Ratios of Offshore
Structures," OTC 3861,
Houston, Texas, May, 1980.
- Chatfield, C. 1975 The Analysis of Time Series: Theory
and Practice, John Wiley and Sons,
Halstead Press, New York.
- Chave, A.D. 1980 "Applications of Time Series Analysis to
Geophysical Data," Ph.D. Thesis,
Massachusetts Institute of Technology and
Woods Hole Oceanographic Institution,
WHOI 80-35, June, 1980.
- Childers, D.G. 1978 Modern Spectrum Analysis, IEEE
(Editor) Press, John Wiley and Sons, New York.
- Claerbout, J.F. 1976 Fundamentals of Geophysical Data
Processing, McGraw-Hill, New York.
- Cook, M.F. 1981 Dynamic Analysis of Offshore Single-Pile
Davidson, M. Platform by Finite Element Method,"
Lin, W.M. MIT 2.093 Term Project, May, 1981.

LIST OF REFERENCES (Cont.) -171-

- Coppolino, R.N. 1980 "Detectability of Structural Failures
Rubin, S. in Offshore Platforms by Ambient
Vibration Monitoring," OTC 3865,
Houston, Texas, May, 1980.
- Crandall, S.H. 1973 Random Vibration, Academic
Press, New York.
- Duggan, D.M. 1980 "Measured and Predicted Vibrational
Wallace, E.R. Behavior of Gulf of Mexico Platforms,"
Caldwell, S.R. OTC 3864, Houston, Texas, May, 1980.
- Enochson, L. 1976 "A Digital Technique for Damping
Measurement of Fixed Platforms,"
OTC 2556, Houston, Texas, May, 1976.
- Fougere, P.F. 1976 "Spontaneous Line Splitting in Maximum
Zawalick, E.J. Entropy Power Spectrum Analysis,"
Radoski, H.P. Physics of the Earth and Planetary
Interiors, Vol 12, pp. 201-207.
- Fougere, P.F. 1977 "A Solution to the Problem of
Spontaneous Line Splitting in Maximum
Entropy Power Spectrum Analysis,"
Journal of Geophysical Research,
Vol. 82, No. 7, March, 1977.
- Gersch, W. 1973 "Estimation of Power Spectra with
Sharpe, D.R. Finite-Order Autoregressive Models,"
IEEE Transactions on Automatic
Control, Vol. AC-18, August, 1973,
pp. 367-369.
- Gold, B. 1969 Digital Processing of Signals,
Rader, C.M. McGraw-Hill, Inc., New York.
- Goodwin, G.C. 1977 Dynamic System Identification:
Payne, R.L. Experimental Design and Data Analysis,
Academic Press, New York.
- Gundy, W.E. 1980 "Damping Measurements of Offshore
Scharton, T.D. Platform," OTC 3863,
Thomas, R.L. Houston, Texas, May, 1980.
- Haykin, S. 1976 "The Complex Form of the Maximum
Kesler, S. Entropy Method for Spectral Estimation,"
Proceedings of IEEE, Vol. 64,
May, 1976, pp. 822-823.
- Haykin, S. 1979 Nonlinear Methods of Spectral Analysis,
(Editor) Topics in Applied Physics, Vol. 34,
Springer-Verlag, New York.

- Morf, M.
Vieira, A.
Kailath, T. 1978 "Covariance Characterization by Partial Autocorrelation Matrices," *The Annals Of Statistics*, Vol. 6, No. 3, March, 1978, pp. 643-648.
- Morf, M. 1978 "Recursive Multichannel Maximum Entropy Spectral Estimation," *IEEE Transactions on Geoscience Electronics*, Vol. GE-16, No. 2, April, 1978, pp. 85-94.
- Ng, A.T. 1977 "Multiple Channel Maximum Entropy Spectral Analysis and Its Applications," S.M. Thesis, Massachusetts Institute of Technology, January, 1977.
- Nuttall, A.H. 1976 "Multivariate Linear Predictive Spectral Analysis Employing Weighted Forward and Backward Averaging: A Generalization of Burg's Algorithm," NUSC Technical Report 5501, October, 1976.
- Nuttall, A.H. 1976 "Fortran Program for Linear Predictive Spectral Analysis of a Complex Univariate Process," NUSC Technical Report 5505, December, 1976.
- Oppenheim, A.V.
Schaffer, R.W. 1975 Digital Signal Processing, Prentice-Hall, Englewood Cliffs, New Jersey.
- Otnes, R.K.
Enochson, L. 1972 Digital Time Series Analysis, John Wiley and Sons, New York.
- Rabiner, L.R.
Gold, B. 1975 Theory and Application of Digital Signal Processing, Prentice-Hall, Inc., Englewood Cliffs, New Jersey.
- Rissanen, J. 1973 "Algorithms for Triangular Decomposition of Block Hankel and Toeplitz Matrices with Application to Factoring Positive Matrix Polynomials," *Mathematics of Computation*, Vol. 27, No. 121, January, 1973, pp. 147-154.
- Robinson, E.A. 1967 Multichannel Time Series Analysis with Digital Computer Programs, Revised Edition, Holden-Day, San Francisco.
- Robinson, E.A. 1978 Digital Signal Processing and Time Series Analysis, Holden-Day, San Francisco.

LIST OF REFERENCES (Cont.) -174-

- Rubin, S. 1979 Ambient Vibration Survey of an Offshore Platform," Presented at ASCE Spring Convention, Boston, Massachusetts, April 2-6, 1979.
- Ruhl, J.A. 1976 "Offshore Platforms: Observed Behavior and Comparisons with Theory," OTC 2553, Houston, Texas, May, 1976.
- Ruhl, J.A. 1979 "Forced Vibration Tests of a Deepwater Platform," OTC 3514, Houston, Texas, May, 1979.
- Siebert, W.M. 1979 "6.003: Signals and Systems," Class Notes, Department of Electrical Engineering and Computer Science, Massachusetts Institute of Technology, Cambridge, Massachusetts.
- Stevenson, A.E. 1978 Ambient Vibration Monitoring for Assessing the Structural Health of Offshore Production Platforms," ASME 78-PET-71, Presented at Energy Technology Conference and Exhibition, Houston, Texas, November 5-9, 1978.
- Rubin, S.
- Strand, O.N. 1977 "Computer Programs for Maximum Entropy Spectral Analysis of Real and Complex Single-Channel Time Series," NOAA Technical Memorandum ERL WPL-19, 1977.
- Yeung, J.M.
- Chadwick, R.B.
- Strand, O.N. 1977 "Computer Programs for Maximum Entropy Spectral Analysis of Real and Complex Multichannel Time Series," NOAA Technical Memorandum ERL WPL-22, April, 1977.
- Strand, O.N. 1977 "Multichannel Complex Maximum Entropy (Autoregressive) Spectral Analysis," IEEE Transactions on Automatic Control, Vol. AC-22, No. 4, August, 1977, pp.634-640.
- Strang, G. 1980 Linear Algebra and Its Applications, Second Edition, Academic Press, New York.
- Ulrych, T.J. 1974 "Cross-Spectral Analysis Using Maximum Entropy," Geophysics, Vol. 39, No. 3, June, 1974, pp. 353-354.
- Jensen, O.
- Ulrych, T.J. 1975 "Maximum Entropy Spectral Analysis and Autoregressive Decomposition," Reviews of Geophysics, Vol. 13, pp. 183-200.
- Bishop, T.N.

